

THE UNIVERSITY OF CALGARY

**Modelling the Catalytic Oxidation of  
N-Butane to Maleic Anhydride  
in a Circulating Fluidized Bed Reactor**

by

Todd Pugsley

A THESIS

SUBMITTED TO THE FACULTY OF GRADUATE STUDIES  
IN PARTIAL FULFILLMENT OF THE REQUIREMENTS FOR THE DEGREE OF  
MASTER OF SCIENCE

DEPARTMENT OF  
CHEMICAL AND PETROLEUM ENGINEERING

CALGARY, ALBERTA

JANUARY, 1992

© Todd Pugsley 1992



National Library  
of Canada

Bibliothèque nationale  
du Canada

Canadian Theses Service    Service des thèses canadiennes

Ottawa, Canada  
K1A 0N4

The author has granted an irrevocable non-exclusive licence allowing the National Library of Canada to reproduce, loan, distribute or sell copies of his/her thesis by any means and in any form or format, making this thesis available to interested persons.

L'auteur a accordé une licence irrévocable et non exclusive permettant à la Bibliothèque nationale du Canada de reproduire, prêter, distribuer ou vendre des copies de sa thèse de quelque manière et sous quelque forme que ce soit pour mettre des exemplaires de cette thèse à la disposition des personnes intéressées.

The author retains ownership of the copyright in his/her thesis. Neither the thesis nor substantial extracts from it may be printed or otherwise reproduced without his/her permission.

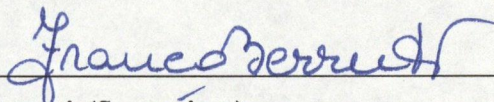
L'auteur conserve la propriété du droit d'auteur qui protège sa thèse. Ni la thèse ni des extraits substantiels de celle-ci ne doivent être imprimés ou autrement reproduits sans son autorisation.

ISBN 0-315-75119-3

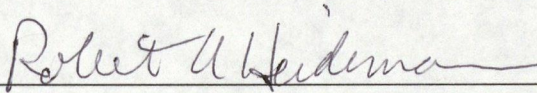
Canada

THE UNIVERSITY OF CALGARY  
FACULTY OF GRADUATE STUDIES

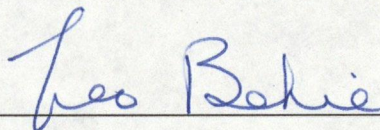
The undersigned certify that they have read, and recommend to the Faculty of Graduate Studies for acceptance, a thesis entitled, "Modelling the Catalytic Oxidation of N-Butane to Maleic Anhydride in a Circulating Fluidized Bed Reactor" submitted by Todd Pugsley in partial fulfillment of the requirements for the degree of Master of Science.



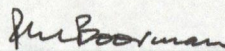
Dr. F. Berruti (Supervisor)  
Department of Chemical and Petroleum Engineering



Dr. R. A. Heidemann  
Department of Chemical and Petroleum Engineering



Dr. L. A. Behie  
Department of Chemical and Petroleum Engineering



Dr. P. M. Boorman  
Department of Chemistry

Feb. 24, 1992

Date

## ABSTRACT

A Circulating Fluidized Bed (CFB) is a gas-solid contactor in which solids are transported vertically in a riser by a high velocity gas stream. Upon exiting at the top of the riser, the solids are separated from the gas and returned to the bottom of the riser. CFB reactors are becoming increasingly attractive for conducting specific catalytic reactions due to their particular intrinsic features. A comprehensive computer simulation has been developed which combines the hydrodynamics of the CFB riser with a kinetic model for the catalytic oxidation of *n*-butane to maleic anhydride.

In this study, the hydrodynamics of the CFB riser have been modelled according to a two zone, core-annulus type of flow structure. Solid catalyst particles are assumed to move upward in the core and downward in the annulus, with interchange of solids between the two regions and the gas phase is assumed to move upward in the core only. A predictive hydrodynamic model has been incorporated which calculates the axial average voidage profile in the riser given the solids circulation rate, superficial gas velocity, solids and gas physical properties, and riser geometry, namely, height, diameter, and exit configuration.

The catalytic oxidation of *n*-butane to maleic anhydride has been simulated for an arbitrarily chosen 20 meter high, 30 centimeter diameter CFB riser. During the reaction, the catalyst undergoes rapid deactivation, which has been described utilizing a simple first order deactivation model at the catalyst surface. This rapid deactivation could correspond

to the mode in which the catalyst is reacting in different oxidation states. Studies have been carried out to investigate the effect of changes in solids circulation rate, superficial gas velocity, and inlet reactant concentrations on the reactor performance. Reactor performance is evaluated in terms of *n*-butane conversions, and product yields and selectivities.

The intrinsic kinetic model used in the simulation was developed in the literature for the partial oxidation of *n*-butane to maleic anhydride in a fixed bed reactor. Fixed bed reactor catalysts are of limited activity to avoid hot spot formation from rapid reaction rates. Hot spots are eliminated in a CFB reactor, and thus a much more active catalyst is employed. It is recommended that further studies into the reaction be undertaken with the specific catalyst used in a CFB catalytic reactor.

The proposed model is successful in describing the key features of the operation, in assessing the effect of the various operating parameters on the reactor performance, and in combining the complex riser hydrodynamics with a specific reaction kinetics model. The proposed simulation can easily accommodate different reaction kinetics and can therefore predict the performance of a CFB reactor for any catalytic process. The model represents a basis for feasibility studies, scale up, and process control of catalytic operations performed in Circulating Fluidized Bed reactors.

## ACKNOWLEDGEMENTS

I would like to take this opportunity to express my sincere thanks to those who have assisted and encouraged me during this work. Firstly, I would like to acknowledge my advisor, Dr. Franco Berruti for numerous consultations and invaluable feedback. He was not just my supervisor, but also a good friend without whose guidance, this work would not have been completed.

Also, thanks goes out to Bruce Milne who had written a computer program for the Berruti-Kalogerakis model prior to my arrival at the University of Calgary. This became an early starting point for my reaction simulation. I would also like to thank Bruce for several discussions along the way. Similarly, I would like to thank Robert Wong for the excellent work on the predictive hydrodynamic model incorporated into this work, and for numerous valuable brainstorming sessions on CFB behavior.

Furthermore, I would like to acknowledge the collaboration on this project with Dr. Jamal Chaouki of the Département de Genie Chimique, École Polytechnique de Montréal and Dr. Greg Patience now at DuPont. The pioneering experimental work of Dr. Patience during his Ph.D. studies at École Polytechnique was used extensively in the development of the hydrodynamic model.

This work was supported through the Natural Sciences and Engineering Research Council

of Canada (NSERC) scholarship and the Archibald Wayne Dingman Memorial Scholarship from the University of Calgary, and they are gratefully acknowledged.

Last, but certainly not least, I am indebted to my family for their continual interest in and support of my seemingly endless studies.

## TABLE OF CONTENTS

Approval Page	ii
Abstract	iii
Acknowledgements	v
Table of Contents	vii
List of Tables	x
List of Figures	xi
Nomenclature	xiii

### CHAPTER 1 - INTRODUCTION

1.1 Historical Background	1
1.2 CFB Design and Operation	2
1.3 CFB as a Catalytic Reactor	6
1.4 Outline of Study	10

### CHAPTER 2 - HYDRODYNAMIC MODEL

2.1 Overview of Riser Flow Structure	11
2.2 Berruti-Kalogerakis Model	12
2.3 Predictive Modelling of the Axial Solids Holdup	15
2.4 Predictive Model of Wong (1991)	16
2.4.1 Acceleration Zone	16

2.4.2 Developed Flow Zone	19
2.4.3 Deceleration Zone	20
2.4.4 Solids Interchange Coefficients	21
2.5 Summary of Hydrodynamic Model	24
2.6 Radial Gas Mixing	25
2.6.1 Previous Investigations into Gas Mixing	25
2.6.2 Proposed Radial Gas Mixing Model	26

### CHAPTER 3 - REACTION KINETICS

3.1 Reaction Kinetics Rate Expressions	28
3.2 Role of the VPO Catalyst	34
3.3 Kinetics of Catalyst Deactivation	37

### CHAPTER 4 - COMPUTER SIMULATION

4.1 Isothermal Operation and Reactor Energy Balance	39
4.2 Core and Annulus Mass Balances	41
4.3 Simulation Conditions	44
4.4 Solution of Mathematical Model	48

### CHAPTER 5 - SIMULATION RESULTS AND DISCUSSION.

5.1 Effect of Feed Concentration on CFB Reactor Performance	50
5.2 Effect of CFB Operating Conditions on Reactor Performance	61

5.3 Results of Catalyst Deactivation Model	72
5.4 Effect of Operating Temperature	76
5.5 Influence of the Core and Annular Regions	79
5.6 Comparison of the CFB Reactor Model with CSTR and PFR Reactor Models	91

## CHAPTER 6 - CONCLUSIONS AND RECOMMENDATIONS

6.1 Conclusions	94
6.2 Recommendations	96

## CHAPTER 7 - REFERENCES

7.1 References	98
----------------	----

## LIST OF TABLES

3.1 Kinetic Parameters for the Oxidation of <i>n</i> -Butane	32
3.2 Activation Energies	32
4.1 Properties of Solid Catalyst Particles	45

## LIST OF FIGURES

1.1	Schematic of a CFB	4
1.2	Schematic of a CFB as a Catalytic Reactor	8
4.1	Temperature Profile of a CFB Combustor	40
4.2	Slip Velocity for Different Reactor Systems	43
5.1	Single Pass Butane Conversion for Butane/Air Mixtures	51
5.2	Variation of Butane Conversion with Feed Concentration	53
5.3	Total Butane Reaction Rate for Butane/Air Mixtures	54
5.4	Butane Reaction Rate to CO <sub>2</sub> for Butane/Air Mixtures	56
5.5	Single Pass Product Yields for 1 mol% Butane in Air	57
5.6	Single Pass Product Yields for 5 mol% Butane in Air	58
5.7	Maleic Anhydride Selectivity for Butane/Air Mixtures	60
5.8	Effect of Solids Circulation Rate on Conversion and Solids Holdup	63
5.9	Effect of Inlet Superficial Gas Velocity on Conversion and Holdup	64
5.10	Superficial Gas Velocity Profile, $U_{oi} = 6$ m/s	66
5.11	Superficial Gas Velocity Profile, $U_{oi} = 4$ m/s	67
5.12	Solids Interchange Coefficients for $G_s = 400$ kg/m <sup>2</sup> s	69
5.13	Solids Interchange Coefficients for $G_s = 800$ kg/m <sup>2</sup> s	70
5.14	Effect of Catalyst Deactivation on Single Pass Butane Conversion	73
5.15	Single Pass Product Yields for 70% Catalyst Deactivation	75
5.16	Axial Reactor Temperature Profile	77

5.17	Effect of Reactor Temperature on Single Pass Butane Conversion	78
5.18	Single Pass Product Yields for Reactor Temperature of 623 K	80
5.19	Effect of Reactor Temperature on Maleic Anhydride Selectivity	81
5.20	Contribution to Reaction by the Core and Annular Regions	83
5.21	Relative MAN Production Rates from the Core and Annular Regions	85
5.22	Three Models for the Axial Variation of the Annular Voidage	86
5.23	Contribution to Reaction by the Core and Annular Regions	88
5.24	Relative MAN Production Rates from the Core and Annular Regions	89
5.25	Single Pass Butane Conversion for the Three Annular Voidage Models	90
5.26	Comparison of CFB Reactor Model with CSTR and PFR Models	92

## NOMENCLATURE

$a$	deactivation parameter ( $s^{-1}$ )
$A_w$	available heat transfer surface area at the reactor wall ( $m^2$ )
$c_B$	<i>n</i> -butane concentration (mol/L)
$c_O$	oxygen concentration (mol/L)
$c_{MA}$	maleic anhydride concentration (mol/L)
$c_{i,c}$	concentration of the $i^{th}$ species in the core (mol/L)
$c_{i,a}$	concentration of the $i^{th}$ species in the annulus (mol/L)
$C_p$	heat capacity of reactor feed (J/mol K)
$D_{AB}$	diffusivity of butane in air ( $m^2/s$ )
$D_p$	mean particle diameter (m)
$D_t$	riser diameter (m)
$E$	upward solids mass flux in the core ( $kg/m^2 s$ )
$E_A$	activation energy (kJ/mol)
$f_{io}$	smooth pipe interfacial friction factor (-)
$F_t$	molar flow of reactor feed (mol/s)
$g$	gravitational acceleration constant ( $m/s^2$ )
$G_s$	overall solids circulation rate ( $kg/m^2 s$ )
$h_w$	solids-to-wall heat transfer coefficient ( $W/m^2 K$ )
$\Delta H_{Ri}$	heat of reaction of the $i^{th}$ reaction (J/mol)
$k$	proportionality constant in the acceleration zone ( $m^{-1}$ )

$k_1$	kinetic constant for maleic anhydride formation ( $\text{mol}^{(1-\alpha)}\text{L}^\alpha/\text{g s}$ )
$k_2$	kinetic constant for $\text{CO}_2$ formation ( $\text{mol}^{(1-\beta)}\text{L}^\beta/\text{g s}$ )
$k_3$	kinetic constant for MAN decomposition ( $\text{mol}^{(\delta-\gamma)}\text{L}^{(1-\delta-\gamma)}/\text{g s}$ )
$k_g$	gas crossflow from core to annulus (m/s)
$K_1$	equilibrium constant in Buchanan and Sundaresan kinetics (-)
$K_2$	equilibrium constant in Buchanan and Sundaresan kinetics (-)
$K_{ac}$	annulus-to-core solids interchange coefficient (m/s)
$K_B$	equilibrium constant in Centi kinetics (mol/L)
$K_{ca}$	core-to-annulus solids interchange coefficient (m/s)
$L_{acc}$	length of the acceleration zone (m)
$P_B$	<i>n</i> -butane partial pressure (Pa)
$P_{MA}$	maleic anhydride partial pressure (Pa)
$P_{O_2}$	oxygen partial pressure (Pa)
$P$	total pressure (Pa)
$q_0$	number of deactivated catalytic sites for a totally deactivated catalyst (-)
$q(t)$	number of deactivated catalytic sites at any time <i>t</i> (-)
$Q$	upward solids mass flowrate in the core (kg/s)
$r_1, r_{MA}$	rate of maleic anhydride formation from <i>n</i> -butane (mol/g s)
$r_2, r_{CO_2}$	rate of $\text{CO}_2$ formation from <i>n</i> -butane (mol/g s)
$r_3, -r_{MA}$	rate of maleic anhydride decomposition (mol/g s)
$r_i$	rate of the $i^{\text{th}}$ reaction, where $i = 1, 2, 3$ (mol/g s)
$r_c$	core radius (m)

$r_d$	rate of catalyst deactivation (mol/g s)
$R$	riser radius (m)
$R_g$	universal gas constant (J/g K)
$Re$	Reynolds number (-)
$Re_p$	particle Reynolds number (-)
$R_s$	net radial flux (kg/m <sup>2</sup> s)
$S$	Stokes number (-)
$S$	product selectivity, moles of product formed per moles converted (-)
$t$	time (s)
$T$	temperature (K)
$T_f$	reactor feed temperature (K)
$T_w$	cooling water temperature in reactor membrane wall (K)
$U_{com}$	combined phase core velocity (m/s)
$U_{gc}$	gas velocity in the core (m/s)
$U_o$	riser superficial gas velocity (m/s)
$U_s$	average solids velocity (m/s)
$U_{sa}$	solids velocity in the annulus (m/s)
$U_{sc}$	solids velocity in the core (m/s)
$U_{s\infty}$	solids velocity at the end of the acceleration zone (m/s)
$U_t$	terminal settling velocity of a single solids particle (m/s)
$V_g$	gas velocity (m/s)
$W$	downward solids mass flux in the core (kg/m <sup>2</sup> s)

$x$	axial location in the riser (m)
$X$	<i>n</i> -butane conversion, moles converted per moles fed (-)
$Y$	product yield, moles of product formed per moles fed (-)

#### Greek Letters

$\alpha, \beta, \delta, \gamma$	kinetic constants, exponents in Centi rate expressions (-)
$\alpha_1, \alpha_2$	kinetic constants, exponents in Sharma rate expressions (-)
$\alpha$	limiting core suspension density ( $\text{kg/m}^3$ )
$\Gamma$	ratio of solids holdup at $x = 0$ to solids holdup at $x = L_{\text{acc}}$ (-)
$\epsilon_{\text{app}}$	apparent axial voidage (-)
$\epsilon_{\text{ann}}$	annular voidage (-)
$\epsilon_{\text{avg}}$	average axial voidage (-)
$\epsilon_{\text{b}}$	apparent voidage at riser bottom (-)
$\epsilon_{\text{c}}$	core voidage (-)
$\epsilon_{\text{mf}}$	voidage at minimum fluidization conditions (-)
$\epsilon_0$	actual voidage at riser bottom (-)
$\epsilon_{\infty}$	voidage at the end of the acceleration zone (-)
$\mu_{\text{g}}$	gas viscosity (Pa·s)
$\zeta$	constant quantifying diffuse nature of core/annulus interface (-)
$\varphi$	slip factor (-)
$\phi$	proportionality constant in $K_{\text{ac}}$ expression (-)
$\rho_{\text{b}}$	bulk density of solids ( $\text{kg/m}^3$ )

$\rho_{\text{com}}$	combined phase core density ( $\text{kg/m}^3$ )
$\rho_{\text{g}}$	gas density ( $\text{kg/m}^3$ )
$\rho_{\text{s}}$	solids particle density ( $\text{kg/m}^3$ )

## CHAPTER 1

### INTRODUCTION

#### 1.1 Historical Background

The use of fluidized bed technology dates back some 65 years to Winkler's coal gasifier, the first large-scale appearance of the fluidized bed. The imminent entry of the United States into World War II pushed the need for high octane aviation fuels. This led to a consortium of companies developing the Fluid Catalytic Cracking (FCC) technology for gasoline production from petroleum cuts. The first commercial unit went into operation in 1942 at Exxon's Baton Rouge, Louisiana refinery (Kunii and Levenspiel, 1991). Early FCC units operated at low pressures (2 to 3 psig) and superficial gas velocities of 1.2 to 1.8 m/s, what is now classified as the turbulent fluidization regime. It was soon realized that by lowering the gas velocity, a dense aggregative fluidized bed was formed which allowed completion of reaction and regeneration steps (Perry, 1984). As a result, investigations into higher velocity operation faded into the background.

In the late 1950's and early 1960's, Sasol developed a high gas velocity, solids recirculation system for producing synthetic gasoline from  $H_2$  and CO gases. Unlike the more complicated FCC units, this system was composed of a single loop solids recirculation system. This was followed by the Lurgi sand cracker for mineral processing. This single loop, solids recirculation network, known as a Circulating Fluidized Bed

(CFB) became more prominent in the mid-1970's with the onset of the energy crisis as countries looked for alternative energy sources (Dry and La Nauze, 1990). The Circulating Fluidized Bed Combustor (CFBC) was designed to burn low grade coal, wood waste or peat and was very successful to that end. In recent years, the CFB has come full circle to be considered as the perfect candidate for some catalytic reactions producing certain specialty chemicals. Potential applications of a CFB for catalytic reactions include fast reactions with rapid, reversible catalyst deactivation, reactions with a desired intermediate such as the partial oxidation of hydrocarbons, or highly exothermic or endothermic reactions (Contractor and Chaouki, 1990). As a result of the application of CFB technology in mineral processing, combustion, and catalytic reactions, research into high gas velocity operation has come out of the shadows to become an extremely active area.

## **1.2 CFB Design and Operation**

A Circulating Fluidized Bed (CFB) reactor is a type of gas solid contacting device in which solid particles are transported vertically by a high velocity gas stream. Riser gas superficial velocity is normally in the range of 3 - 10 m/s compared with less than 1 m/s for conventional bubbling beds. Operation is thus in the range between bubbling fluidization and pneumatic conveying.

At these velocities, solids carryover at the exit is large. Solids exiting at the top of the riser are separated from the gas stream and returned to the riser by gravity through a

vertical standpipe. Separation is most commonly achieved with a cyclone. Figure 1.1 illustrates a schematic representation of a CFB combustor.

The gas is fed at the base of the riser while solids are introduced by re-injection from the vertical standpipe. In combustion processes, secondary air is added along the riser to improve combustion. Secondary gas injection or staged addition of reagents may be beneficial for catalytic reactions as well. Gianetto et al. (1990) investigated the partial oxidation of propylene to acrolein for both stoichiometric feed oxygen and 100% excess feed oxygen. The first case resulted in higher acrolein selectivity with the maximum selectivity occurring at a longer residence time, while the excess feed oxygen case produced the maximum selectivity at a shorter residence time. They concluded that an optimum could be obtained by direct oxygen concentration control along the riser length. This oxygen control could be varied depending on the oxygen kinetic order of a particular reaction.

The gas solid reaction occurs in the riser. There is normally a denser gas-solid phase at the base of the riser where the solids and gas are introduced. As the bed becomes leaner axially, a smooth pressure drop is seen from the bottom to the top of the riser. On a plot of pressure drop versus velocity, a fluidized bed experiences a constant pressure drop between the minimum fluidization velocity and the initiation of entrainment. It is the high velocities beyond this point and the associated decrease in pressure drop which correspond to operation of a CFB.

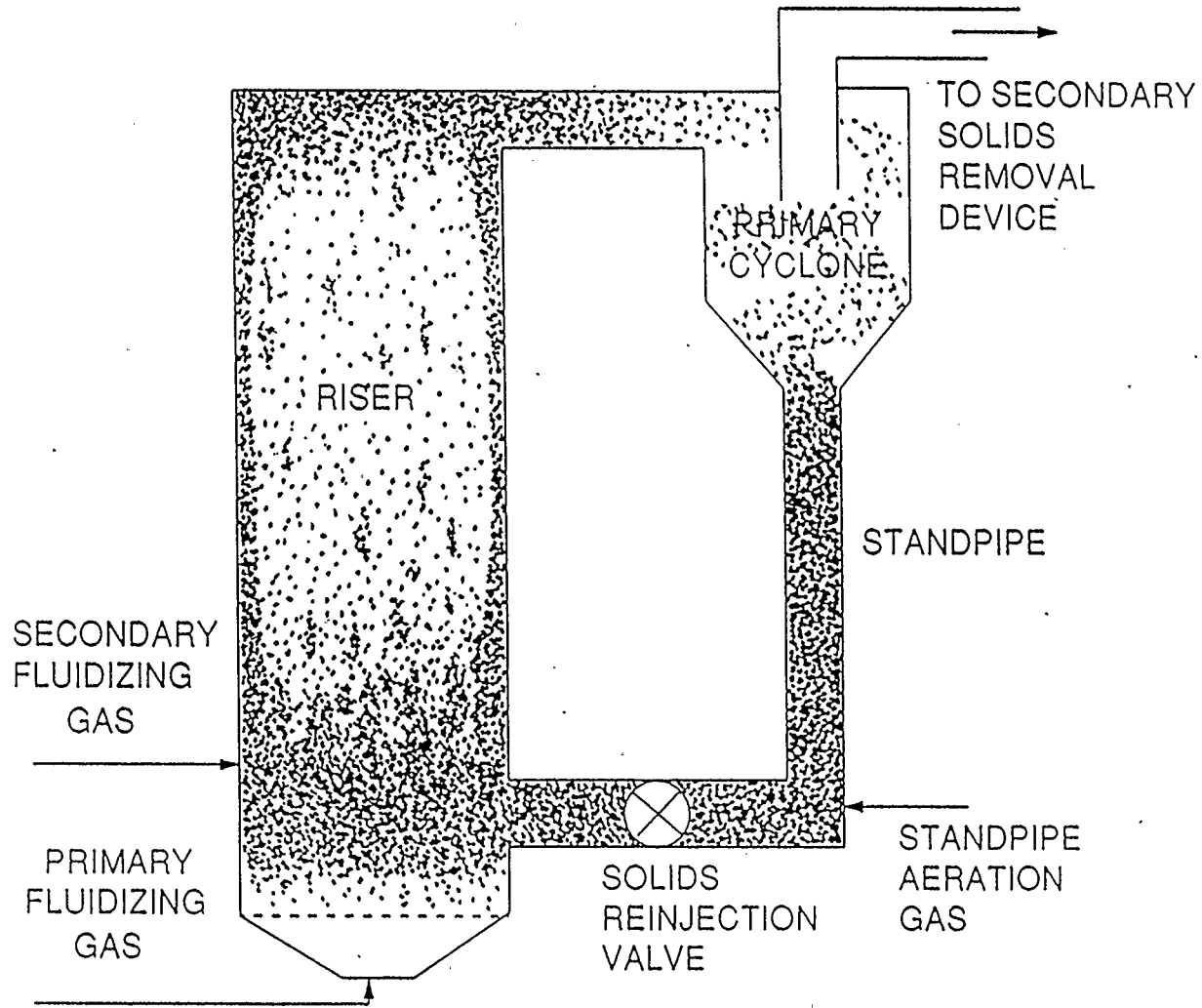


Figure 1.1 - Schematic of a Circulating Fluidized Bed Combustor

Because of the high gas velocities, tube banks can not be inserted to remove heat from the bed as they are typically used in a conventional fluidized bed. Instead, the riser is generally surrounded by water walls which raise steam due to the high heat transfer from solids to the wall.

For gas-solid separation, conventional vertical cyclones are the most common. It has been found that separation efficiency increases with increased solids loading (Dry and La Nauze, 1990) and the large clusters of particles associated with high loadings appear to sweep the smaller particles to the cyclone wall. The need for abrasion-resistant refractory lining makes the cyclone a significant portion of the capital cost.

The vertical standpipe is like an overgrown external cyclone-dipleg arrangement of a conventional fluidized bed. However, it is much larger in terms of diameters, and handles much higher solids flows. The loop seal shown at the base of the standpipe in Figure. 1.1 is a type of check valve arrangement which prevents back flow of gas between the riser and the standpipe.

The key features of a Circulating Fluidized Bed are:

- high gas velocity and solids throughput
- near perfect mixing and thermal inertia leading to near isothermal conditions
- high heat transfer coefficients from solids to wall (200-250 W/m<sup>2</sup>K)
- large pressure drops associated with high bed densities

### 1.3 CFB as a Catalytic Reactor

DuPont in the United States has recently proceeded with the design and construction of a pilot plant for studying the use of a CFB as a catalytic reactor (Contractor et al., 1988). The particular reaction being studied is the partial oxidation of *n*-butane to maleic anhydride (MAN). MAN is an extremely important industrial chemical, used primarily for the production of unsaturated polyester resins, alkyd resins, and specialty copolymers. It is also used in the manufacture of agricultural chemicals, as an additive in lubricating oils, and as a building block for L-aspartic acid, used in making NutraSweet. Annual production in the United States is approaching 190,000 metric tonnes and is increasing by approximately 6% per year to meet increasing demand (Irving-Monshaw and Kislin, 1989). A 3000 tonne/year facility has recently been commissioned in Belgium to produce butyrolactone from direct hydrogenation of maleic anhydride. This method produces butyrolactone at a 10% lower cost than the traditional route from butanediol. Butyrolactone is an intermediate in the manufacture of vitamin B<sub>12</sub> (Chowdrury, 1991).

Traditionally, the production of maleic anhydride from C<sub>4</sub> feedstock was accomplished in a fixed bed reactor. A problem with fixed beds is the development of hot spots within the bed of solids. At high temperatures, the *n*-butane tends to be completely oxidized to CO<sub>2</sub> and water. Thus yield of desired product can be greatly reduced by hot spots in a partial oxidation such as this one. Furthermore, these hot spots can decrease catalyst activity through coke deposition or structural changes. Another consideration is the rapid

reduction of the catalyst activity during the partial oxidation of *n*-butane. This creates the need for frequent catalyst regeneration. Such frequent regeneration requires the need for two or more fixed bed reactors operating on a "swing" system if the process is to be operated continuously. Initial cost of such a system is great. Rapid reduction of the catalyst creates a need for excess oxygen in the feed stream. However, this oxygen will also tend to make CO<sub>2</sub> formation more favorable, again decreasing maleic anhydride yields.

After considering these drawbacks in a fixed bed, the use of a CFB as the reactor in such a process appears to be a classic application. Figure 1.2 is a schematic of a CFB catalytic reactor. Solid catalyst particles are injected from the standpipe and are transported vertically in the high velocity gas stream containing *n*-butane. The reaction occurs along the riser and the catalyst is rapidly deactivated. The solids and gas exit from the riser via a smooth elbow and are separated in the cyclone. The product gas stream containing maleic anhydride and other gases is sent downstream for purification. The deactivated catalyst particles are stripped of any carbonaceous material by an inert such as nitrogen or steam and sent on to the regenerator section where contact with air oxidizes the catalyst surface once again. The regenerated catalyst is gravity fed to the standpipe where it moves to the base of the riser for reinjection into the riser reaction zone.

Contractor and Sleight (1987) discussed the inherent advantages of a CFB in the catalytic partial oxidation of *n*-butane to maleic anhydride. These include:

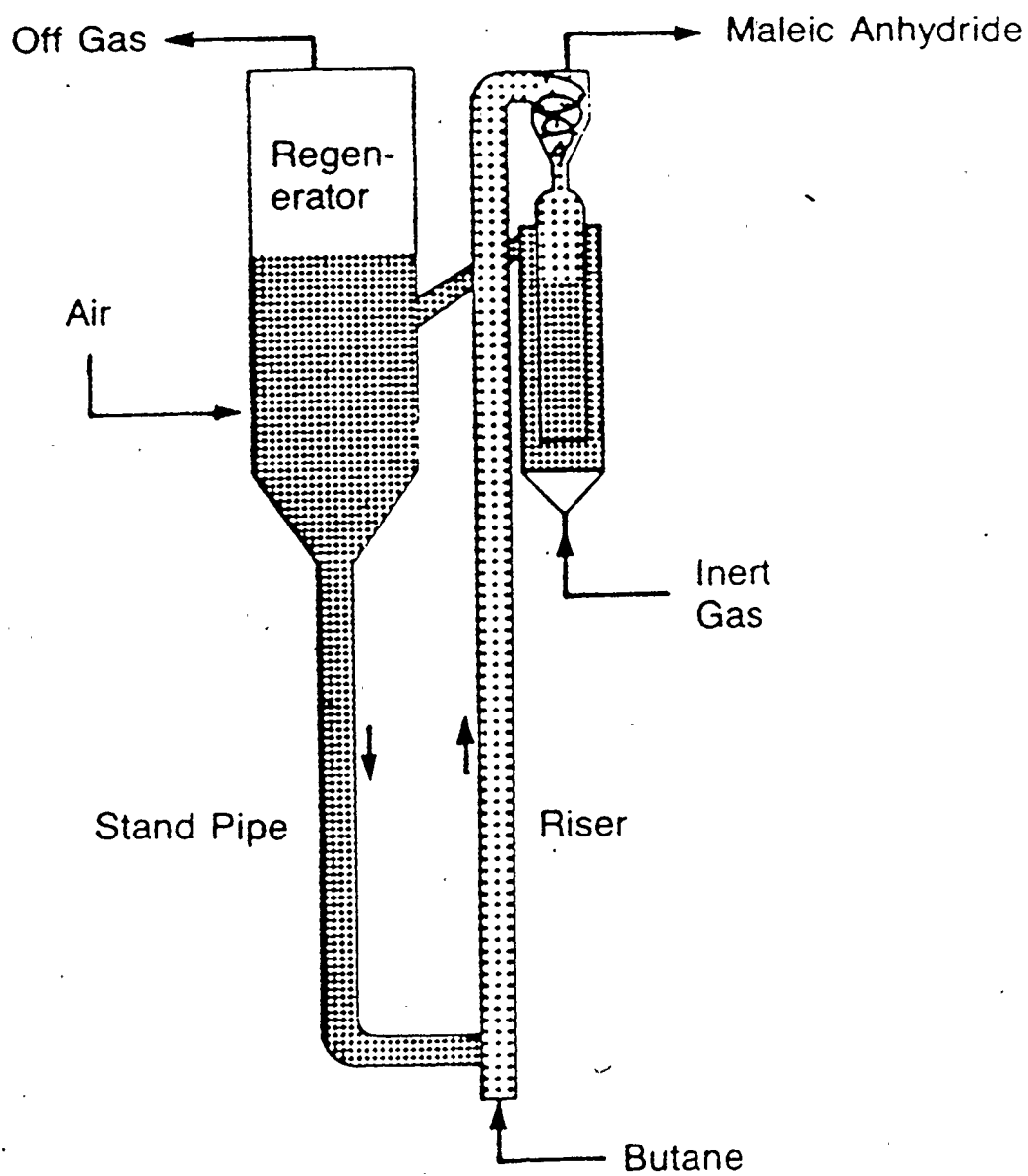


Figure 1.2 - Schematic of a Circulating Fluidized Bed as a Catalytic Reactor  
(Contractor and Sleight, 1987)

1. Separate catalyst reduction and oxidation (regeneration) zones in the riser and vertical standpipe, respectively.
2. Resulting lower oxygen concentration in the feed (since regeneration occurs in a separate section), leading to higher yields and selectivity of maleic anhydride.
3. High throughput associated with high gas velocities.
4. Near isothermal conditions as a result of near perfect mixing, thermal inertia, and high heat transfer coefficients. Hot spots and the corresponding yield losses are eliminated.
5. Separate product gas and regenerator off gas streams (see Figure 1.2) combined with a more concentrated feed stream, resulting in a concentrated product. This eases the load on downstream separation processes.

The high demand for maleic anhydride from *n*-butane coupled with the interest in the Circulating Fluidized Bed technology makes a simulation for predicting reactor performance a valuable tool.

The objective of this study was to develop a comprehensive computer simulation combining CFB hydrodynamics with reaction kinetics of MAN formation which may be used with any reactor size and operating conditions (within the limits of the empirical correlations of the hydrodynamic model). This work included the development of a model adaptable to different kinetics, either for a different reaction in the CFB or new, improved kinetics for the *n*-butane partial oxidation to maleic anhydride.

## 1.4 Outline of Study

The actual flow pattern in a CFB is very complex and is strongly dependent on many variables. In chapter 2, a predictive model is summarized which can be used to calculate the riser hydrodynamic properties given the riser geometry and operating conditions and the gas and solids physical properties. This model can also account for entrance and exit effects, and the acceleration of solids entering at the base of the riser.

The reaction kinetics for the partial oxidation of *n*-butane to maleic anhydride in a fixed bed have been studied extensively by several authors. The results are examined in chapter 3. Also, the behavior of the catalyst in terms of active crystalline phases during the reaction is discussed. A simple catalyst deactivation model has been employed in the simulation and described in detail in chapter 3.

In chapter 4, the actual computer simulation written in UNIX:C language is described. Assumptions are validated, and the mass balance equations for the simulation are presented. The method of solution of these equations is outlined.

Finally, graphical results are presented and discussed in chapter 5. This chapter addresses the usefulness of the simulation and its ability to predict reactor performance and optimal operating conditions.

## CHAPTER 2

### HYDRODYNAMIC MODEL

#### 2.1 Overview of Riser Flow Structure

The flow pattern of solids in the riser of a Circulating Fluidized Bed is extremely complex. The column diameter, height, and exit configuration, particle properties, and gas characteristics all affect the flow structure in the riser. Visual observation in a column of circular cross section indicates the existence of a lean suspension of solids in gas flowing upward in the center of the riser (solids holdup typically in the range of 2 to 15% by volume), with a denser downflow of solids next to the wall. Experimental work of many researchers support this observation. Weinstein et al. (1986) and Bader et al. (1988) both observed decreasing radial voidage profiles in their units, with the most dramatic decrease occurring very close to the wall. The radial location of this sudden change in voidage indicates the interface between the dilute upward flowing region and the dense downward flowing region. Brereton et al. (1988), and Berruti and Kalogerakis (1989) followed these experimental observations with simple models for the flow structure in the riser of a Circulating Fluidized Bed. These models assumed a core/annulus, two-zone type of structure with gas and entrained solids flowing upward in the dilute core region, and dense clusters of solids flowing downward in a thin annular film next to the wall. The CFB riser is also characterized by a dense, turbulent portion at its base where solids are fed into the riser, which eventually becomes leaner as the flow of solids develops and the

particles are accelerated to their steady state upward velocity in the riser.

Though the core/annulus approach is employed in this work to quantify some of the key aspects of the solids and gas flow, it is acknowledged that the real situation is much more complicated. The local voidage of the downward flowing annular region varies greatly with time and axial location and, at times, the annulus can not be seen at all. Also, the interface between the core and annular regions is not well defined. Streamers or clusters of solids may be observed flowing up or down at varying velocities. With the aid of a high speed video camera, Takeuchi and Hirama (1990) observed extremely chaotic and turbulent behavior at the base of the riser while more stable flow was seen at higher elevations. However, even at the higher elevations unstable behavior was periodically observed.

## **2.2 Berruti-Kalogerakis Model**

The model of Berruti and Kalogerakis (1989) is used in this work to evaluate the internal flow structure in the riser. It requires the solids circulation rate, the axial gas superficial velocity, and the average axial riser voidage as inputs. The average riser voidage at any axial location may be obtained from the riser pressure profile. In the formulation of the model, it is assumed that the slip velocity in the core is equal to the terminal settling velocity of a single particle,

$$U_{sc} - U_{gc} = U_t \quad (2.1)$$

and the upward flow of gas is restricted to the core region. Also, the velocity of the downward flowing particles in the annular region is taken as the terminal settling velocity of a single particle, and the annular voidage is assumed to be that of a fluidized bed of particles at minimum fluidization conditions. The end result is the following equation for calculation of the core voidage:

$$\epsilon_c = 1 - \frac{G_s + [1 - (\frac{r_c}{R})^2] \rho_s (1 - \epsilon_{mf}) U_t}{\rho_s (\frac{r_c}{R})^2 [\frac{U_o}{\epsilon_c} (\frac{R}{r_c})^2 - U_t]} \quad (2.2)$$

The axial average voidage profile can be obtained from an experimentally determined pressure drop profile according to,

$$\epsilon_{avg} = 1 - \frac{1}{\rho_s g} \frac{dP}{dx} \quad (2.3)$$

Equation (2.3) assumes that the axial pressure drop profile is due solely to the weight of solids present at any axial location, ignoring frictional effects at the wall. Arena et al. (1986) compared the average axial voidage profile predicted from pressure drop measurement with the profile obtained from trapped solids weighing along the riser length. Pressure drop measurements were found to under-predict the average voidage in the riser and this discrepancy was attributed to the frictional effects of the wall. They indicated that the small diameter column used (4.1 cm ID) may have enhanced the frictional effects.

A solids balance over a volume element of the riser results in the following expression for the core radius:

$$\left(\frac{r_c}{R}\right)^2 = \frac{\epsilon_{\text{avg}} - \epsilon_{\text{mf}}}{\epsilon_c - \epsilon_{\text{mf}}} \quad (2.4)$$

Equations (2.2) and (2.4) may be solved simultaneously to obtain the values of core voidage and core radius at any axial position along the riser. Having obtained these values, the remaining quantities are calculated from the relationships used to formulate Equation (2.2). The interstitial gas velocity in the core can be calculated from

$$U_{\text{gc}} = \frac{U_o}{\epsilon_c} \left(\frac{R}{r_c}\right)^2 \quad (2.5)$$

The upward solids velocity in the core can then be obtained from Equation (2.1). The upward solids flux in the core,  $E$ , at any axial location per unit cross sectional area is given by

$$E = U_{\text{sc}}(1 - \epsilon_c)\rho_s\left(\frac{r_c}{R}\right)^2 \quad (2.6)$$

At any point in the riser, the overall solids circulation rate,  $G_s$ , must equal the difference between the upward and downward solids fluxes,

$$G_s = E - W \quad (2.7)$$

In summary, the Berruti-Kalogerakis model is able to predict the core voidage and core radius, solids fluxes in the core and annular regions, and the gas and solids velocities in the core at any axial location, given the experimental steady state pressure profile in the riser.

### **2.3 Predictive Modelling of the Axial Solids Holdup Profile**

Several authors have formulated correlations for predicting the average axial solids holdup in the riser of a CFB. Choi et al. (1990) and Mori et al. (1990) present empirical correlations for the solids holdup in both the dense and fully developed flow regions. These relations are developed for Geldart type A and B particles, but their use is limited to CFB units of similar geometry (3.8 cm to 5.0 cm ID). Kunii and Levenspiel (1990) developed a predictive model showing a lower region of constant solids holdup, and an upper region with an exponentially decaying solids density. The decay constant was correlated using data from the literature. Zhang et al. (1990) combined Brownian motion with random walk theory to obtain a mathematical model for the axial voidage distribution. The model produces an axial voidage curve which is the combination of two half logarithmic curves. In the dense region, the voidage increases exponentially from its value at the base of the riser, while in the leaner region, the voidage decreases from its value at the riser exit. The values of the voidages at the inlet and outlet, and the height of the interface between the lean and dense phases are obtained from empirical correlations of Li (1980). Wong (1991) compared various predictive correlations found

in literature with the experimental data of Patience (1990) and showed that none of the correlations was successful in providing accurate profiles, especially in the denser portion at the bottom of the riser or for abrupt exit geometry. In the work of Wong (1991), a new predictive model for the axial solids distribution and the internal flow structure of a CFB riser is developed and used in conjunction with the Berruti-Kalogerakis model to calculate the main hydrodynamic characteristics of the solids and gas flows.

## **2.4 Predictive Model of Wong (1991)**

This model considers the CFB riser divided into three sections: an acceleration zone corresponding to the dense region at the base of the riser, a fully developed flow zone immediately above the acceleration zone, and a deceleration zone for risers equipped with an abrupt exit geometry. If the riser has a smooth exit to the cyclone, the fully developed zone is assumed to extend all the way to the outlet. Given the riser diameter, height, and exit configuration, solids and gas flowrates, and physical properties, the axial voidage profiles may be calculated along with the core voidage and radius, core gas and solids velocity, and solids interchange coefficients from core and annulus and from annulus to core, all functions of the axial location along the riser.

### **2.4.1 Acceleration Zone**

In the dense region at the base of the riser of a CFB, a fraction of the total measured

pressure drop between the entrance and the start of the fully developed flow zone can be attributed to the acceleration of the particles to their steady state velocity. If this acceleration component is not separated from the pressure drop data, erroneous voidages will be predicted in the acceleration zone.

A momentum balance on a height element,  $dx$ , in the acceleration zone, neglecting the gas contribution (since  $\rho_s \gg \rho_g$ ) gives

$$1 - \epsilon_{app} = \frac{G_s}{\rho_s g} \left( \frac{dU_s}{dx} + \frac{g}{U_s} \right) \quad (2.8)$$

The solids velocity gradient may be expressed as (Weinstein and Li, 1989)

$$\frac{dU_s}{dx} = k(U_{s\infty} - U_s) \quad (2.9)$$

where  $U_{s\infty}$  is the solids velocity at the end of the acceleration zone. The solids holdup at the end of the acceleration zone is

$$1 - \epsilon_{\infty} = \frac{G_s}{\rho_s U_{s\infty}} \quad (2.10)$$

Equation (2.9) is integrated from the initial solids velocity,  $U_{s0}$ , at the base of the riser, to a velocity  $U_s$  at a point  $x$  in the acceleration zone. Substitution of this result and Equation (2.10) into Equation (2.8) leads to the following expression for the apparent solids holdup in the acceleration zone:

$$\frac{1 - \epsilon_{app}}{1 - \epsilon_{\infty}} = \frac{U_{s\infty}^2 k \Gamma}{g} \exp(-k x) + \frac{1}{1 - \Gamma \exp(-k x)} \quad (2.11)$$

where

$$\Gamma = 1 - \frac{1 - \epsilon_0}{1 - \epsilon_{\infty}} \quad (2.12)$$

This is the ratio of the actual solids holdup at the bottom of the riser, to the solids holdup at the end of the acceleration zone. In order to evaluate this constant, the apparent voidage at the bottom of the riser,  $\epsilon_b$ , must be known.

Wong (1991) proposed two empirical correlations for calculating  $\epsilon_b$ : one for Geldart group B particles, and one for Geldart group A particles. For Geldart type A particles, the expression is

$$\epsilon_b = 0.714 \left( \frac{G_s}{\rho_s U_o} \right)^{-0.02528} D_t^{-0.0794} Re_p^{-0.12016} \quad (2.13)$$

whereas for Geldart type B particles,  $\epsilon_b$  is calculated from:

$$\epsilon_b = 0.249 \left( \frac{G_s}{\rho_s U_o} \right)^{-0.10794} D_t^{-0.23396} Re_p^{0.018583} \quad (2.14)$$

Assuming an inlet solids velocity of zero, and taking  $U_s$  as  $0.99U_{s\infty}$  at the end of the acceleration zone (where  $x = L_{acc}$ ), then the integration of Equation (2.9) gives

$$k = -\ln\left(\frac{0.01}{L_{acc}}\right) \quad (2.15)$$

Thus, if the length of the acceleration zone,  $L_{acc}$ , is known, a value of the proportionality constant,  $k$ , may be determined. Wong (1991) used a modified version of the correlation of Enick et al. (1987) to calculate the length of the acceleration zone:

$$\left(\frac{L_{acc}}{D_t}\right) = 7.92 \times 10^8 \left(\frac{D_t}{D_p}\right)^{-0.7642} \left(\frac{\rho_s}{\rho_g}\right)^{-1.213} \left(1 + \frac{G_s}{U_o \rho_g}\right)^{0.915} (Re)^{0.415} \quad (2.16)$$

#### 2.4.2 Developed Flow Zone

Immediately above the acceleration zone, a fully developed flow zone is assumed where the solids and gas have been accelerated to their steady state velocity, and the average solids holdup remains essentially constant.

Patience et al. (1991), have found that in the fully developed flow regions of Circulating Fluidized Beds, the slip factor, defined as the ratio of the interstitial gas velocity to the solids velocity, is approximately equal to two:

$$\phi = \frac{U_o}{\epsilon_{avg}} \frac{1}{U_{sc}} = 2 \quad (2.17)$$

Knowing that the average solids velocity in the fully developed zone is given by:

Equation (2.17) may be rearranged to solve for the average voidage in the fully developed

$$U_s = \frac{G_s}{\rho_s (1 - \epsilon_{avg})} \quad (2.18)$$

flow zone:

$$\epsilon_{avg} = \frac{U_o \rho_s}{2 G_s + U_o \rho_s} = \epsilon_\infty \quad (2.19)$$

### 2.4.3 Deceleration Zone

The deceleration zone of the CFB riser is that region affected by an abrupt exit configuration. The effect of an abrupt exit is an increased solids holdup in the area around the riser outlet due to internal solids recirculation. This solids densification may also extend downward for a significant portion of the riser, depending upon the operating conditions used. The solids recirculation can significantly increase the solids residence time, especially at higher solids circulation rates and can therefore have implications on the reactor performance, if the solids are active catalyst particles.

In the model of Wong (1991), unlike the acceleration and fully developed zones where the average voidage is determined directly, the calculation of the voidage in the deceleration zone is a boundary value problem involving iterations to determine a fitting parameter. The boundary conditions for the deceleration zone are the voidage at the end of the fully developed flow zone, and the voidage at the top of the riser. The voidage at

the top of the riser is calculated from an empirical correlation developed from data reported in literature for CFBs with abrupt exit configurations. The function involved in the iterative procedure is that used in the calculation of solids interchange coefficients, and shall be reported in the next section. It is noted by Wong (1991) that the data reported in literature for abrupt exit configurations is limited and the empirical correlation for the top voidage is valid only for a narrow range of conditions. The proposed correlation is:

$$\frac{\varepsilon_t}{1-\varepsilon_t} = 130.934 \left\{ U_o \left( \frac{\rho_g^2}{\mu_g (\rho_s - \rho_g)} \right)^{1/3} \right\}^{-0.85786} \left( \frac{G_s}{\rho_s (U_o - U_g)} \right)^{-0.29989} A \quad (2.20)$$

where

$$A = D_t^{-0.53642} Re_p^{-0.10143} Z^{10.3377} \quad (2.21)$$

#### 2.4.4 Solids Interchange Coefficients

The net radial solids flux between the annular and core regions of the riser,  $R_s$ , may be written for any axial location as:

$$R_s = -\frac{1}{2\pi r_c} \frac{dQ}{dx} = K_{ca} \alpha - K_{ac} \rho_s (1 - \varepsilon_{mf}) \quad (2.22)$$

where  $Q$  is the upward solids flowrate,  $r_c$  the core radius, and  $\varepsilon_{mf}$  the annular voidage according to the Berruti-Kalogerakis model. The parameter  $\alpha$  represents the core suspension density, given by

$$\alpha = \rho_s (1 - \epsilon_c) + \rho_g \epsilon_c \quad (2.23)$$

Studies into the mechanism of the exchange of solids between the core and annular regions suggest that it is due to either turbulent diffusion of solids or solid-solid collisions. The model of Wong (1991) uses the empirical expression of Bolton and Davidson (1988), based on a turbulent diffusion mechanism, to calculate the solids interchange coefficient between the core and the annulus:

$$K_{ca} = 0.1 \sqrt{\pi} U_o \frac{(1 - 2.8 \text{Re}^{-1/8})}{(1 + S/12)} \quad (2.24)$$

The determination of the solids annulus-to-core interchange coefficients is based on analogy with gas-liquid countercurrent annular flow. It has been suggested (Senior and Brereton, 1990, Takeuchi and Hirama, 1990) that the diffuse interface between the core and annular regions of a Circulating Fluidized Bed is comparable to that of a gas-liquid annular flow reported in the literature. The expression for the solids annulus-to-core interchange coefficient is then

$$K_{ac} = \frac{\phi \rho_{com} U_{com}^2 f_{i_o}}{2 \rho_b (U_{sc} - U_{sa})} \left(1 + \zeta \left(\frac{R - r_c}{D_t}\right)\right) \quad (2.25)$$

where  $\rho_{com}$  and  $U_{com}$  are the combined phase core density and the combined phase core velocity, respectively, and are defined as follows:

The quantity  $f_{i_o}$  is the smooth pipe friction factor. The proportionality constant,  $\phi$ , is

$$\rho_{\text{com}} = \frac{U_{\text{gc}} \epsilon_c \rho_g + U_{\text{sc}} (1 - \epsilon_c) \rho_s}{U_{\text{gc}} \epsilon_c + U_{\text{sc}} (1 - \epsilon_c)} \quad (2.26)$$

$$U_{\text{com}} = (U_{\text{gc}} \epsilon_c + U_{\text{sc}} (1 - \epsilon_c)) \left(\frac{r_c}{R}\right)^2 \quad (2.27)$$

determined for the case of a negligible solids wall layer thickness such that  $r_c = R$ , and the net solids interchange,  $R_s$ , is zero. The constant  $\xi$ , is a fitting parameter accounting for the wavy, diffuse nature of the core/annulus interface. Its value varies depending on the riser operating conditions and it is normally evaluated by a trial and error method.

Equations (2.22) to (2.27) are used to determine the average voidage profile in the deceleration zone. From the Berruti-Kalogerakis model,

$$E = G_s + W \quad (2.28)$$

Therefore, the upward solids flowrate is

$$Q = (G_s + (1 - (\frac{r_c}{R})^2) \rho_s (1 - \epsilon_{\text{mf}}) U_t) \pi r_c^2 \quad (2.29)$$

Thus, from Equation (2.22):

$$-\frac{1}{2 \pi r_c} \frac{d[(G_s + (1 - (\frac{r_c}{R})^2) \rho_s (1 - \epsilon_{\text{mf}}) U_t) \pi r_c^2]}{dx} = K_{\text{ca}} \alpha - K_{\text{ac}} \rho_s (1 - \epsilon_{\text{mf}}) \quad (2.30)$$

The core voidage may be expressed in terms of the core radius as per the Berruti-Kalogerakis model. The core to annulus interchange coefficient is taken to be the same as that in the fully developed zone. This leaves the iterative procedure as outlined by

Wong (1991) to obtain a value for the constant  $\zeta$ . Using Equation (2.20), the average voidage at the top of the riser may be estimated. Equations (2.2) and (2.4) are then solved simultaneously to obtain the corresponding core voidage and core radius at the top of the riser. Implementing the slip factor criterion of Patience et al. (1991), the average voidage at the bottom of the deceleration zone (i.e. the average voidage at the end of the fully developed flow zone) is calculated. The corresponding core voidage and radius are again determined. The calculated core radii at the top and bottom of the abrupt exit zone become the respective boundary conditions. Equation (2.30) is discretized and the core radius profile is determined from the top to the bottom of the deceleration zone. The parameter  $\zeta$  is varied until the core radius at the bottom of the acceleration zone is equal to the core radius in the fully developed zone, and the bottom boundary condition is satisfied. In this way, the core radius profile may be obtained, and hence the core voidage. Finally, the average voidage profile in the deceleration zone may be calculated.

## 2.5 Summary of Hydrodynamic Model

The hydrodynamic model of Wong (1991) combines a predictive model for determining the average axial voidage profile with the Berruti-Kalogerakis model to describe the internal flow structure of a Circulating Fluidized Bed. The model requires the input of solids circulation rate,  $G_s$ , and the inlet superficial gas velocity,  $U_0$ . From there, the model divides the riser into an acceleration zone, a fully developed flow zone, and a deceleration zone, the latter for abrupt exit riser geometry only. For known gas and solids

physical properties, and a given riser height and diameter, the model successfully predicts the axial average voidage profile along with the core voidage and radius, core gas and solids velocity, and the solids interchange coefficients from core-to-annulus and annulus-to-core.

## **2.6 Radial Gas Mixing**

### 2.6.1 Previous Investigations into Gas Mixing

The predictive model of Wong (1991) successfully calculates the axial voidage profile and internal flow structure of solids in a Circulating Fluidized Bed riser. However, it does not determine all of the characteristics relative to the internal flow structure of the gas, specifically the crossflow of gas between the core and the annular regions. This is a general trend in the current literature; much work has been devoted to studies of the flow structure of solids, but little remains known about the gas phase. Plug flow of gas in the core with little or no flow in the annulus has been widely accepted. Bader et al. (1988) found axial dispersion of gas to be negligible compared to convective transport in the riser. They also determined that 75% of the gas flowed through the middle 20 centimeters of their 30.5 centimeter column. Adams (1988) investigated the diffusion coefficient of gas in a CFB. He found that the presence of solids greatly reduced the diffusion from that in an empty bed. Increased solids circulation rates further reduced the gas mixing. He modelled this behavior based on a turbulent eddy diffusion mechanism. Brereton et al.

(1988) found more pronounced deviations from plug flow of gas. It is believed that the abrupt exit geometry and the small diameter (0.152 meters) of their experimental unit contributed somewhat to this result. They suggested a simple, two-zone model for gas flow incorporating a crossflow coefficient which is assumed constant at any axial location along the riser.

### 2.6.2 Proposed Radial Gas Mixing Model

With so little research into this area, a highly involved model for gas mixing in a CFB riser is not warranted. Originally, the possibility of using the solids interchange coefficients to describe the gas crossflow was considered, but this assumption would have greatly exaggerated the amount of radial gas mixing. In the work presented here, the Higbie penetration theory (Higbie, 1935) is used to calculate the gas crossflow coefficient. The theory was originally developed to describe contact between liquid and gas occurring for a short period of time. Thus a steady state concentration gradient would not have time to develop as the gas moves into the liquid. The gas sees the film of liquid as an infinite medium. This results in the following expression for the mass transfer coefficient:

$$k = \sqrt{\frac{4D_{AB}\epsilon}{\pi t}} \quad (2.31)$$

Extending this theory to the Circulating Fluidized Bed, the crossflow of gas is assumed to occur in the core to annulus direction only. The voidage in Equation (2.31) may be taken as the annular voidage and the gas diffusivity is that of *n*-butane in air. The

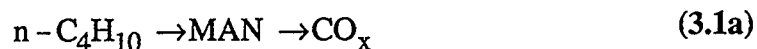
exposure time,  $t$ , is the residence time of gas in a volume element of the riser. The concept of this volume element will be explained in Chapter 4, where the computer simulation is described in detail. Thus, the transfer of gas from the core to the annular region is described by a diffusional mass transfer mechanism, involving the contact of eddies of solids with an upward flowing gas stream.

## CHAPTER 3

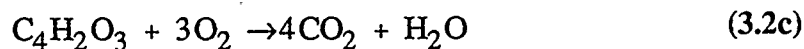
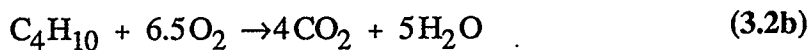
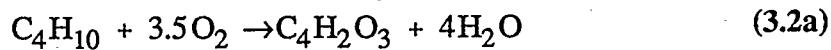
### REACTION KINETICS

#### 3.1 Reaction Kinetics Rate Expressions

Maleic anhydride can be produced from *n*-butane utilizing a Vanadium Phosphorus Oxide (VPO) catalyst. Over the years, several studies have been undertaken to derive kinetic expressions for the partial oxidation and to determine the intermediates formed during the reaction. Escardino et al. (1973) proposed a triangular reaction mechanism whereby *n*-butane formed both maleic anhydride (MAN) and total oxidation products (CO, CO<sub>2</sub>, and H<sub>2</sub>O) in a parallel reaction scheme, and the maleic anhydride subsequently partially decomposed, in a series reaction, to total oxidation products. These series and parallel reaction steps are, respectively:



The chemical equations corresponding to these reaction steps are:



For the *n*-butane feed concentrations employed in the work of Escardino et al. (1973) (less than 1 mol%), the system was well modelled by three pseudo-first order reactions of the form:

$$r_i = k_i p_i \quad (3.3)$$

where  $p_i$  is the partial pressure of the species  $i$  involved in the reaction.

Wohlfahrt and Hoffman (1980) using higher *n*-butane feed concentrations arrived at the following rate equations:

$$-r_B = \frac{k c_B c_O^{0.285}}{1 + K c_B} \quad (3.4)$$

$$r_{MA} = \frac{k c_{MA} c_O^{0.285}}{1 + K c_B} \quad (3.5)$$

where  $(-r_B)$  and  $r_{MA}$  are the rates of butane depletion and maleic anhydride decomposition respectively, and  $c_B$ ,  $c_O$ , and  $c_{MA}$  are the concentrations of *n*-butane, oxygen, and maleic anhydride, respectively.

Experimental results obtained by these authors, however, indicated that the catalyst employed favored the formation of total oxidation products. This resulted in low yields and selectivities of maleic anhydride. Also, their results were for a temperature range of 400 to 500 °C which would further enhance total oxidation.

Centi et al. (1985) determined the reaction kinetics for this partial oxidation for a highly active and selective catalyst and within a temperature range of 300 to 340 °C utilizing a packed bed experimental reactor. The only total oxidation products they observed were CO<sub>2</sub> and water. The kinetic analysis was performed under both differential and integral conditions. For the integral reactor (conversions of 0 to 100%) the differential reactor model showed agreement up to about 60% conversion, when experimental maleic anhydride yield began to decrease. This confirmed the decomposition reaction of maleic anhydride to carbon dioxide at high conversions. Centi et al. (1985) formulated the following rate equations, valid for conversions of 0 to 100%:

$$r_1 = r_{MA} = \frac{k_1 K_B c_B c_O^\alpha}{1 + K_B c_B} \quad (3.6)$$

$$r_2 = r_{CO_2} = k_2 c_O^\beta \quad (3.7)$$

$$r_3 = (-r_{MA}) = k_3 c_{MA} \frac{c_O^\gamma}{c_B} \quad (3.8)$$

where  $r_{MA}$  is the rate of maleic anhydride formation from *n*-butane,  $r_{CO_2}$  is the rate of CO<sub>2</sub> formation from *n*-butane, and  $(-r_{MA})$  is the rate of maleic anhydride decomposition. The decomposition reaction (Equation (3.8)) showed a strong dependence on the ratio of residual oxygen to *n*-butane concentrations.

Centi et al. (1985) also investigated the effect of the reaction temperature on the kinetics,

and reported values of the activation energies for the three reactions. The model of these authors was used in the simulation, thus the kinetic parameters at 300, 320, and 340 °C are summarized in Table 3.1 and the activation energies are reported in Table 3.2.

Buchanan and Sundaresan (1986) found substantial inhibition of the reaction by maleic anhydride and water. These authors arrived at a rate expression of the form

$$r_i = \frac{k_i p_B R_g T}{1 + K_1 \left( \frac{p_B}{p_{O_2}^n} \right) + K_2 \left( \frac{p_{MA}}{p_{O_2}^n} \right)} \quad (3.9)$$

where subscript "i" denotes the three reaction pathways of Equations (3.1) and (3.2), and "n" can be 0.5 or 1.0. Centi et al. (1988) note that the maleic anhydride and water effects are lumped into a single term involving only the maleic anhydride partial pressure ( $p_{MA}$  in denominator of Equation (3.9)).

The most recent studies on the intrinsic kinetics of this reaction have been undertaken by Martin and Emig (1989), Sharma et al. (1991), and Bej and Rao (1991). Martin and Emig (1989) compared the Rideal-Eley model with a mechanistic model developed by the authors. The Rideal-Eley model is of the following form:

$$r_i = \frac{k_i p_B K_{O_2} p_{O_2}}{1 + K_{O_2} p_{O_2} + K_{H_2O} p_{H_2O}} \quad (3.10)$$

The Rideal-Eley model adequately described the experimental *n*-butane conversion and

Temperature (°C)	$k_1 (10^{-7})$ ( $\text{mol}^{1-\alpha} \text{L}^\alpha / \text{g s}$ )	$k_2 (10^{-7})$ ( $\text{mol}^{1-\beta} \text{L}^\beta / \text{g s}$ )	$k_3 (10^{-7})$ ( $\text{mol}^{\delta-\gamma} \text{L}^{1-\delta-\gamma} / \text{gs}$ )
300	3.357	2.001	0.440
320	4.621	4.364	0.606
340	6.230	9.040	0.966

$$K_B = 2616 \text{ mol/L} \quad \alpha = \beta = 0.2298 \quad \gamma = 0.6345 \quad \delta = 1.151$$

**Table 3.1 - Kinetic Parameters for the Oxidation of *n*-Butane to MAN (Centi, 1985).**

Reaction	1	2	3
$E_A$ , (kJ/mol)	45.1	110.0	57.4

**Table 3.2 - Activation Energies (Centi, 1985)**

product selectivities, while the mechanistic model did not. Sharma et al. (1991) studied the kinetics for a temperature range of 300 to 380 °C and *n*-butane feed concentrations up to 3 mol%. The rate equations were modelled by power law kinetics and included an inhibition term due to product adsorption. The rate equations proposed were:

$$r_1 = r_{MA} = \frac{k_1 p_B^{\alpha 1}}{(1 + K_2 p_{MA})} \quad (3.11)$$

$$r_3 = (-r_{MA}) = \frac{k_3 p_{MA}}{(1 + K_2 p_{MA})^2} \quad (3.12)$$

$$r_2 = r_{CO_2} = k_2 p_B^{\alpha 2} \quad (3.13)$$

where  $r_{MA}$ ,  $r_{CO_2}$ , and  $(-r_{MA})$  have the same meaning as in Equations (3.6) to (3.8). Based on the proposed reaction scheme, the rates of reaction are independent of oxygen concentration. The kinetic model predicts reactant and product distributions very well. However, the experimental results indicate that the formation of total oxidation products is favored. Presumably, the catalyst employed is not very selective toward maleic anhydride. Bej and Rao (1991) investigated the possibility of modelling the reaction as either based on a Langmuir-Hinshelwood model or on a Redox model at the catalyst surface. The Redox model employed gave the following expression for the total rate of *n*-butane consumption:

where  $\alpha$  is the moles of oxygen required to convert one mole of *n*-butane to maleic anhydride. Four different forms of the Langmuir-Hinshelwood model were employed

$$(-r_B) = \frac{k_1 k_2 P_B P_{O_2}^n}{k_1 P_{O_2}^n + \infty k_2 P_B} \quad (3.14)$$

depending on the assumptions of the affinity of the active sites for butane and oxygen.

They investigated a temperature range of 420 to 440 °C and a maximum concentration of 2.5 mol% *n*-butane in the feed. The results are for differential reactor conditions corresponding to less than 10% conversion. Their studies indicate selectivities to MAN of 80 to 90% and MAN yields of 5 to 8% depending on the magnitude of the conversion. They also found that a Redox model with a zero-order dependence on oxygen concentration ( $n = 0$  in Equation (3.14)) best fit the experimental data. Unfortunately, the final kinetic rate expression presented in Equation (3.14) is for the total rate of *n*-butane depletion rather than for the separate expressions for the parallel and series reaction schemes.

### 3.2 Role of the VPO Catalyst

The Vanadium Phosphorus Oxide (VPO) is characterized by a number of crystalline phases. The transformation of these phases during the oxidation is a function of the reactant concentrations, the reaction temperature, and the time on stream (Centi et al., 1988). The activity and selectivity of the VPO catalyst are most often attributed in the literature to the presence of the orthophosphate ( $VOPO_4$ ) and the vanadyl pyrophosphate ( $(VO)_2P_2O_7$ ) crystalline phases. The oxidation state of the vanadium in the

orthophosphate phase is  $V^{+5}$ , while the oxidation state in the pyrophosphate phase is  $V^{+4}$ . The vanadium present in the catalyst is the main oxygen carrier, and during the reaction with the hydrocarbon, the orthophosphate phases are transformed, via a reduction process, to the pyrophosphate phases. This is written in terms of the valence change as  $V^{+5} \leftrightarrow V^{+4}$ . Contractor (1988), found the average oxidation state of the catalyst to be about 4.1, with the difference in the average valence between the oxidized and reduced state of the catalyst to be 0.2. This result indicates that most of the active catalyst exists in the  $V^{+4}$  oxidation state, and that the surface of the catalyst provides most of the oxygen needed for the reaction.

With most of the oxygen required for the reaction provided by the catalyst surface, it is possible to operate the reactor in the absence of or with minimal concentrations of gas phase oxygen. In the process described by Contractor (1988), oxygen was not fed to the riser zone. Results indicated that the reactor could be successfully operated for several thousand catalyst reduction/regeneration cycles in the absence of gas phase oxygen while obtaining selectivities of approximately 75%, constant up to 50% *n*-butane conversions, and decreasing to about 60% at 90% conversion. Due to the absence of oxygen in the feed, very high *n*-butane concentrations were attainable. Contractor (1988) investigated the effect of up to 50 mol% *n*-butane feed concentrations on conversion. The increased concentrations resulted in high initial reaction rates, but rapid depletion of the available surface oxygen. Thus a maximum conversion was observed corresponding to 20 mol% *n*-butane in the feed stream, and any further increase in concentration did not result in any

further conversion. The residence times of solids in these experiments was in the range of two to four seconds, so that even though the surface oxygen was depleted, there was no time for significant buildup of reduced layers on the catalyst surface. For that reason, it was possible to increase both conversion and selectivity by operating the riser with oxygen in the feed. Contractor (1988) found that 6 mol% oxygen in the feed increased conversion 4%, while selectivity remained unchanged. A feed of 16 mol% oxygen increased conversion 6%, however selectivity decreased measurably. The presence of highly active oxygen species on the catalyst surface having no significant buildup of reduced layers was presumed to be the reason for the selectivity losses at higher oxygen feed concentrations. Contractor (1988) found that the presence of these oxygen species could be controlled and high selectivities re-established by stripping the regenerated catalyst before it entered the riser reactor zone. Selectivities of 90% are reported for operation with the stripped catalyst and gas phase oxygen addition. The CFB reactor lends itself well to this style of operation because of the ability for secondary reagent injection.

The results of the kinetic studies presented in section 3.1 may be explained based on the structure of the catalyst (Centi et al., 1988). The catalytic behavior will be different for fresh and equilibrated catalysts. The kinetic model of Centi et al. (1985) is indicative of a fresh catalyst possessing large amounts of surface oxygen and readily forming the  $(VO)_2P_2O_7$  crystalline phase. At higher than 80% conversion, the maleic anhydride begins to decompose, and this decomposition is found to correspond to an increase in the ratio of residual concentration of oxygen to *n*-butane. The fresh catalyst surface becomes over-

oxidized and the maleic anhydride is unstable. For the case of the equilibrated catalyst, the maleic anhydride formed is stable for conversions up to more than 95%, and the ratio of hydrocarbon to oxygen has little effect on the catalyst behavior. This explains why the model of Buchanan and Sundaresan (1986) has a parameter "n" which can take values of 0.5 or 1.0 without affecting the fit to the data, and the models of Sharma, et. al. (1991) and Bej and Rao (1991) have a zero order dependence on oxygen. The work of these authors employed an equilibrated catalyst.

### 3.3 Kinetics of Catalyst Deactivation

The activity of the Vanadium Phosphorus Oxide (VPO) catalyst has been found to decrease rapidly as the partial oxidation reaction proceeds. Smith (1981) developed a simple model in which catalyst deactivation is assumed to occur by blocking of the active sites and the rate of a desired chemical reaction becomes proportional to the number of sites still unblocked. If  $q(t)$  corresponds to the number of blocked sites at time  $t$ , and  $q_0$  to the number of blocked sites corresponding to total deactivation, with the rate of reaction proportional to the number of still active sites, the rate of maleic anhydride formation, for example, becomes

$$r_{MA}(t) = r_{MA} \left(1 - \frac{q(t)}{q_0}\right) = r_{MA} (1 - \phi(t)) \quad (3.15)$$

The rate of deactivation depends on how  $\phi(t)$  varies with time. The reduction of VPO catalyst due to reaction is an example of parallel deactivation, where the reactants form

products and at the same time deactivate the catalyst. Smith (1981) modelled this deactivation as a first order reaction at the catalyst surface. Thus the rate of deactivation may be written as:

$$r_d = q_0 \frac{d\phi(t)}{dt} = k_d c_B (1 - \phi(t)) \quad (3.16)$$

Upon integration, Equation (3.16) gives

$$1 - \phi(t) = \exp\left[-\left(\frac{k_d}{q_0} c_B\right)t\right] = \exp[-at] \quad (3.17)$$

Substitution of Equation (3.17) into Equation (3.15) provides the expression for the rate of reaction incorporating catalyst deactivation:

$$r_{MA}(t) = r_{MA} \exp[-at] \quad (3.18)$$

The severity of catalyst deactivation is characterized by the value of the parameter "a". Relatively larger values of "a" will result in rapid deactivation, and if  $a = 0$ , no deactivation is occurring.

## CHAPTER 4

### COMPUTER SIMULATION

The computer simulation, written in UNIX:C language, combines the predictive hydrodynamic model with reaction kinetics to provide a comprehensive model of the Circulating Fluidized Bed reactor performance.

#### 4.1 Isothermal Operation and Reactor Energy Balance

As stated in section 1.2, the near perfect mixing and high heat transfer coefficients which can be typically obtained in CFBs, result in near isothermal operating conditions in the riser. The review by Grace (1990) reports the temperature in the riser and standpipe of the CFB combustor shown in Figure 4.1 and temperature fluctuations of no greater than 20 °C are seen. From a practical engineering point of view, this reactor is indeed operating under isothermal conditions. The exothermicity of the oxidation of *n*-butane very large. Kunii and Levenspiel (1991) reported a value for the heat of reaction of 1420 kJ/mol. This is more than three times that of coal combustion. Despite the large values of the heat of reaction, Contractor (1987) reported a complete elimination of hot spots in the riser of a CFB catalytic reactor for maleic anhydride production. In this work, the CFB catalytic reactor is thus modelled as an isothermal reactor.

The assumption of isothermal operation is supported by the solution of the reactor energy

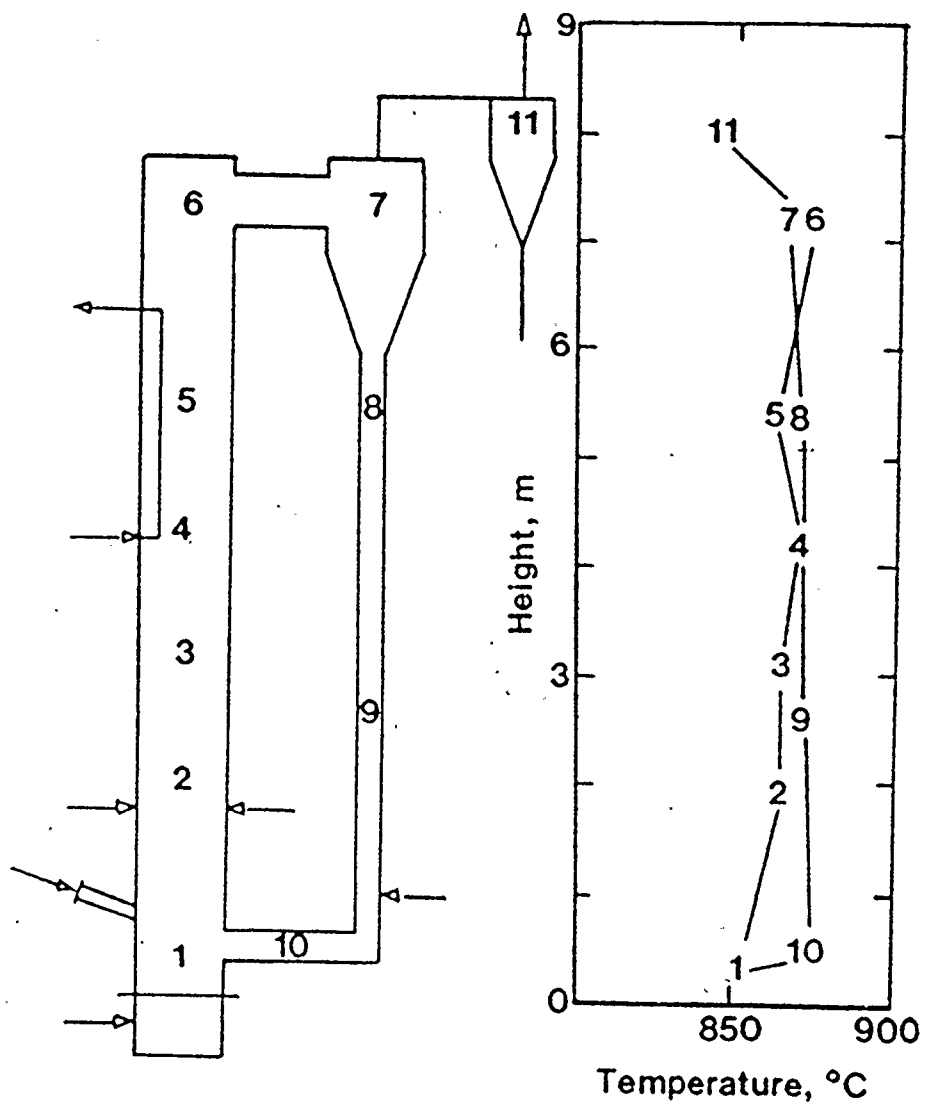


**Figure 4.1 - Temperature Profile of a Circulating Fluidized Bed Combustor (Grace, 1990)**

balance. The reactor operates non-adiabatically with heat removed at the reactor wall. Therefore, at steady state, the heat flowing into a volume element of the reactor plus the heat generated due to the reaction is equal to the heat removed at the wall. This is formulated as:

$$h_w(T_w - T)dA_w = F_t C_p dT + \sum_{i=1}^3 \Delta H_{Ri}(r_i dV) \quad (4.1)$$

where  $\Delta H_{Ri}$  is the heat of reaction for reaction  $r_i$  ( $i=1,2,3$ ),  $h_w$  is the solids to wall heat transfer coefficient, and  $T_w$  is the temperature of the cooling water in the membrane walls. A constant heat transfer coefficient of  $150 \text{ W/m}^2 \text{ K}$  is assumed, and the temperature of the cooling water is chosen as constant at  $30 \text{ }^\circ\text{C}$ .

## 4.2 Core and Annulus Mass Balances

The partial oxidation of *n*-butane to maleic anhydride is assumed to occur in both the core and the annulus, the proportion of which is dependent on the local solid catalyst concentration, as calculated by the hydrodynamic model. The simulation of the reaction requires solution of the mass balance for each species,  $i$ , reacted or formed. In the core region, where the gas is flowing, the steady state mass balance includes a net convective input term plus the reaction term which is equal to the gas crossflow to the annulus. The reaction term,  $r_i$  in Equations (4.2) and (4.3) below, is positive for products formed and negative for reactants consumed. The core mass balance is written as follows (Patience, 1990):

$$-\frac{\partial}{\partial x}(V_g c_{i,c}) + \rho_p(1 - \varepsilon_c)r_i - \frac{2k_g}{r_c}(c_{i,c} - c_{i,a}) = 0 \quad (4.2)$$

In the annular region, there is no convective input term. The gas input to the annulus is due to crossflow from the core. The annular region mass balance is thus

$$\rho_p(1 - \varepsilon_{ann})r_i + \frac{2k_g r_c}{(R^2 - r_c^2)}(c_{i,c} - c_{i,a}) = 0 \quad (4.3)$$

The units of the rate of reaction term,  $r_i$ , in Equations (4.2) and (4.3) are mol/g<sub>cat</sub>·s. In order to incorporate the reaction rate expression into the mass balance equations, the pseudo-homogeneous system was assumed. Such a reactor assumes no concentration gradients within a volume element, which is valid for reactions which are kinetically controlled. The half life of this reaction was estimated assuming that the reaction occurs in a constant volume batch reactor. This calculation results in a half life of approximately 50 ms, indicative of an extremely fast reaction which would not normally be kinetically controlled. However, for a mean particle diameter of 75 μm, typical of the VPO catalyst used in the reactor, the Thiele modulus is of the order of 10<sup>-2</sup> and the effectiveness factor is one. Thus, intraparticle resistance is negligible. Furthermore, the high slip velocities typical of circulating fluidized bed operation result in excellent mass transfer between the gas phase and the catalyst surface. Figure 4.2 indicates, in a qualitative manner, that the slip velocity is at a maximum in the circulating fluidized bed regime. Therefore, mass

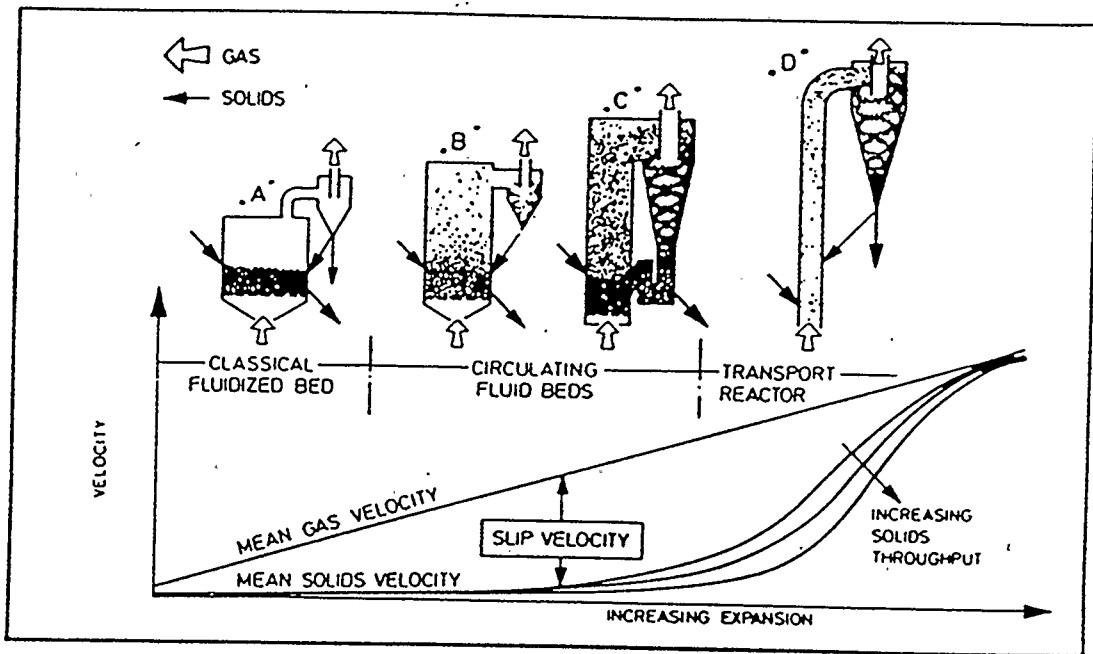


Figure 4.2 - Slip Velocity for Different Reactor Systems

transfer or interparticle resistance will also be negligible. The negligible intraparticle and interparticle resistances indicate the reaction is kinetically controlled even though it is very fast, and thus the pseudo-homogeneous assumption is valid for the reactor.

### 4.3 Simulation Conditions

The simulation makes use of the predictive hydrodynamic model of Wong (1991) to obtain the average axial voidage profile in an arbitrarily chosen 20 meter high, 30 centimeter diameter column having a smooth exit to the cyclone. Simulation of a CFB reactor having an abrupt exit to the cyclone was not considered in this work because of the current narrow range of applicability of the empirical formula used in the hydrodynamic model for estimating the voidage at the top of the riser. Also, as discussed in section 2.4.3, internal recirculation of solids due to an abrupt exit geometry leads to an increased solids holdup and can significantly increase the solids residence time. The internal recirculation and increased residence time of solids will have a detrimental effect on reactor performance if the solids are deactivated catalyst particles. Figure 1.2 indicated a smooth elbow configuration connecting the riser exit to the cyclone. The column was investigated for solids fluxes ranging from 400 to 800 kg/m<sup>2</sup>-s and superficial gas velocities ranging from 4 to 6 m/s. Butane in air mixtures of 1, 5, 20, and 50 mol% were employed to establish the effect of feed concentration on reactor performance. The assumed physical properties of the solid VPO catalyst are summarized in Table 4.1. The temperature range investigated in the simulation is 300 to 350 °C. The riser reactor is

Solids Property	
Mean Particle Diameter, $\mu\text{m}$	75
Particle Density, $\text{kg/m}^3$	1500
Bulk Density, $\text{kg/m}^3$	630
Voidage @ Minimum Fluidization	0.50
Velocity @ Minimum Fluidization, m/s	0.0029
Particle Terminal Velocity, m/s	0.05

**Table 4.1 - Assumed Physical Properties of VPO Catalyst**

assumed to operate at atmospheric pressure, so that the gas behaves ideally. The temperature dependence of the gas density is then obtained through the molar volume. A linear dependence of gas viscosity is assumed over the small temperature range investigated.

The current limitation of the simulation is the kinetic model used. The kinetics of Centi et al. (1985) (Equations (3.6) to (3.8)) have been selected for use in this work. The catalyst used by these authors, unlike many other studies, is very selective toward the desired maleic anhydride. Also, since the simulation presently considers only the riser section and not the re-injection of regenerated solids from the standpipe, the results of Centi et al. (1985) for fresh catalyst are more suitable than the results of other authors using equilibrated catalyst. However, the major drawback of Centi et al. (1985) and all other kinetic models available in the literature is that they were developed using fixed bed reactor technology. This was a natural development because until recently, maleic anhydride production in a fixed bed reactor had been the technology of choice. The reaction rate expressions for the catalyst used in a CFB riser reactor are expected to be radically different. Catalysts used in fixed bed operation have limited activity to avoid hot spot formation during rapid reaction at the reactor inlet. Since the excellent mixing and large heat transfer coefficients in CFBs eliminate hot spots, a much more active catalyst is employed. Intrinsic reaction rate expressions developed for the less active fixed bed reactor catalyst will not be able to accurately predict the CFB reactor performance. Appreciably higher *n*-butane conversions, and maleic anhydride yields and selectivities

are expected in the CFB due to the active catalyst employed. Also, Contractor (1987) reports the use of a highly attrition resistant catalyst to which colloidal silica has been added before spray drying. Presumably, this will also change the reaction kinetics from those of a fixed bed catalyst. Furthermore, the catalyst in a CFB riser reactor experiences rapid cycles of reduction and oxidation in the riser and standpipe, respectively, and perhaps stripping of non-selective surface oxygen species before re-injection to the riser. Matros (1985) indicated that, depending on the reaction mechanism, cyclical operation may enhance the overall reaction rate. Lang et al. (1989) studied the effect of feed composition cycling on maleic anhydride production from butadiene on a Te-promoted vanadia molybdate catalyst. These conditions were much more representative of CFB operation than previous works. In one such experiment, a reactant stream of 0.8 mol% butadiene in nitrogen was introduced, followed by a 100 mol% nitrogen pulse, and finally an 80 mol% nitrogen-20 mol% oxygen mixture. These pulses were all of equal duration. This experiment was equivalent to operation in a CFB catalytic reactor where reactants are fed to the riser in the absence of gas phase oxygen, products are desorbed and separated, and oxygen is introduced in the regeneration step. Lang et al. (1989) found selectivity increased from 50% under steady state operation to 54% during the cyclical operation. Lang et al. (1989) acknowledged that selectivities could potentially be further increased by using different catalyst and reactants to obtain better agreement with the selectivity data reported by Contractor (1988).

#### 4.4 Solution of Mathematical Model

The riser height of 20 meters is divided into 100 equal elements of 20 centimeters each. The length of the acceleration zone is calculated, and the hydrodynamic model is invoked (Wong, 1991) to obtain the average axial voidage profile. From the Berruti-Kalogerakis model, the core voidage and core radius are obtained for each element. For a given inlet concentration of reactants to the first volume element, the reaction rates may be calculated from Equations (3.6) to (3.8) using the kinetic data of Table 3.1. From the stoichiometry of the chemical reactions (3.1) and (3.2), the rates of water formation and oxygen depletion are calculated. It should be noted that since the majority of gas flows in the core region, the reactant concentration in the annular region in the first element is taken to be zero. This sets up the concentration gradient required for the mass transfer of gas from the core to the annulus.

Taking the gas velocity in the core ( $V_g$  in Equation (4.2)) as constant with height within each of the small elements, then the axial concentration gradient of species "i" in the element,  $\partial c_i / \partial x$ , may be determined. If the partial derivative is put in discrete form, and with the inlet concentrations to the first element known, the outlet concentration of species "i" from each element may be found. This concentration becomes the input to the next element where the mass balances of Equations (4.2) and (4.3) are performed again. These results then become the input to the next element, and the procedure is continued to the reactor exit.

By keeping track of the molar flows of each species reacted or formed, the moles of gas generated by the reaction will be known. This is converted to a volumetric flow of gas via the molar volume at reaction conditions. In this way, the increase in gas velocity in the riser due to gas generation may be calculated and the hydrodynamic model updated at the end of each interval, in order to evaluate the new flow structure corresponding to increasing values of the gas superficial velocity.

The *n*-butane conversion, yields of maleic anhydride and CO<sub>2</sub>, and maleic anhydride selectivity are calculated at each 20 centimeter interval. The conversion, X, is defined as:

$$X = \frac{\text{moles of butane converted}}{\text{moles of butane fed}} \quad (4.4)$$

Maleic anhydride selectivity, S, is defined here as:

$$S = \frac{\text{moles maleic anhydride formed}}{\text{moles of butane converted}} \quad (4.5)$$

Finally, the yield of maleic anhydride, Y<sub>MA</sub>, is defined as:

$$Y_{MA} = \frac{\text{moles of maleic anhydride formed}}{\text{moles of butane fed}} = SX \quad (4.6)$$

and the yield of carbon dioxide, Y<sub>CO<sub>2</sub></sub>, as:

$$Y_{CO_2} = \frac{\text{moles of CO}_2 \text{ formed}}{\text{moles of butane fed}} \quad (4.7)$$

## CHAPTER 5

### SIMULATION RESULTS AND DISCUSSION

Using the computer simulation described in the previous chapter, the performance of the Circulating Fluidized Bed catalytic reactor for maleic anhydride production from the partial oxidation of *n*-butane was evaluated corresponding to various operating conditions. This evaluation involved examination of the conversion of *n*-butane, product yields and selectivities. A mixture of *n*-butane in air can form a potentially explosive mixture. For this reason, the experiments of Sharma et al. (1991) used *n*-butane concentrations of less than 3 mol%. However, as indicated by Contractor et al. (1988), the reaction in a CFB may be carried out in the absence of gas phase oxygen, allowing higher *n*-butane concentrations. The simulation was performed for various *n*-butane concentrations up to 50 mol%. The effects of different inlet superficial gas velocities and solids circulation rates on reactor performance were considered. Also, the respective influences of catalyst deactivation kinetics and reaction temperature were studied. Results from these numerous trials are presented graphically and discussed in this chapter.

#### 5.1 Effect of Feed Concentration on CFB Reactor Performance

The conversion of *n*-butane along the riser length for various *n*-butane inlet feed concentrations is shown in Figure 5.1. The *n*-butane conversion was found to decrease

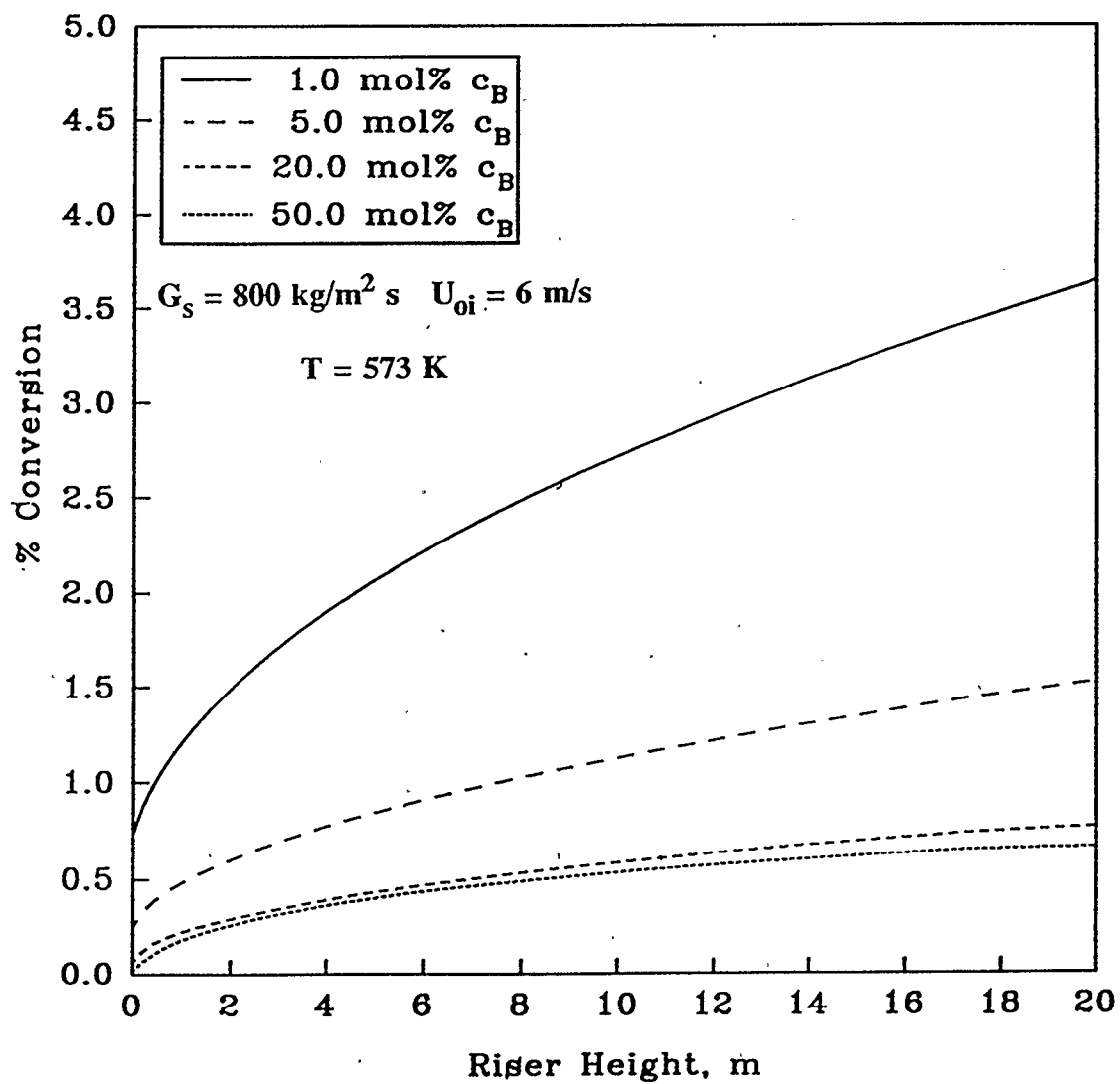


Figure 5.1 - Single Pass Butane Conversion for Various Butane in Air Mixtures

with increasing *n*-butane concentration in the feed. For a mixture of 1 mol% *n*-butane in air, conversions of 3.5% are realized, while they drop to 0.5% or less for more concentrated feed streams. Figure 5.1 indicates that a limit is reached whereby an increase in the *n*-butane concentration in the feed has only a marginal effect on the conversion. In Figure 5.2, the *n*-butane conversion at the riser exit is plotted as a function of the inlet feed concentration. A sharp drop in the conversion is seen in the 5 to 10 mol% range. For an *n*-butane feed concentration greater than approximately 25 mol%, conversion is essentially unchanged, but a greater gas recycle capacity will be required and, therefore, gains from such operation would be minimal.

The effect of *n*-butane concentration may be explained by a closer examination of the kinetic model of Centi et al. (1985). When discussing the consumption of *n*-butane, it is necessary to look at the parallel reactions described by Equations (3.1) and (3.2). The rate expression for the formation of maleic anhydride from *n*-butane exhibits a first order dependence on *n*-butane concentration in the numerator, and an inhibition term in the denominator. The kinetic expression for the complete oxidation of *n*-butane to CO<sub>2</sub> has a weak dependence on the oxygen concentration only. Figure 5.3 presents the rate of *n*-butane consumption to form both maleic anhydride and CO<sub>2</sub>. This is the total rate of reaction occurring in both the core and annular regions, the proportion of each determined by the solids holdup predicted from the hydrodynamic model. Although the *n*-butane concentration increases by a factor of 20, the reaction rate for 20 mol% *n*-butane is only 1.5 times the reaction rate at 1 mol%. The increase in reaction rate is lessened by the

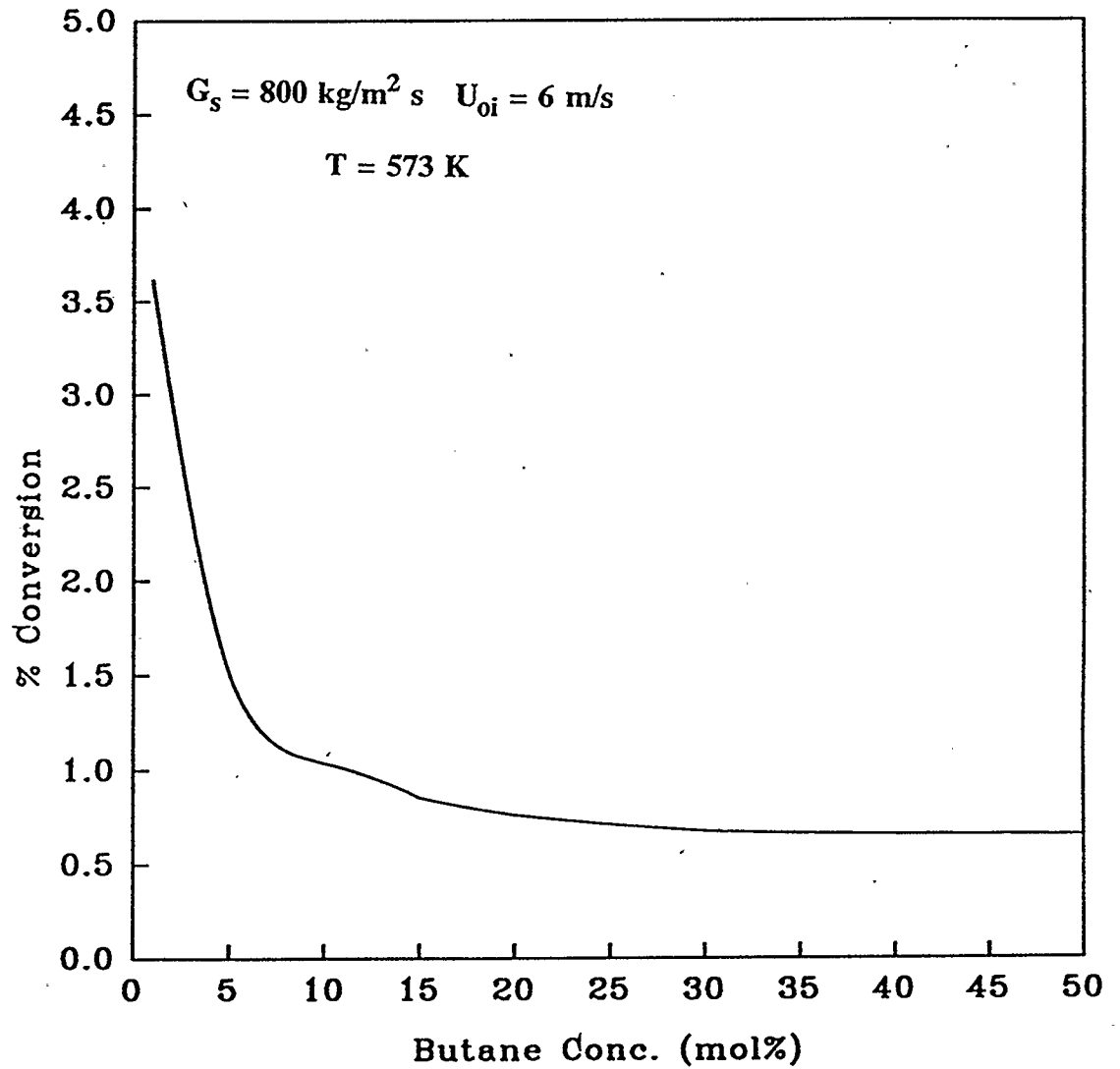


Figure 5.2 - Variation of Butane Conversion with Butane Feed Concentration

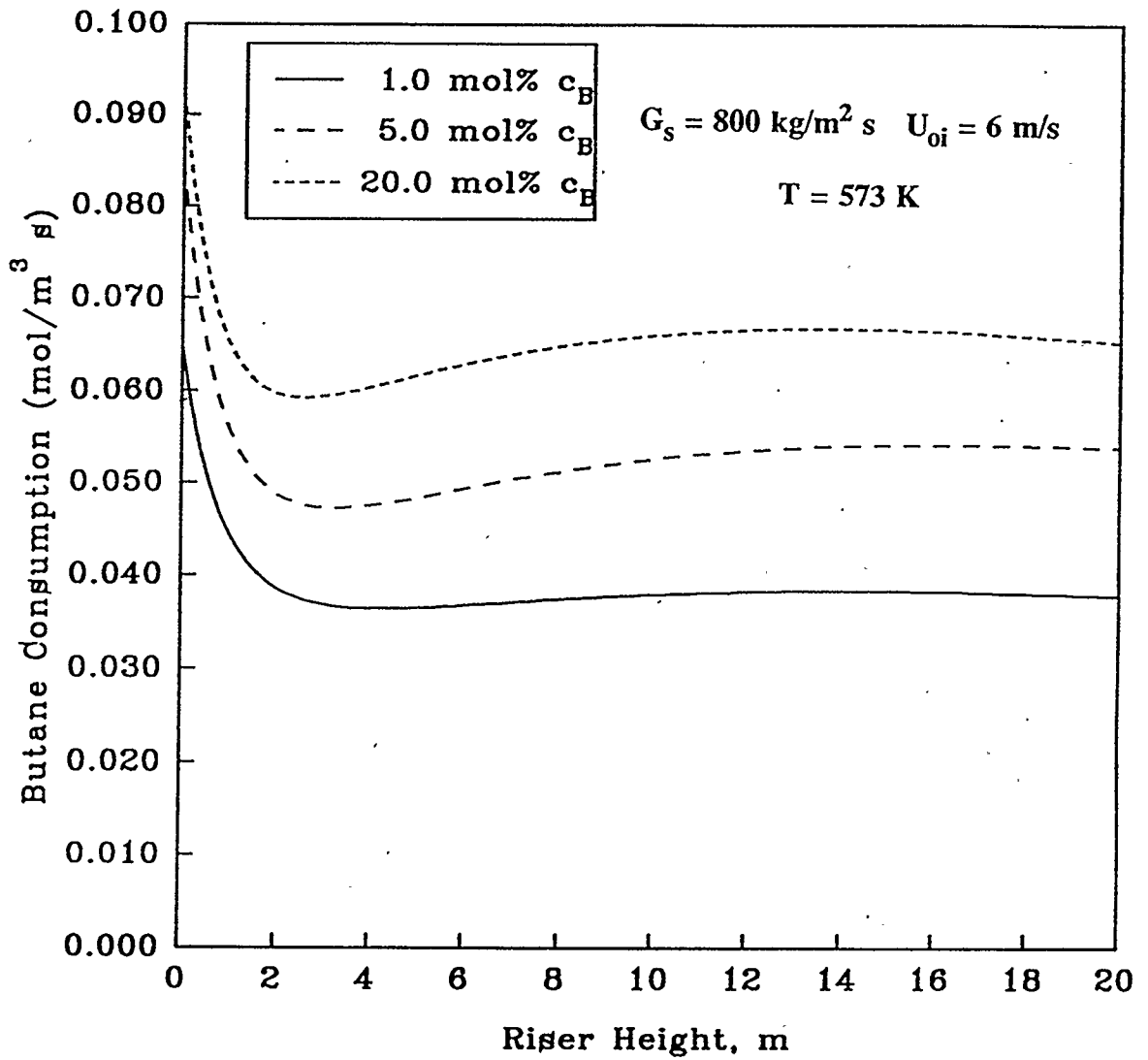


Figure 5.3 - Total Butane Reaction Rate for Various Butane in Air Mixtures

inhibition term in the denominator of the rate expression for the formation of maleic anhydride represented by Equation (3.6). In Figure 5.4, the rate of  $\text{CO}_2$  formation from *n*-butane is plotted along the riser length. As the concentration of *n*-butane is increased in the air/butane mixture, the concentration of oxygen must decrease. Therefore, the rate of  $\text{CO}_2$  formation must decrease. However, due to the weak dependence on oxygen in Equation (3.7), this decrease is very slight. Conversion is defined in the simulation as the moles of *n*-butane converted per mole of *n*-butane fed. For an increase in *n*-butane in the feed, the rate of reaction does not increase as much accordingly, and thus the overall conversion is decreased. Since the decrease in the rate of  $\text{CO}_2$  formation is insignificant, it is primarily the effect of the inhibition term that leads to this result.

With the competing series and parallel reactions, the conversion includes formation of both desired and undesired products. Figures 5.5 and 5.6 compare the yields of maleic anhydride and  $\text{CO}_2$  along the riser length for two different air/butane mixtures. Figure 5.5 indicates that for 1 mol% *n*-butane in the feed, the yield of  $\text{CO}_2$  is actually greater than the yield of maleic anhydride. When the feed concentration is increased to 5 mol% as shown in Figure 5.6, the yields of both maleic anhydride and  $\text{CO}_2$  decrease, but the yield of the desired product, maleic anhydride, is now greater than the yield of  $\text{CO}_2$ . This is obviously a more profitable situation. These results indicate that although higher conversions are attained at relatively lower feed concentrations of *n*-butane, such an operating condition is not advantageous as the  $\text{CO}_2$  yield exceeds that of the maleic anhydride. The ability to operate a CFB reactor in the absence of gas phase oxygen now

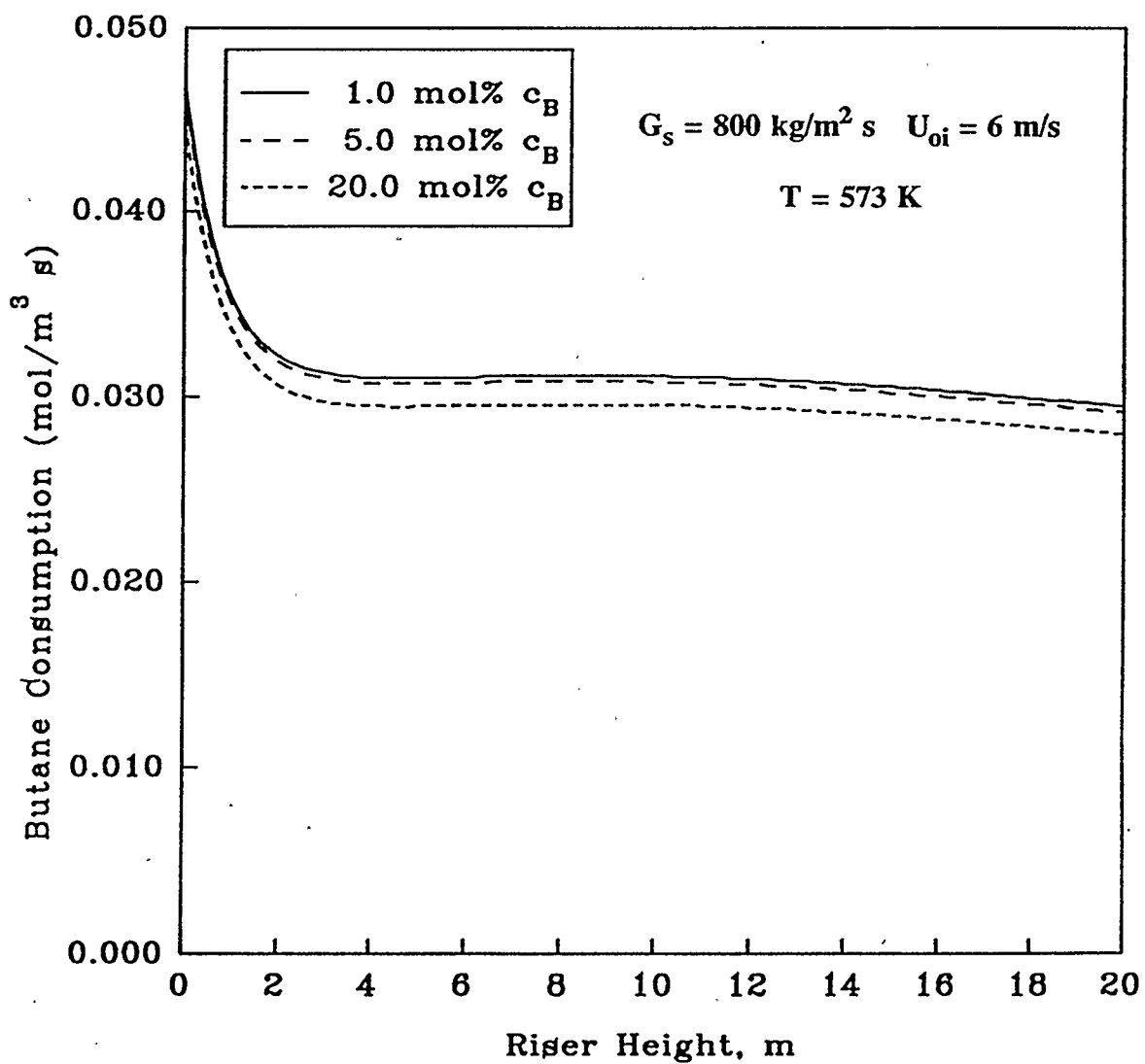


Figure 5.4 - Butane Reaction Rate to  $\text{CO}_2$  for Various Butane in Air Mixtures

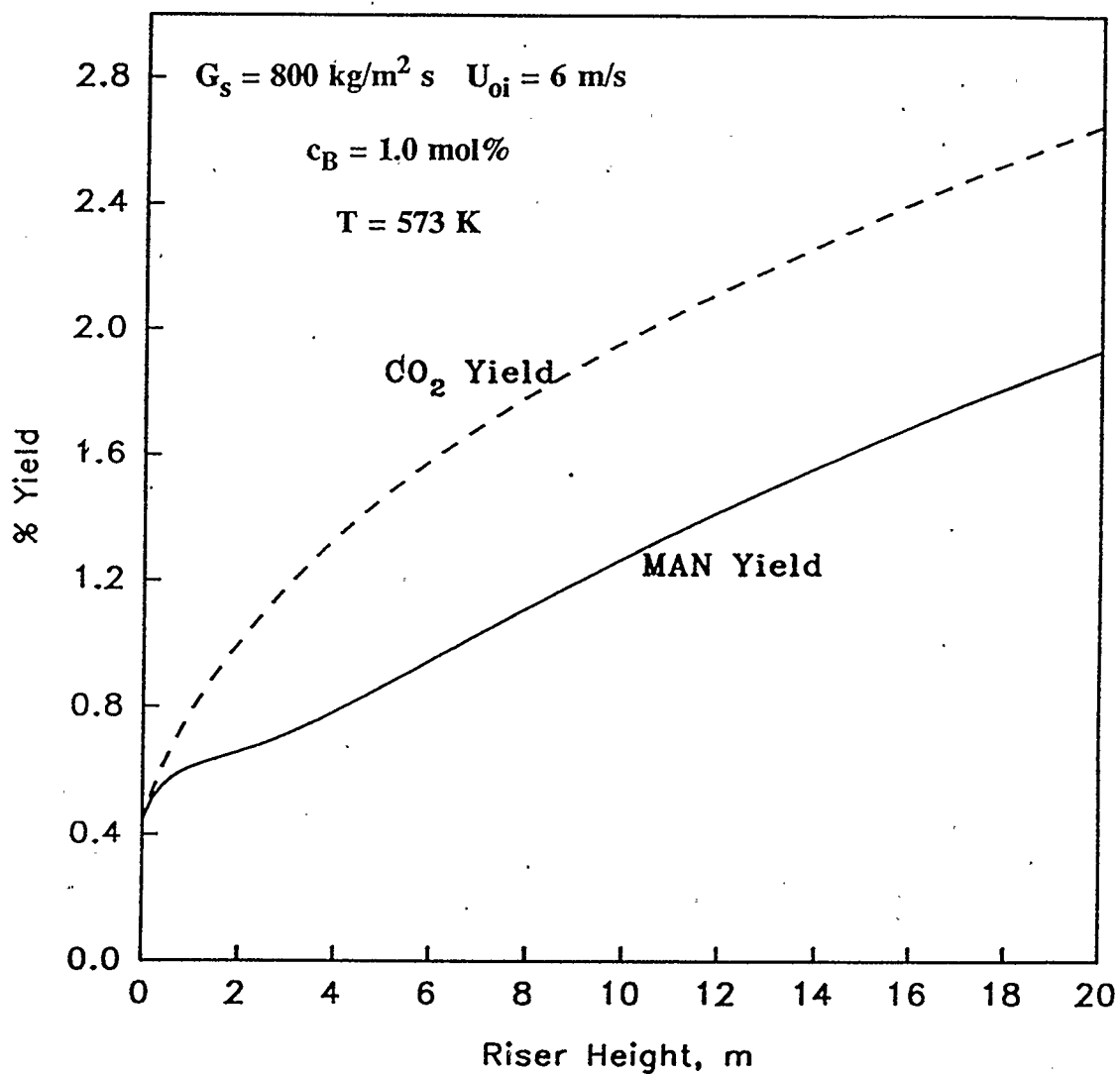


Figure 5.5 - Single Pass Product Yields for  
1 mol% Butane in Air Mixture

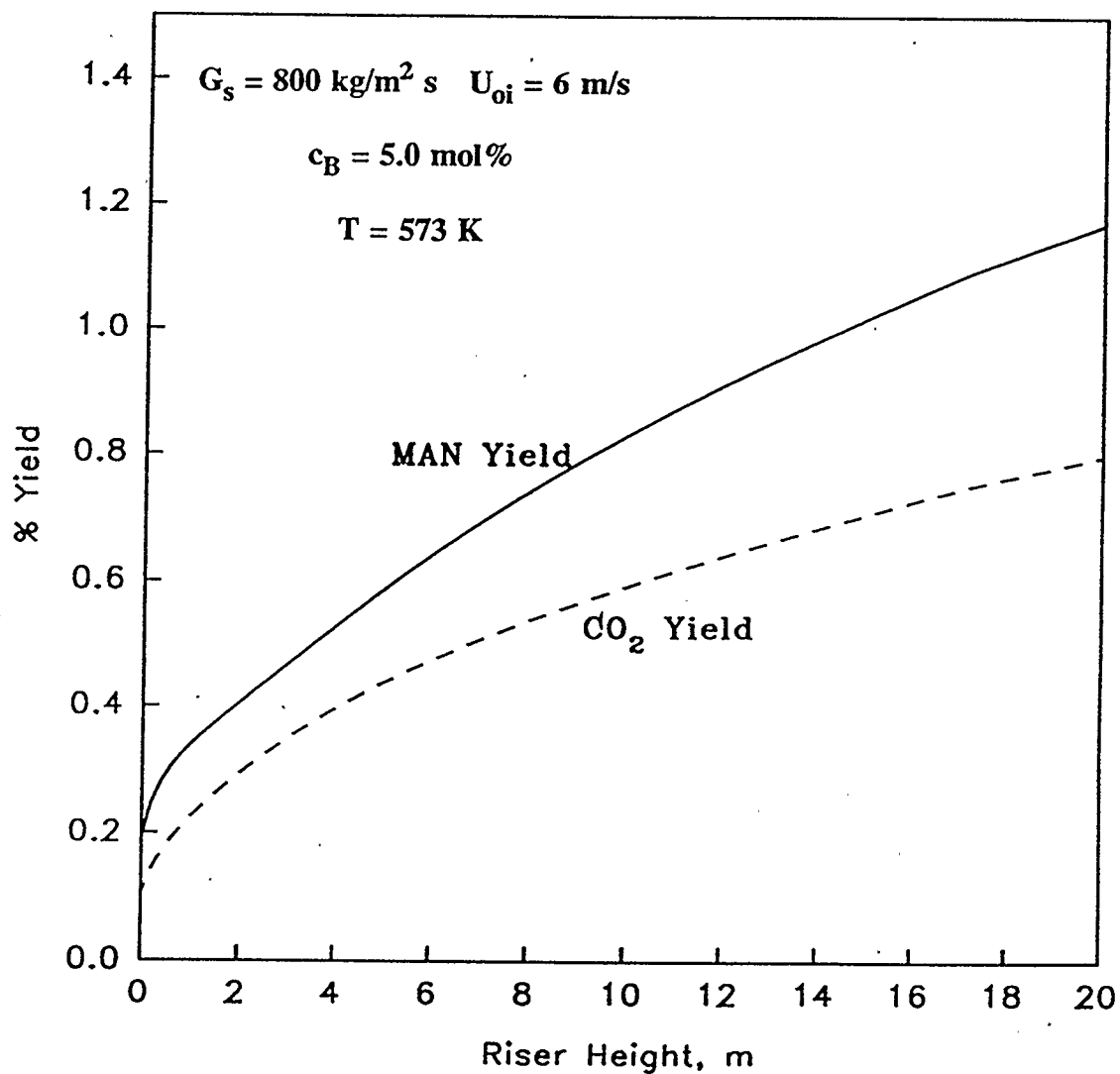


Figure 5.6 - Single Pass Product Yields for  
5 mol% Butane in Air Mixture

becomes important, as the resulting higher *n*-butane concentrations will result in improved yields of maleic anhydride.

Figure 5.7 shows the selectivity to maleic anhydride (MAN) along the riser defined in this work as the moles of MAN produced per mole of *n*-butane converted. Lower concentrations of *n*-butane in the feed result in lower selectivity. At concentrations of 20 mol% or greater, selectivities of 80% are realized. Experimental graphical data at 360 °C presented by Contractor, et. al. (1988) indicate selectivities of 75% to 80% for *n*-butane concentrations in the range of 12 to 50%. Thus the results of this work at 300 °C agree favorably with that data. The initial drop in selectivity seen at the lower concentrations in Figure 5.7 may be attributed to the relatively greater initial oxygen concentration in the feed. For a 1 mol% *n*-butane concentration in an air/butane mixture, the corresponding oxygen concentration is 20.8 mol%. Therefore, the initial reaction rate for CO<sub>2</sub> formation is favored, and a drop in selectivity is observed. For 20 mol% *n*-butane in the feed, the initial oxygen concentration is 16.8 mol% and a flatter selectivity profile is seen. Once again, the advantage of operating the CFB reactor in the absence of gas phase oxygen and increased *n*-butane concentrations is reinforced as the higher feed concentrations result in significantly improved selectivities. These selectivity results agree with the previous results of the product yields. Low yields at low *n*-butane concentrations correspond to low maleic anhydride selectivities.

Though the conversions and yields are very small, throughput from CFB reactors is very

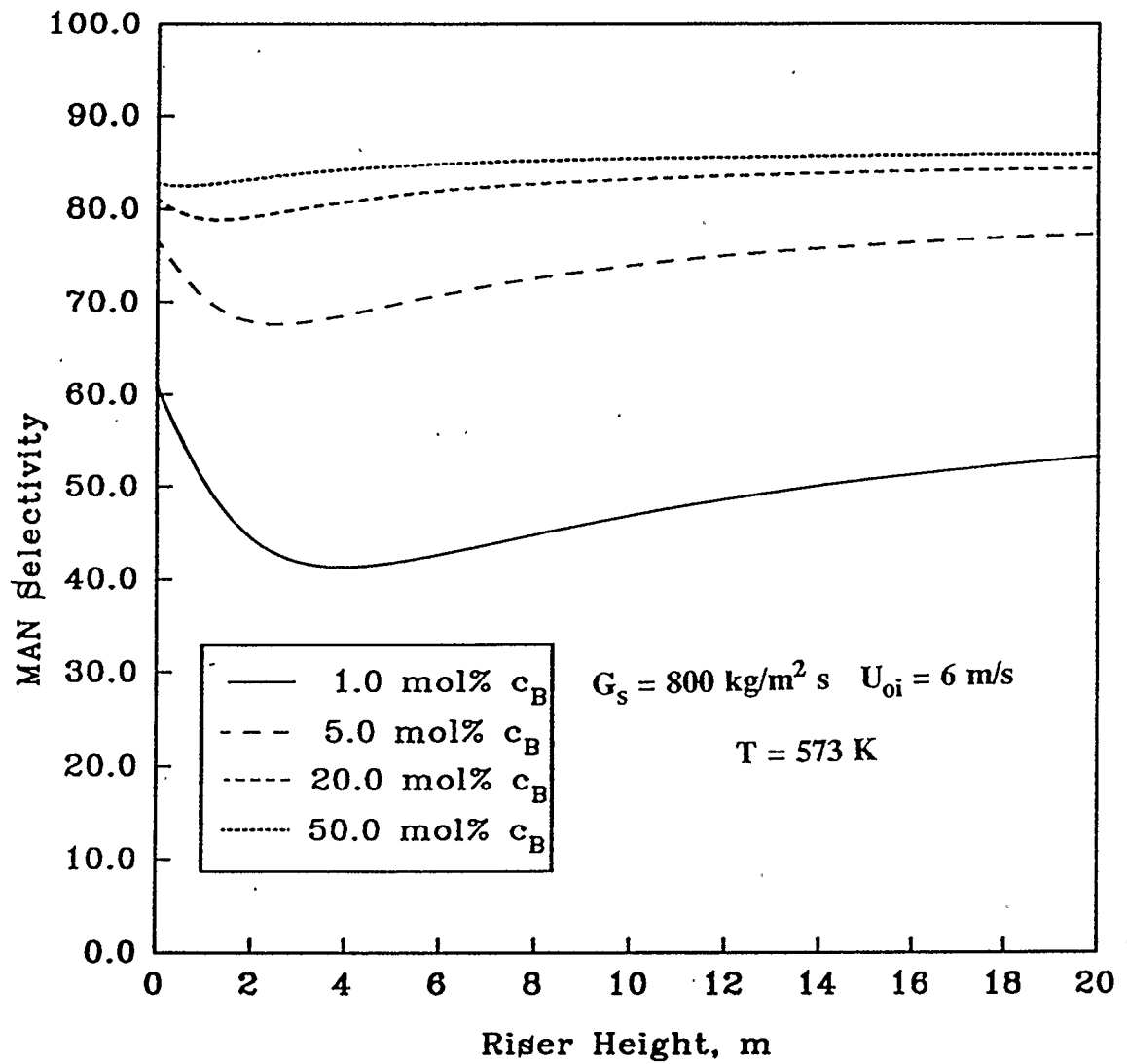


Figure 5.7 - Maleic Anhydride Selectivity for Various Butane in Air Mixtures

large and maleic anhydride production can be significantly higher than that from a fixed bed operation. As mentioned previously in section 4.3, the kinetics of Centi et al. (1985) are based on fixed bed technology. Kinetics based on CFB operation would possibly yield higher conversions due to the reduced gas phase oxygen and increased catalyst activity. Furthermore, there is the potential for enhanced reaction rates due to the cyclic operation between the riser and the regenerator (Matros, 1985, Lang et al., 1989). Centi (1991) states that the productivity of this reaction is, in fact, small. Ordinarily, one kilogram of catalyst is required to produce one gram of maleic anhydride. Contractor et al. (1988) indicate that it is possible to convert a maximum of two grams of *n*-butane for every kilogram of catalyst in a CFB reactor. Contractor et al. (1988) also state that it is possible to improve this conversion by addition of small amounts of gas phase oxygen in the riser. The potential for secondary air injection along the CFB riser would be valuable for this purpose.

## 5.2 Effect of CFB Operating Conditions on Reactor Performance

The use of the predictive hydrodynamic model in this simulation allows the effect of operating parameters such as solids circulation rate and superficial gas velocity to be carefully studied. These variables will affect the local solids catalyst holdup in the riser and hence the conversions and yields.

The *n*-butane conversion for solids circulation rates of 400, 600, and 800 kg/m<sup>2</sup>-s is

presented along with the corresponding actual solids holdup for each circulation rate in Figure 5.8. The inlet gas superficial velocity is maintained at 6 m/s, and *n*-butane concentration in the feed is 5 mol%. An increased solids circulation rate results in a greater solids holdup. This improves the contact between gas and solids and therefore a higher conversion is achieved. It should be observed that at the inlet of the riser, solids holdup is increased from about 28% solids at the low solids circulation rate to roughly 35% solids at the highest solids circulation rate. This increase in solids holdup is important because the catalyst will be most active when it re-enters the riser after regeneration in the standpipe.

In Figure 5.9, the *n*-butane conversion along the riser is presented for inlet superficial gas velocities of 4, 5, and 6 m/s along with the corresponding solids holdups. The solids circulation rate and *n*-butane feed concentration are 800 kg/m<sup>2</sup>·s and 5 mol%, respectively. The effect of increased superficial gas velocity is a dilution of the bed and thus a decrease in solids holdup. As a result, a decrease in the conversion of *n*-butane is seen at higher gas velocities. Again, the dense bed at the base of the riser exhibits the greatest solids holdup.

Figures 5.8 and 5.9 confirm that it is beneficial to operate at the highest possible solids loadings and lower gas velocities. A potential problem with such a scenario is choking as the incoming gas can not push the very dense bed of solids up through the riser. However, the high initial reaction rates and the resulting gas generation in the dense bed

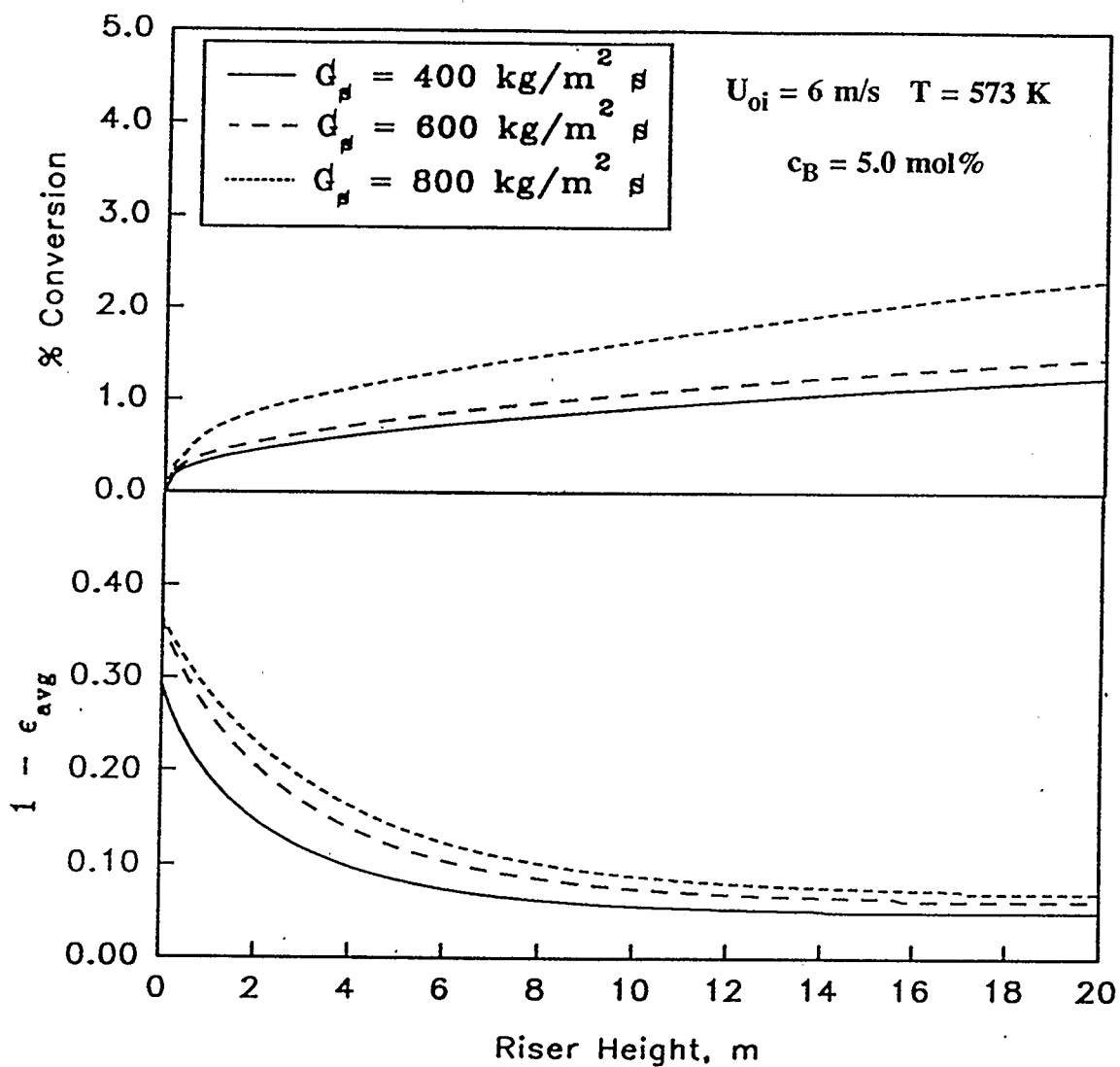


Figure 5.8 - Effect of Solids Circulation Rate on Butane Conversion and Solids Holdup

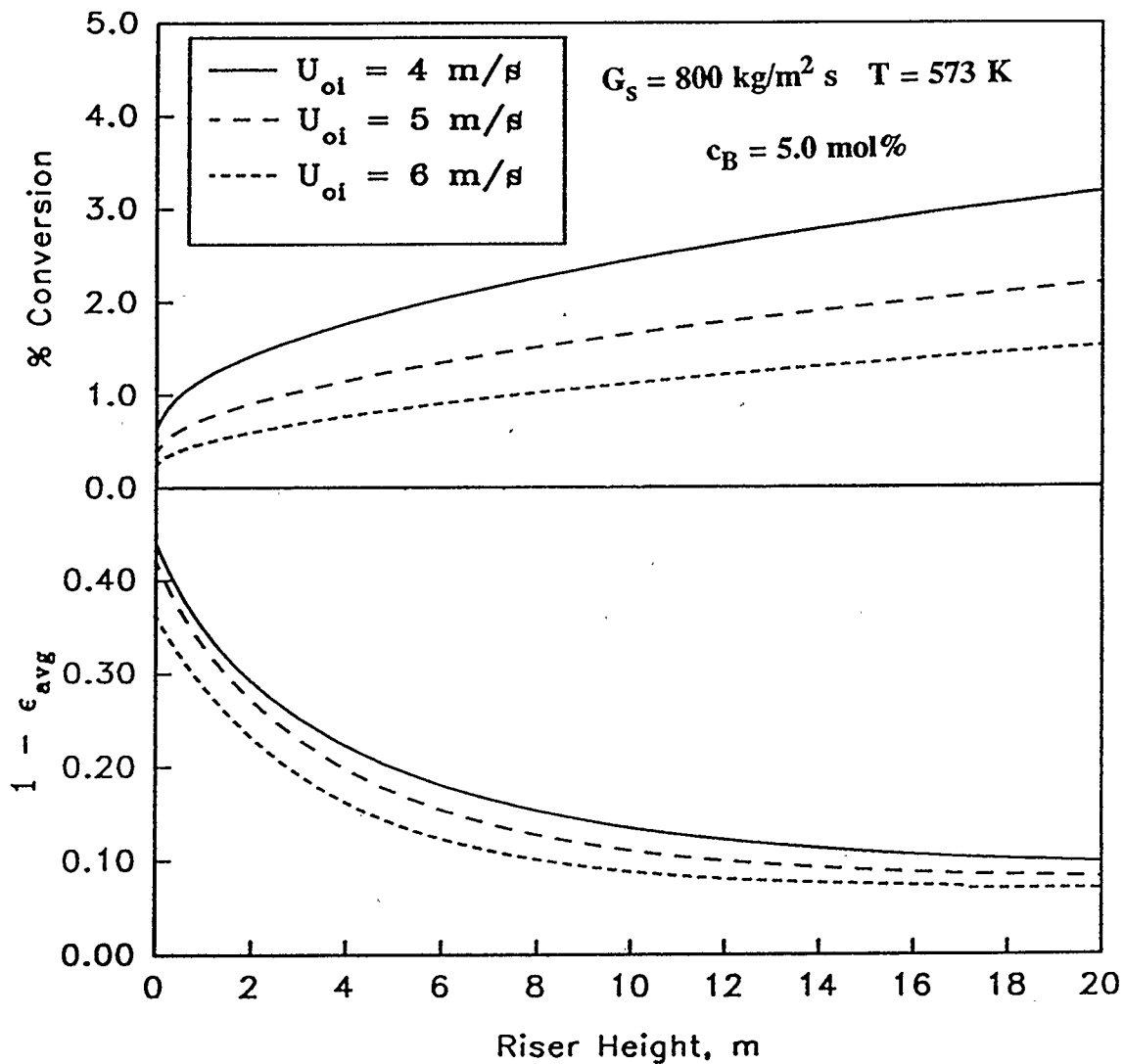


Figure 5.9 - Effect of Inlet Superficial Gas Velocity on Butane Conversion and Solids Holdup

will tend to increase the gas superficial velocity. Operating at low gas velocities and high solids loadings will minimize this effect, and the gas generation due to reaction will prevent choking. An example of gas generation due to reaction is presented in Figure 5.10. For a solids circulation rate of  $800 \text{ kg/m}^2\cdot\text{s}$  and an *n*-butane feed concentration of 5 mol%, the gas superficial velocity becomes more than double the inlet value of 6 m/s. This sudden jump is due to the rapid initial reaction rate previously presented in Figure 5.3. The superficial gas velocity profile decreases slightly along the riser length as the reaction rate decreases and the core radius increases. This sudden increase in gas superficial velocity in the denser bed at the base of the riser should be enough to prevent choking. In order to estimate the inlet gas velocity corresponding to the onset of choking for a given solids circulation rate, a correlation presented by Chong and Leung (1986) for vertical pneumatic transport of Geldart type A particles was used. For a solids circulation rate of  $800 \text{ kg/m}^2\cdot\text{s}$ , the correlation predicts the onset of choking at a velocity less than 4.7 m/s. For the case presented in Figure 5.10 with an inlet superficial gas velocity of 6 m/s, choking will not be a factor. In Figure 5.11, the gas superficial velocity profile along the riser length is presented for operation with an inlet gas velocity of 4 m/s. Based on the correlation, choking should occur in this case. However, as indicated in Figure 5.11, the superficial gas velocity is again more than doubled due to the reaction occurring. As a result, the potential for choking is eliminated. Thus, operation at the relatively low inlet gas velocity of 4 m/s with a solids circulation rate of  $800 \text{ kg/m}^2\cdot\text{s}$  is attainable. In an industrial scale CFB riser reactor, it is conceivable that solids circulation rates of more than  $1500 \text{ kg/m}^2\cdot\text{s}$  could be achieved at gas velocities in the range of 6 to 8 m/s. The

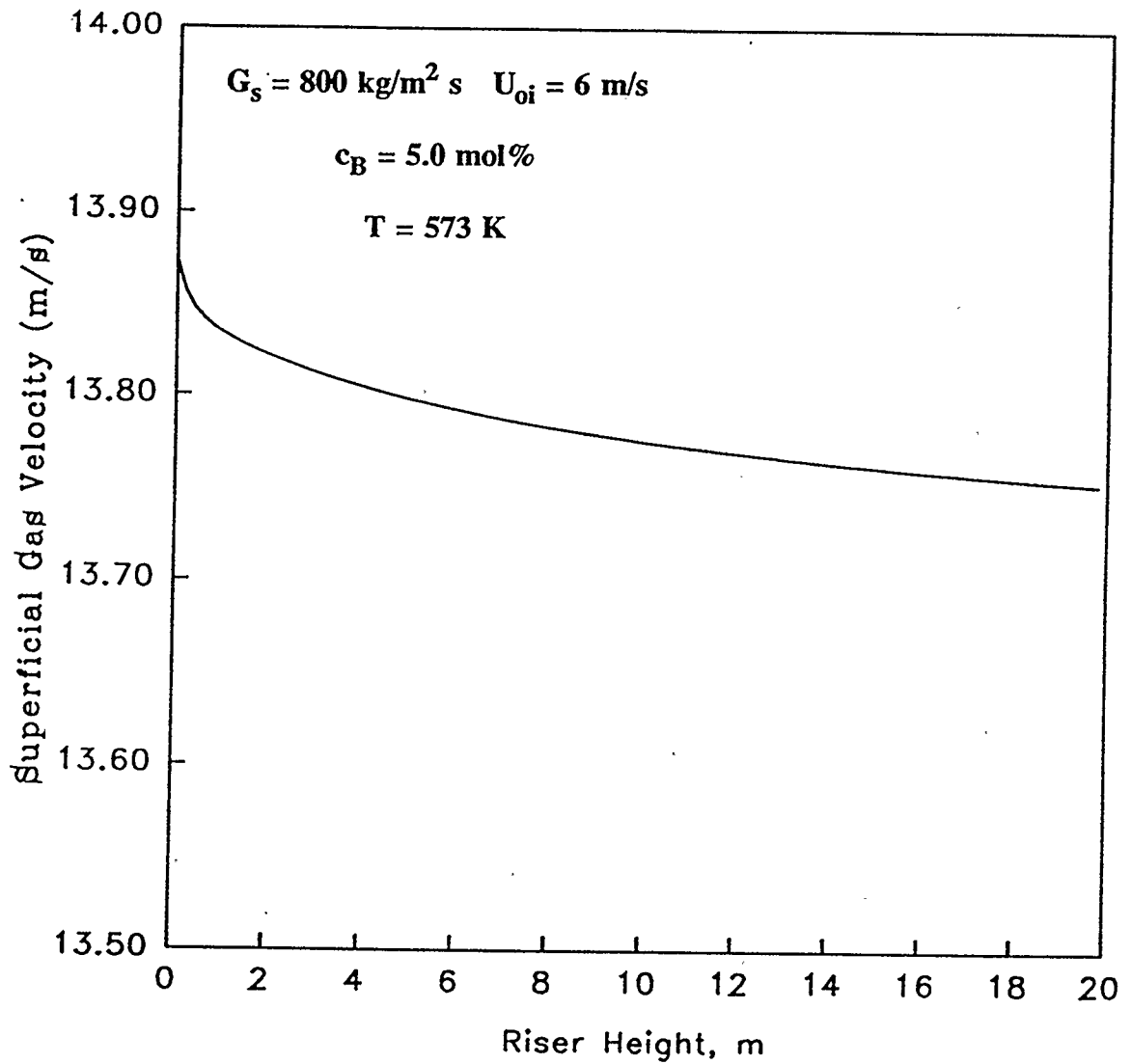


Figure 5.10 - Superficial Gas Velocity Profile  
 $U_{oi} = 6 \text{ m/s}$

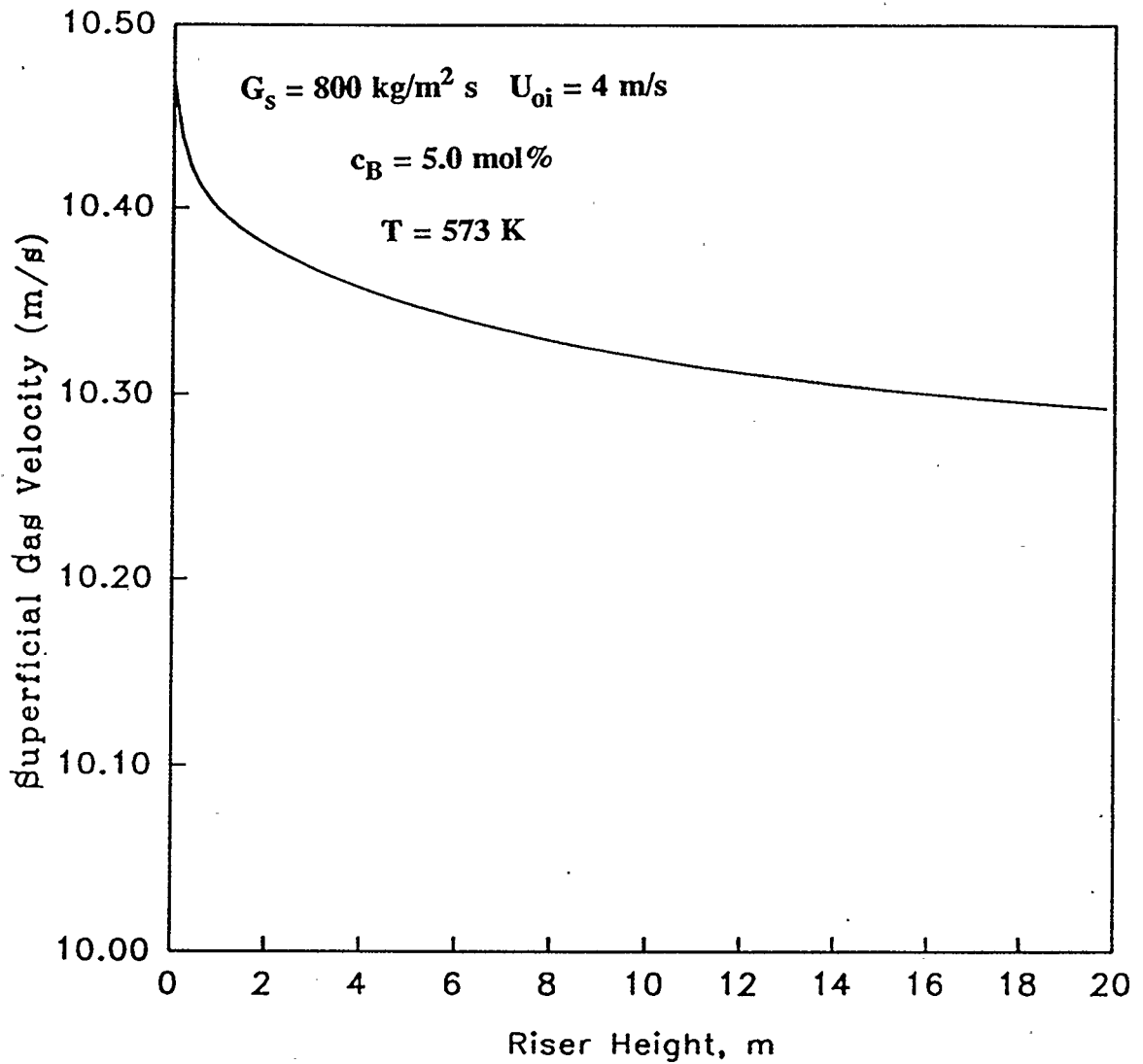


Figure 5.11 - Superficial Gas Velocity Profile

$U_{oi} = 4 \text{ m/s}$

high solids holdup corresponding to the lower gas velocity must be balanced by the high throughput required for profitable operation. These high gas velocities and solids circulation rates were not studied in this work because they are outside the limits of the empirical correlations of the hydrodynamic model, however, the simulation does indicate the potential for operation at gas velocities and solids circulation rates and thus very good gas-solid contacting.

The predictive hydrodynamic model is able to quantitatively describe the internal flow structure of the CFB riser by calculating the solids interchange coefficients between the core and annular regions. As expected, the solids circulation rate has an effect on this interchange. In Figure 5.12 and Figure 5.13, the solids interchange coefficients for solids circulation rates of  $400 \text{ kg/m}^2\cdot\text{s}$  and  $800 \text{ kg/m}^2\cdot\text{s}$ , respectively, are shown as a function of axial location. The gas superficial velocity for both cases is equal to  $6 \text{ m/s}$ . Increased solids loading for a given gas velocity will affect the interaction between solid particles as collisions become more frequent. With the core to annulus interchange coefficients based on a turbulent diffusion model, the increased solids loading will increase turbulence and thus will enhance transfer of solids from the core region to the annular region. This effect will, in turn, favor the formation of larger, dense clusters in the annulus. As mentioned in section 2.4, the annulus to core solids interchange coefficient model is developed from an analogy with gas-liquid counter-current annular flow. The interchange is inversely related to the vertical momentum change of solids removed from the annular region (Wong, 1991). The larger clusters associated with higher solids loadings will have

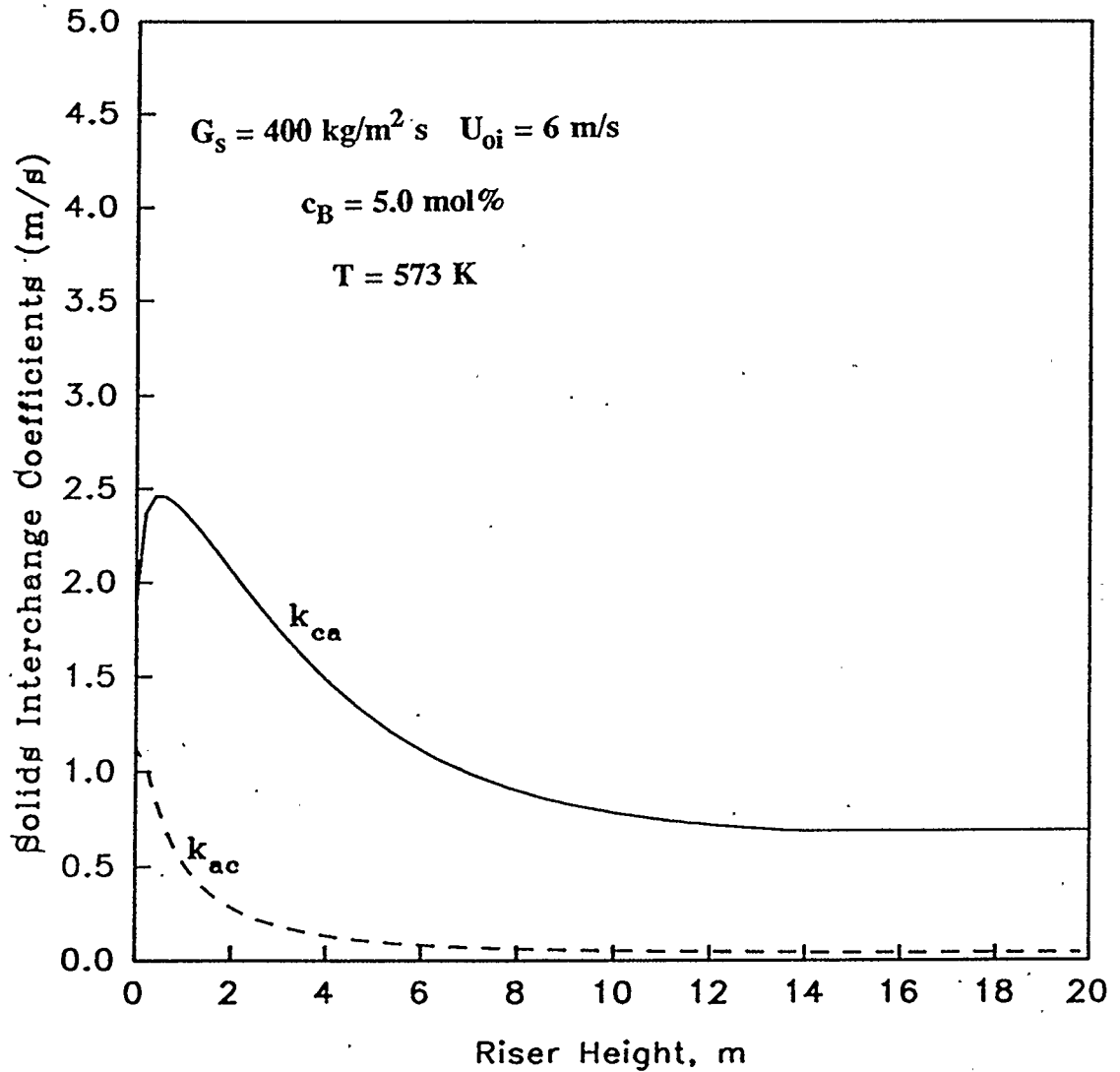


Figure 5.12 - Solids Interchange Coefficients  
for a Solids Circulation Rate of  $400 \text{ kg/m}^2 \cdot \text{s}$

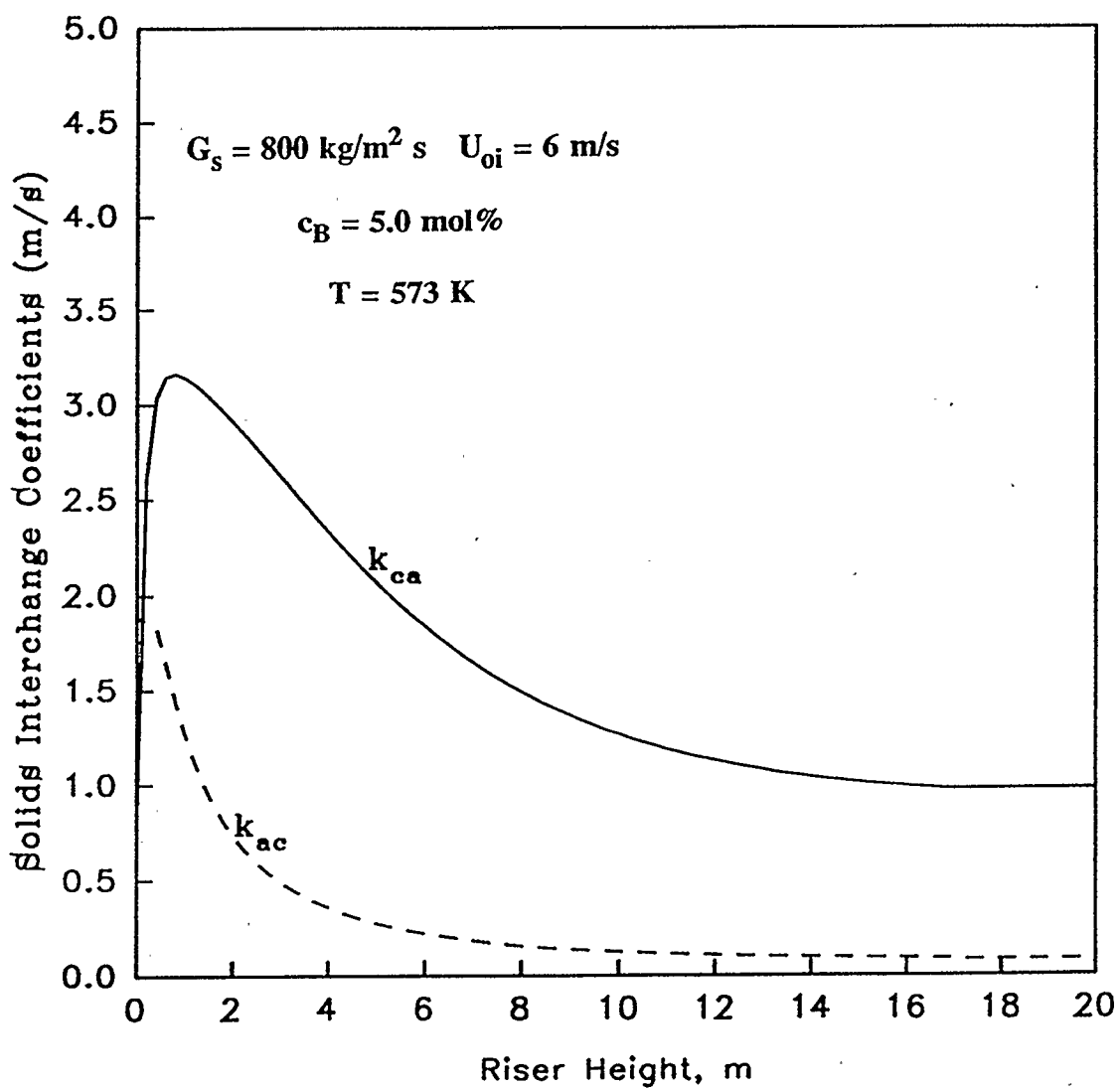


Figure 5.13 - Solids Interchange Coefficients  
for a Solids Circulation Rate of  $800 \text{ kg/m}^2 \text{ s}$

a greater downward velocity, and thus the vertical momentum change as solids are swept into the core will be less. As a result, the annulus-to-core solids interchange coefficient will increase. Figures 5.12 and 5.13 do indeed depict an increase of both interchange coefficients with increased solids circulation rate.

Except for a short distance at the base of the riser, the core-to-annulus solids interchange coefficient is always greater than the annulus-to-core solids interchange coefficient. This explains, in part, the fact that the annular film becomes thicker towards the base of the riser, as observed experimentally by numerous authors. The net transfer of solids is therefore from the core to the annulus, and some of these solids will fall down along the wall and re-enter the core at the riser bottom. Thus, at the riser bottom, the annulus-to-core interchange coefficient is momentarily greater as these solids rejoin the upward flow in the core. This effect is less pronounced for the lower solids circulation rate as the solids will have less tendency to fall all the way to the bottom. A maximum value of the core-to-annulus interchange coefficient is seen at approximately one meter from the riser bottom. This sharp rise is due to the rapid formation of the core/annular structure as solids accelerate from the base of the riser. After that point, the interchange declines as the flow becomes fully developed, and the core becomes leaner.

The interchange of solid catalyst between the core and the annulus has an influence on the performance of the CFB catalytic reactor. Flow of solids from the core to the annular region in the lower region of the riser will remove active catalyst from the core where the

majority of the reacting gas is flowing. At higher riser elevations, less active catalyst may be transferred to the annulus and later returned to the core where it is contacted with fresh gas. The magnitude of the solids interchange coefficients are indicative of the degree of mixing occurring in the riser. At the higher solids circulation rates, the mixing of solids will be higher, and thus a uniform temperature is maintained. At the base of the riser, large amounts of heat will be released as the reaction occurs very fast, but the solids interchange will prevent the formation of hot spots and the associated yield losses.

### 5.3 Results of Catalyst Deactivation Model

The preceding results were obtained assuming a catalyst deactivation corresponding to a value of 20% at the outlet of the riser. This section investigates the importance of catalyst deactivation as it is modelled here. Values of the decay constant "a" in Equation (3.16) were chosen such that the catalyst was 20%, 50%, and 70% deactivated upon exiting to the cyclone. Feed concentration and riser operating conditions were held constant. As shown in Figure 5.14, increased catalyst deactivation reduces conversion along the riser. For approximately the first three meters of riser length, the conversion is unaffected, but beyond this point the conversion profiles begin to separate. At the riser inlet, the catalyst has just been regenerated and exposure to reaction conditions does not show a noticeable effect. Reaction occurs rapidly at this level, however, and after three meters the transformation of the catalyst crystalline phases at the expense of the surface oxygen layers becomes significant. The higher degree of deactivation, resulting in reduced

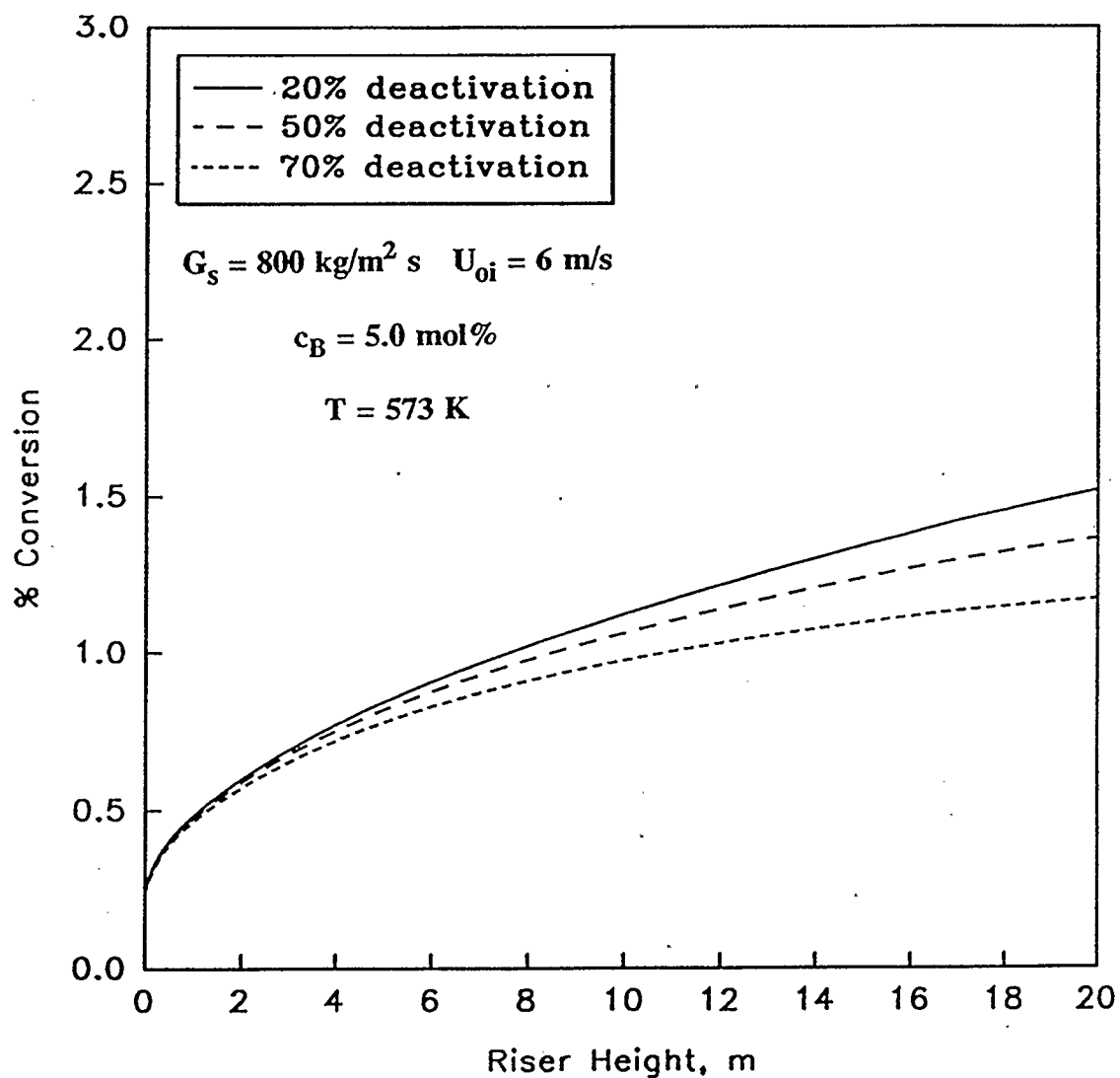


Figure 5.14 - Effect of Catalyst Deactivation on Single Pass Butane Conversion

conversion, will consequently reduce the yields of both maleic anhydride and  $\text{CO}_2$ . This is shown by comparing the results reported in Figure 5.6 (previously referenced and having 20% deactivation) and Figure 5.15 where deactivation is 70%. The yield of maleic anhydride is 1.2% for 20% deactivation, but drops to 1.0% for 70% deactivation. The results of this simple catalyst deactivation model indicate that reduction of the catalyst activity as the reaction proceeds has only a slight effect on the reactor performance. One of the key features of a CFB reactor is the short residence times of solids and gas. The average residence time of solids in the riser simulated in this work is approximately two seconds. Although the VPO catalyst is rapidly deactivated, the influence of this deactivation is minimized because, on the average, the solid catalyst passes rapidly through the riser. As discussed in the previous section, internal recirculation of solids can result in spent catalyst contacting fresh feed, but this factor is not incorporated into this simplified deactivation model. This is due to the complexity of the solids RTD curves in a CFB as illustrated in the work of Patience et al. (1990) where large fluctuations indicative of secondary flow patterns were observed. The work of Patience et al. (1990) used sand particles in the Geldart type B category, and in general there is a lack of RTD data for solids having the same characteristics as the VPO catalyst used in this work. More experimental and modelling work on solids RTD is needed before such effects can be incorporated into the present simulation.

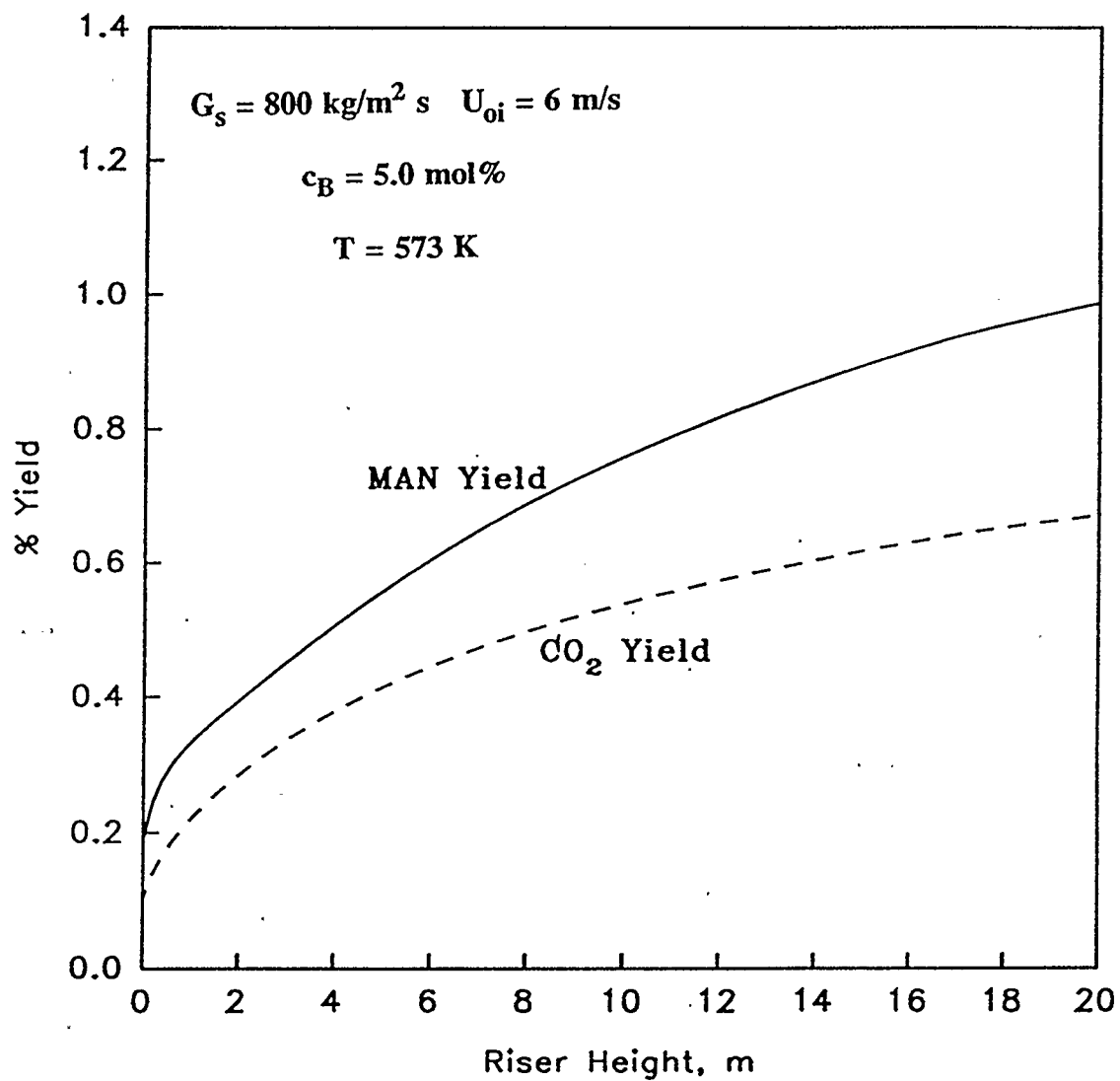
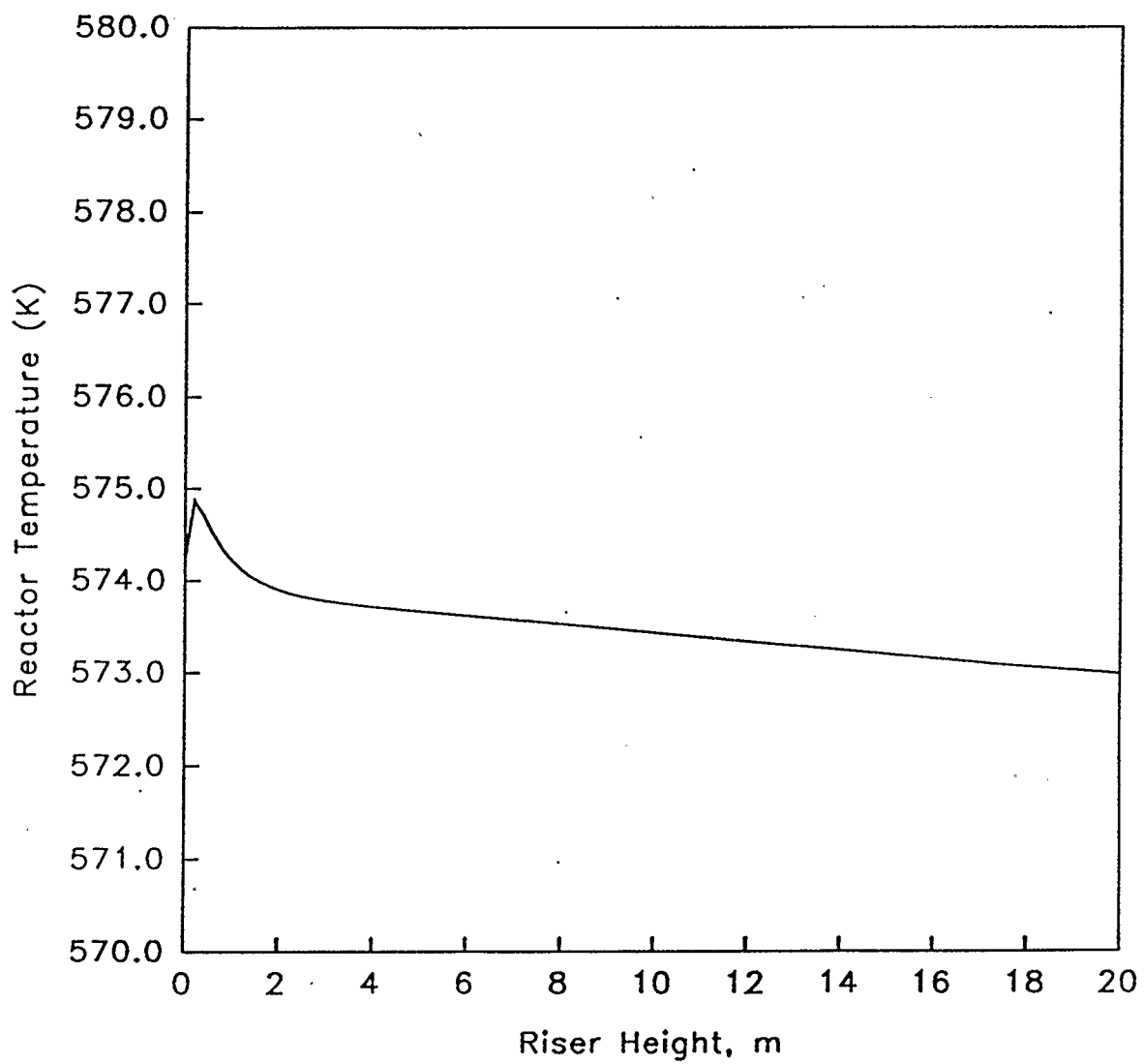


Figure 5.15 - Single Pass Product Yields for 70% Catalyst Deactivation

#### 5.4 Effect of Operating Temperature

Equation (4.1) may be solved to obtain the axial temperature profile in the reactor. Figure 5.16 indicates a maximum temperature variation of approximately 3 K along the riser length. An increase in temperature is seen at the riser inlet where the reaction rate is the greatest. However, this increase is only about 2 K, and will not affect the reactor performance. The combination of high solids-to-wall heat transfer coefficient, and low conversion per pass result in this small temperature variation. The heat release associated with conversions of the order of 2% will be considerably less than if a high single pass conversion was obtained, and the heat that is generated will be removed at the reactor wall. Figure 5.16 indicates that the reactor is operating isothermally. Figure 4.1 indicated a 20 °C temperature increase in the riser of a CFB combustor, but the higher solids circulation rates in CFB catalytic reactors and, in this case, low single pass conversions result in an even smaller temperature variation. The ability to maintain isothermal operating conditions in the reactor is very important for optimal reactor performance.

The activation energies describing the temperature dependence of the reaction kinetics were presented in Table 3.2. This data was used in the simulation to investigate the effect of the isothermal operating temperature on reactor performance. Simulations were performed at 573 K, 593 K, and 623 K, for a solids circulation rate of 800 kg/m<sup>2</sup>·s and an inlet superficial gas velocity of 6 m/s. The feed concentration was 5 mol% *n*-butane. Figure 5.17 presents the effect of temperature on *n*-butane conversion. As the temperature



**Figure 5.16 - Axial Reactor Temperature Profile**

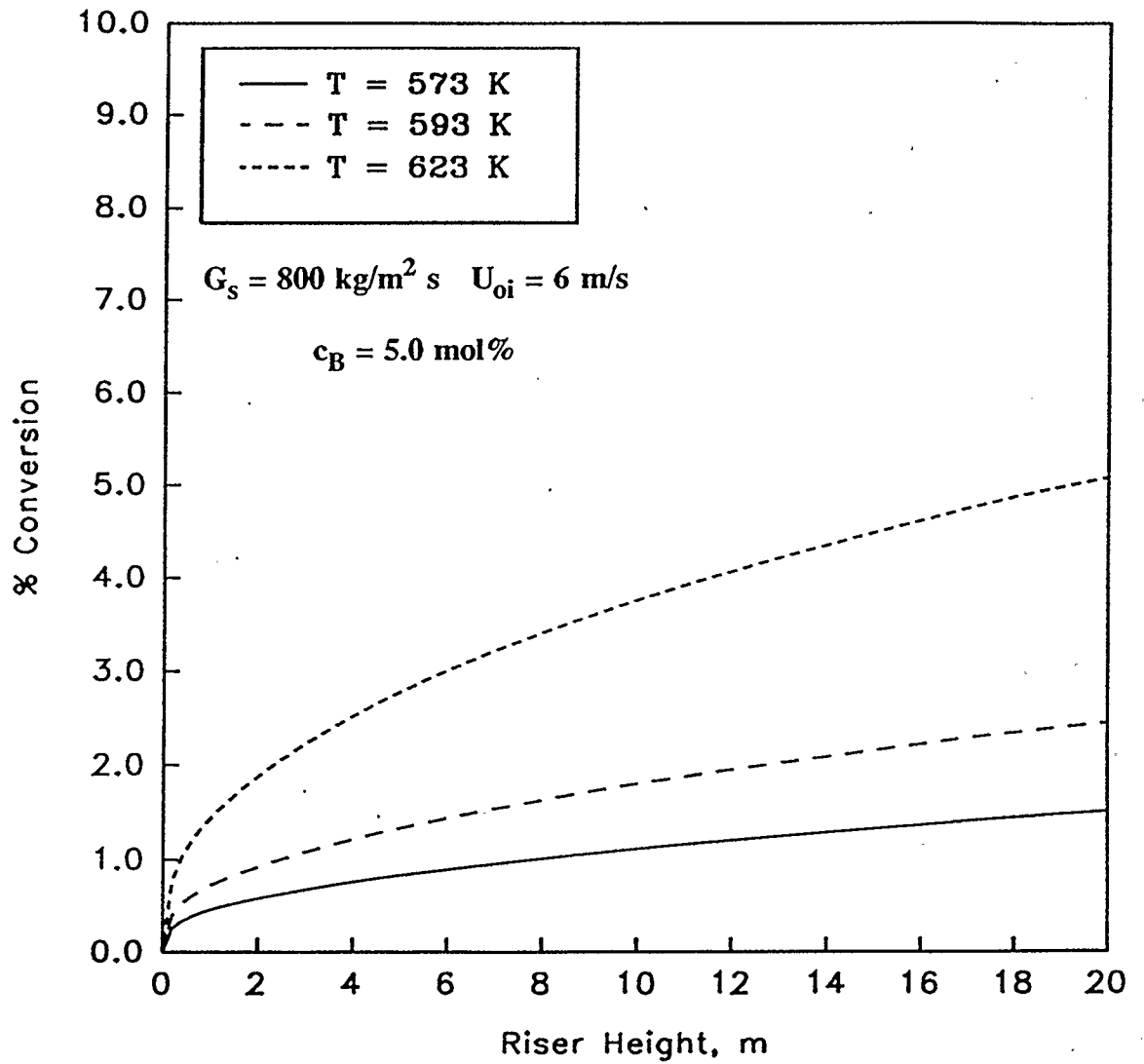


Figure 5.17 - Effect of Reactor Temperature on Single Pass Butane Conversion

is increased, the reaction proceeds more rapidly and thus conversion is greater. Conversion at 623 K is almost five times that at 573 K. However, the higher operating temperatures will allow the large activation energy barrier associated with the parallel reaction path of total oxidation of *n*-butane to CO<sub>2</sub> to be overcome. Thus the formation of CO<sub>2</sub> from *n*-butane will become more favorable. Figure 5.18 shows that at 623 K, the yield of CO<sub>2</sub> is in fact greater than the yield of maleic anhydride. Although the maleic anhydride yield has increased from 1.2% (Figure 5.6) to almost 2.5%, the CO<sub>2</sub> yield at 623 K is 4.0% as compared to 0.75% at the lower temperature. The selectivity to maleic anhydride along the riser as a function of reaction temperature is presented in Figure 5.19. With the formation of CO<sub>2</sub> favored, the selectivity decreases significantly from 75% at 573 K to 50% at 623 K. Based on the kinetics of Centi et al. (1985), operation at elevated temperatures is detrimental to the formation of maleic anhydride. These results are also indicative of the yield losses possible with formation of localized hot spots. Once again, this reaffirms the attractiveness of the near isothermal operating conditions which are obtained in Circulating Fluidized Beds.

## 5.5 Influence of the Core and Annular Regions

It is interesting to investigate the separate contributions of the core and the annulus to the reaction. While the majority of the gas flows upward in the solids-lean core region, the annular region will have a higher concentration of catalyst. Furthermore, although the annulus is very dense, it is also very thin, which will affect the reaction rate per unit

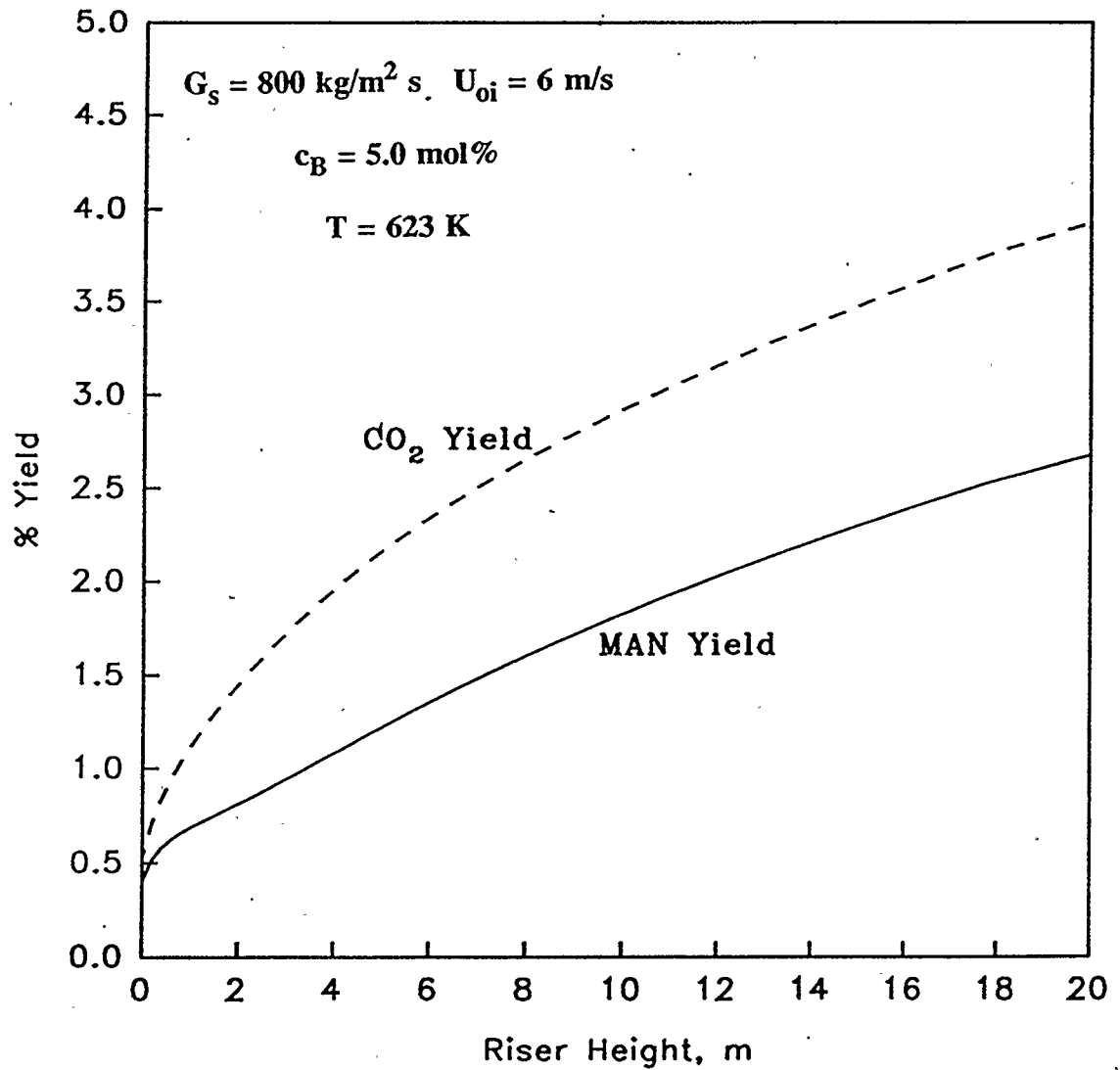


Figure 5.18 - Single Pass Product Yields for a Reactor Temperature of 623 K

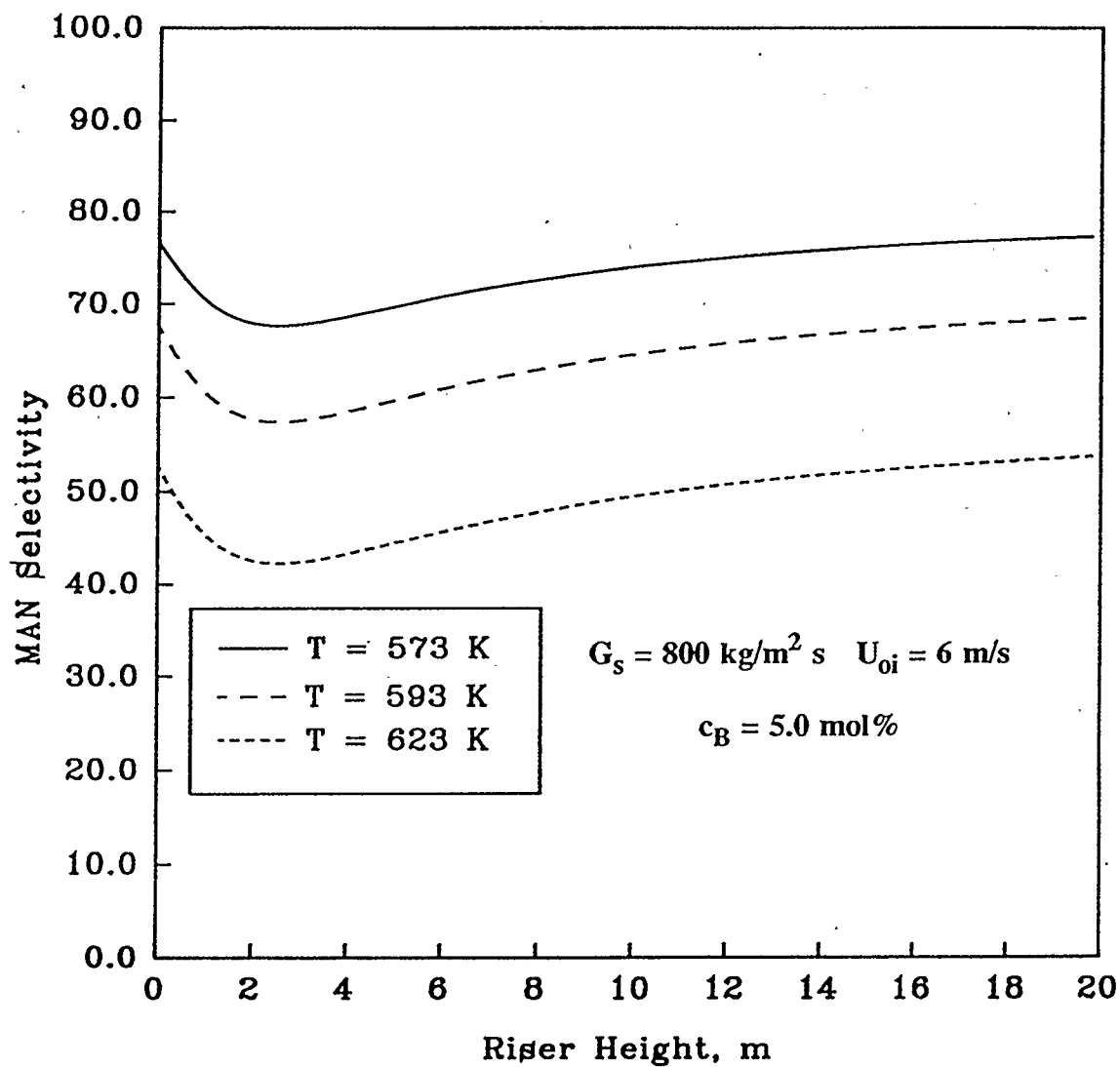


Figure 5.19 - Effect of Reactor Temperature on Maleic Anhydride Selectivity

volume of bed.

Figure 5.20 separates the contribution to the reaction by the core and the annular regions. The model assumes that, initially, all of the gas fed to the riser is in the core region. The high initial concentration of reactants combined with the large solids holdup in the core at the base of the riser results in a high initial reaction rate in the core and essentially zero reaction rate in the annulus. The solids holdup in the core quickly decreases however; as illustrated earlier in Figure 5.8 and some of the upward flowing gas is transferred to the annulus. Also, the rapid initial reaction rate depletes a large portion of the reactants. These factors combine to give the steep decline in reaction rate in the core seen in Figure 5.20. The gas concentration gradient between the core and the annulus is initially very large because all of the gas is concentrated in the core. Thus, with crossflow of gas modelled by a mass transfer mechanism, the annulus gas concentration rises quickly. This fact, combined with the constant solids holdup corresponding to minimum fluidization voidage as assumed in the development of the hydrodynamic model, leads to a rapid initial rise in reaction rate in the annular region. After eight to ten meters, the rate of reaction levels off as reactants are depleted and mass transfer between the core and the annulus is lessened.

Simultaneous solution of Equation (2.2) and Equation (2.4) of the hydrodynamic model gives the value for the core radius at any axial location. For a height element  $\Delta z$ , the volume of the core and the annulus may be determined. The product of the bed volume

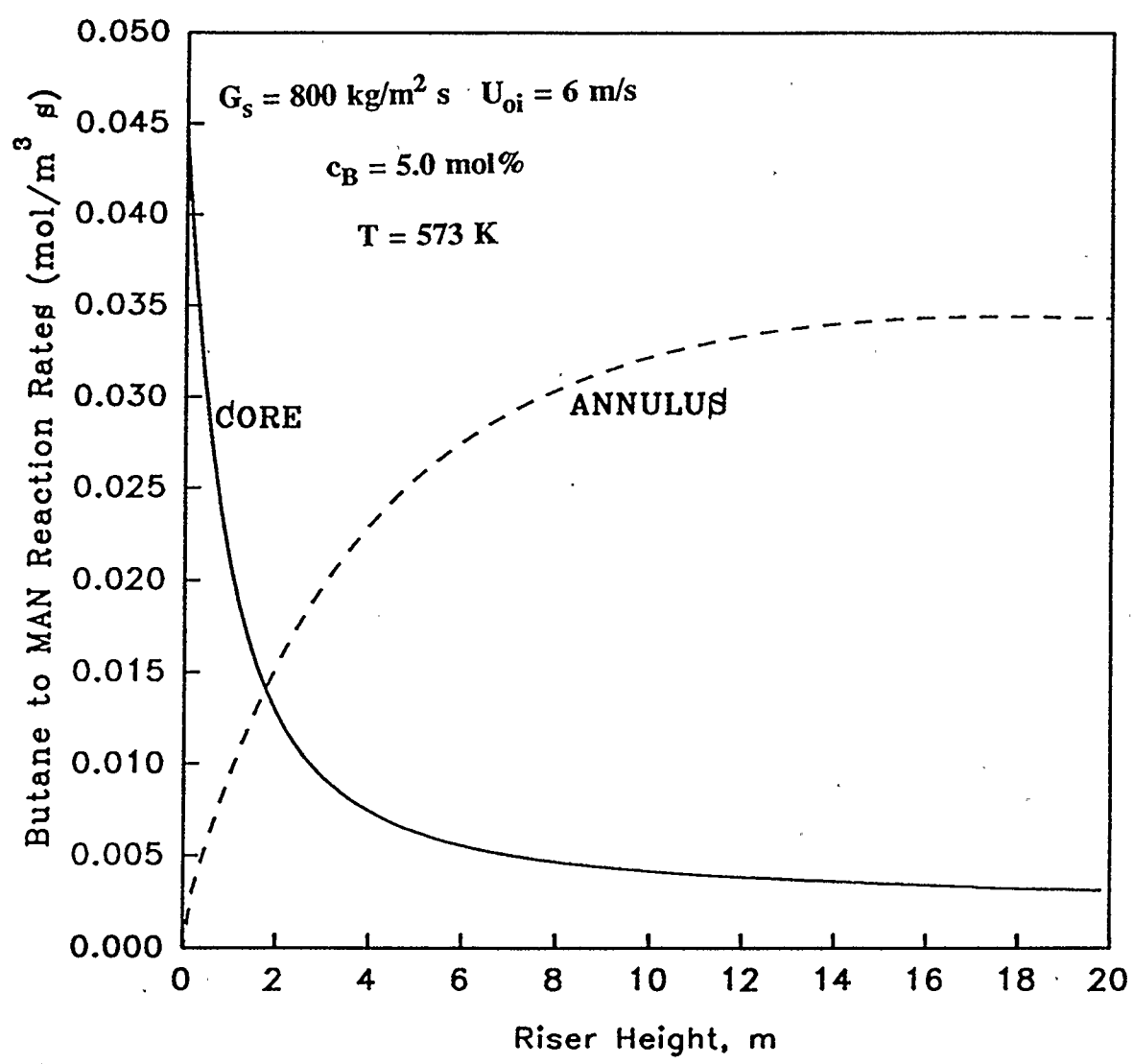
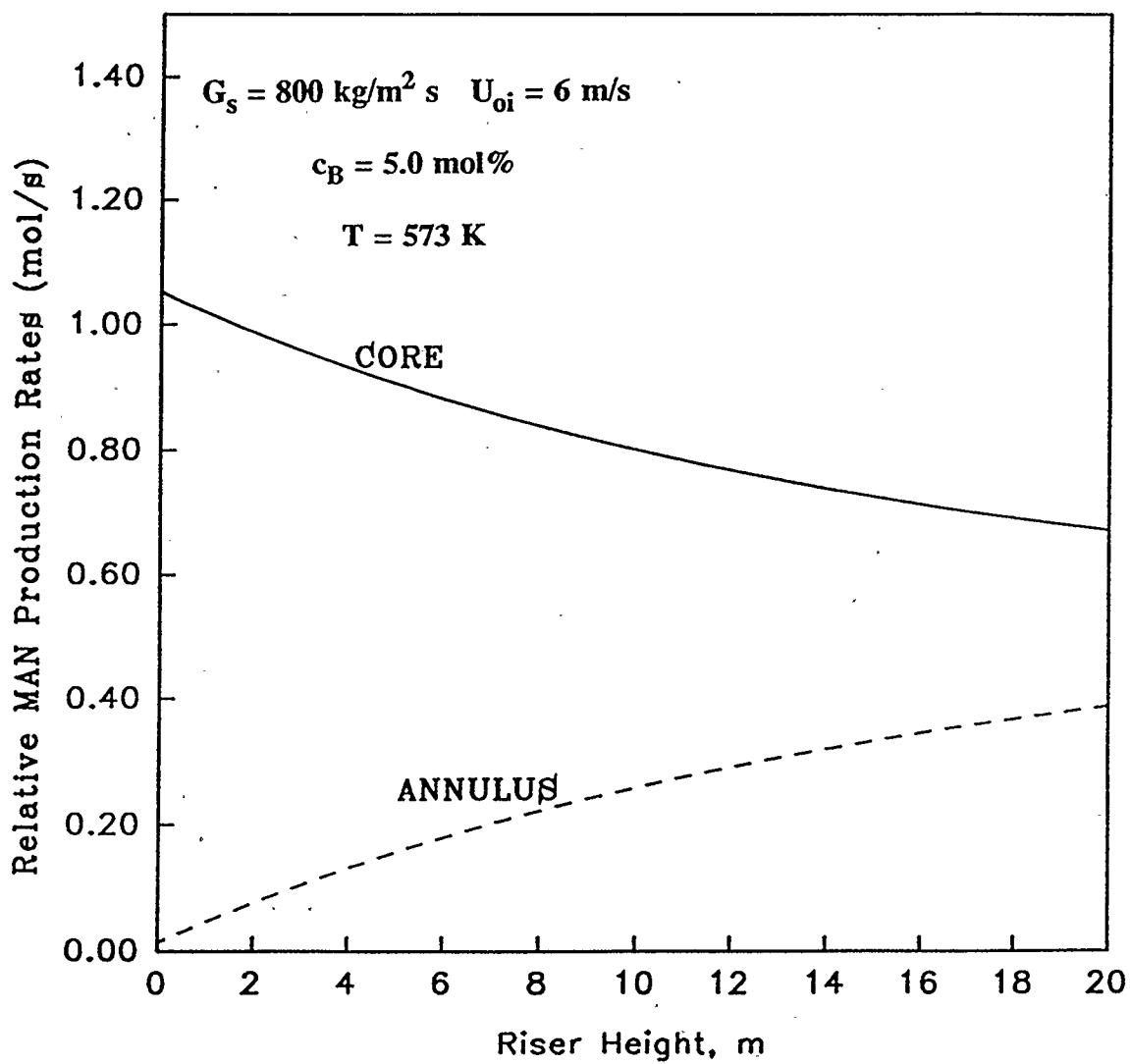


Figure 5.20 - Contribution to Reaction by the Core and Annular Regions for a 5 mol% Butane in Air Mixture

and the reaction rate gives the molar flow out of the volume element. In this way, the separate contribution of the core and the annulus to the overall production rate of maleic anhydride may be examined. This is presented in Figure 5.21 where it is seen that at all points along the riser, the production rate of maleic anhydride is greater in the core than in the annulus. Although the reaction rate in the annulus is greater than that in the core, it is offset by the small volume of the thin annular region.

Results comparing the relative influence of the core and annular region arise from the use of the model of Berruti and Kalogerakis (1989) which assumes the voidage in the annulus to be that of the solid particles at minimum fluidization conditions. As mentioned in section 2.1, the local voidage in the annulus may change greatly as a function of time and location along the riser. In order to better fit experimental data, Berruti and Kalogerakis (1989) took the time averaged voidage in the annulus to be half the minimum fluidization voidage. This represented intermittent flow of clusters of solids at minimum fluidization conditions and solids free voids in the annular region in equal proportions. Realizing the potential influence of the representation of the annular voidage, the simulation described in this work was run for three different models representing the annular voidage profile. The axial variation of the annular voidage for the three models is shown in Figure 5.22. Model 1 is the Berruti-Kalogerakis model assuming a constant annular voidage equal to the minimum fluidization voidage of a bed of particles. Model 2 is a linear variation of the annular voidage with height from the minimum fluidization voidage at the base of the riser, to an arbitrarily chosen voidage of 0.80 at the outlet. Model 3 corresponds to an



**Figure 5.21 - Relative MAN Production Rates from the Core and Annular Regions for a 5 mol% Butane in Air Mixture**

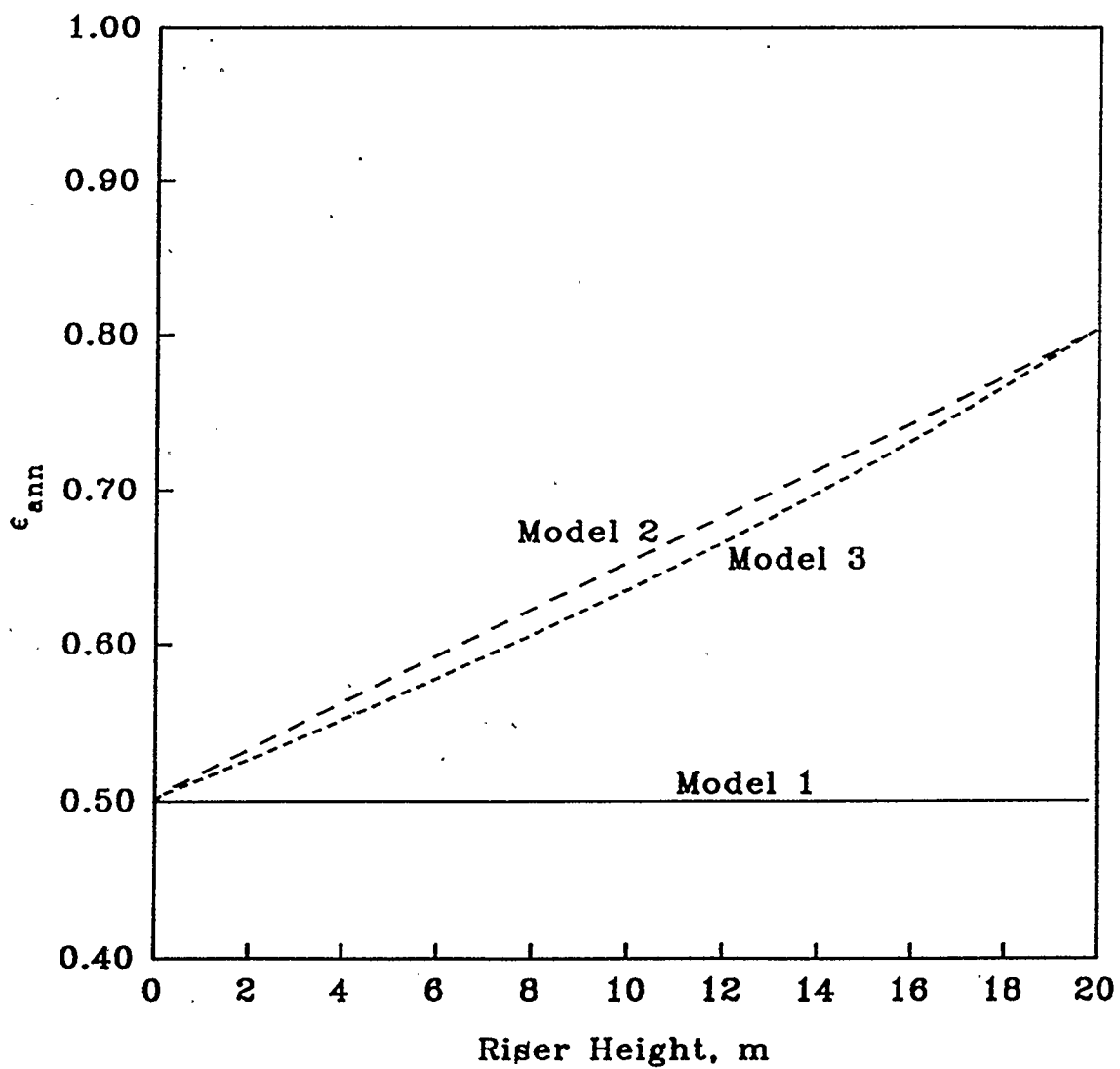
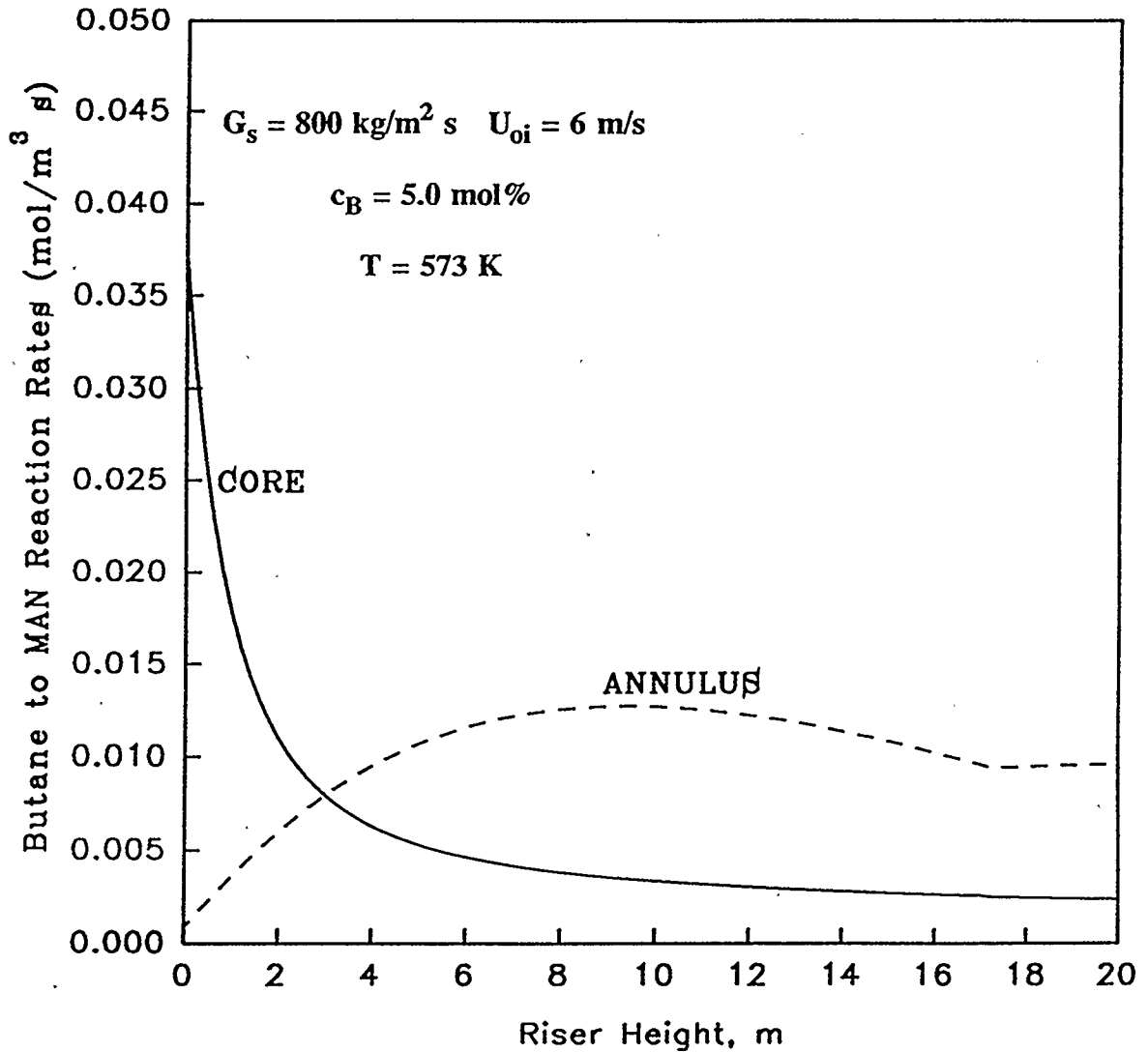


Figure 5.22 - Three Models for the Axial Variation of the Annular Voidage

exponential variation with height between the same limits. While there is a large difference between model 1 and the other two models, models 2 and 3 result in very similar annular voidage profiles. In this way, the sensitivity of the simulation to this parameter can be studied for both small and large changes.

Figures 5.23 and 5.24 are identical to Figures 5.20 and 5.21, but are the results assuming the linearly decreasing annular voidage of model 2. As before, the reaction rate for the formation of maleic anhydride from *n*-butane in the core decreases rapidly while the annular reaction rate rises from a zero initial value. However, in this case, the reaction rate in the annulus reaches a maximum and then decreases after eight to ten meters. At that point, the effect of the decreasing annular density and reduced gas mass transfer from core to annulus combine to reduce the reaction rate in the annulus. Although the exact nature of the annular voidage is not easily quantified, the results obtained with this simple linear variation model seem more realistic than a continuous increase and levelling out as represented in Figure 5.20. Despite the significant change in the reaction rate in the annulus, it is seen from Figure 5.24 that the relative production rates in the core and annular regions remain essentially the same as before. The molar flow from the two regions is insensitive to the value of the annular voidage. Figure 5.25 presents the conversion for the three different annular voidage models. As expected, since the molar flows out of the core and annulus remained the same, conversion is also essentially constant for all three models.



**Figure 5.23 - Contribution to Reaction by the  
 Core and Annular Regions for  
 a 5 mol% Butane in Air Mixture**

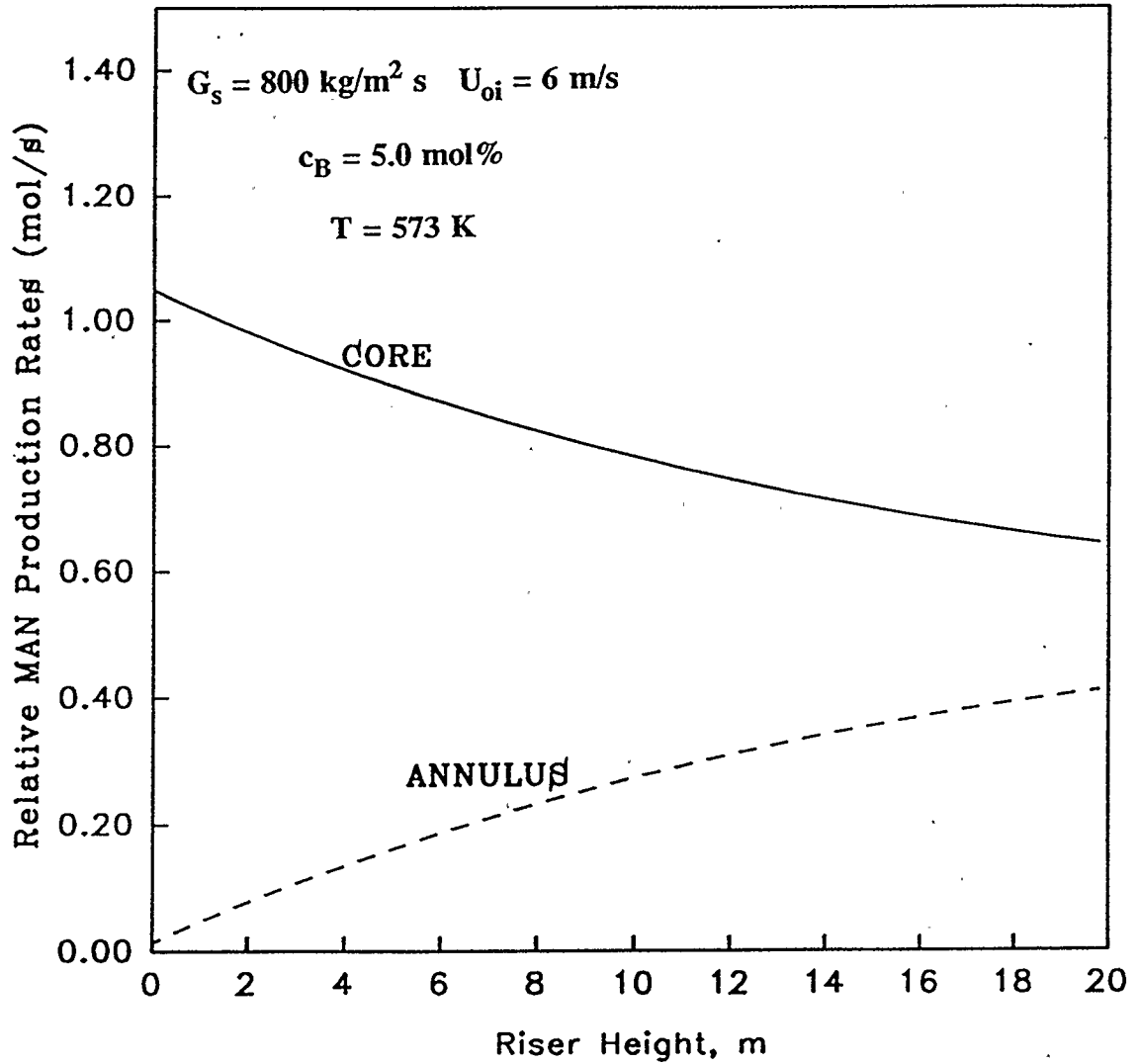


Figure 5.24 - Relative MAN Production Rates from the Core and Annular Regions for a 5 mol% Butane in Air Mixture

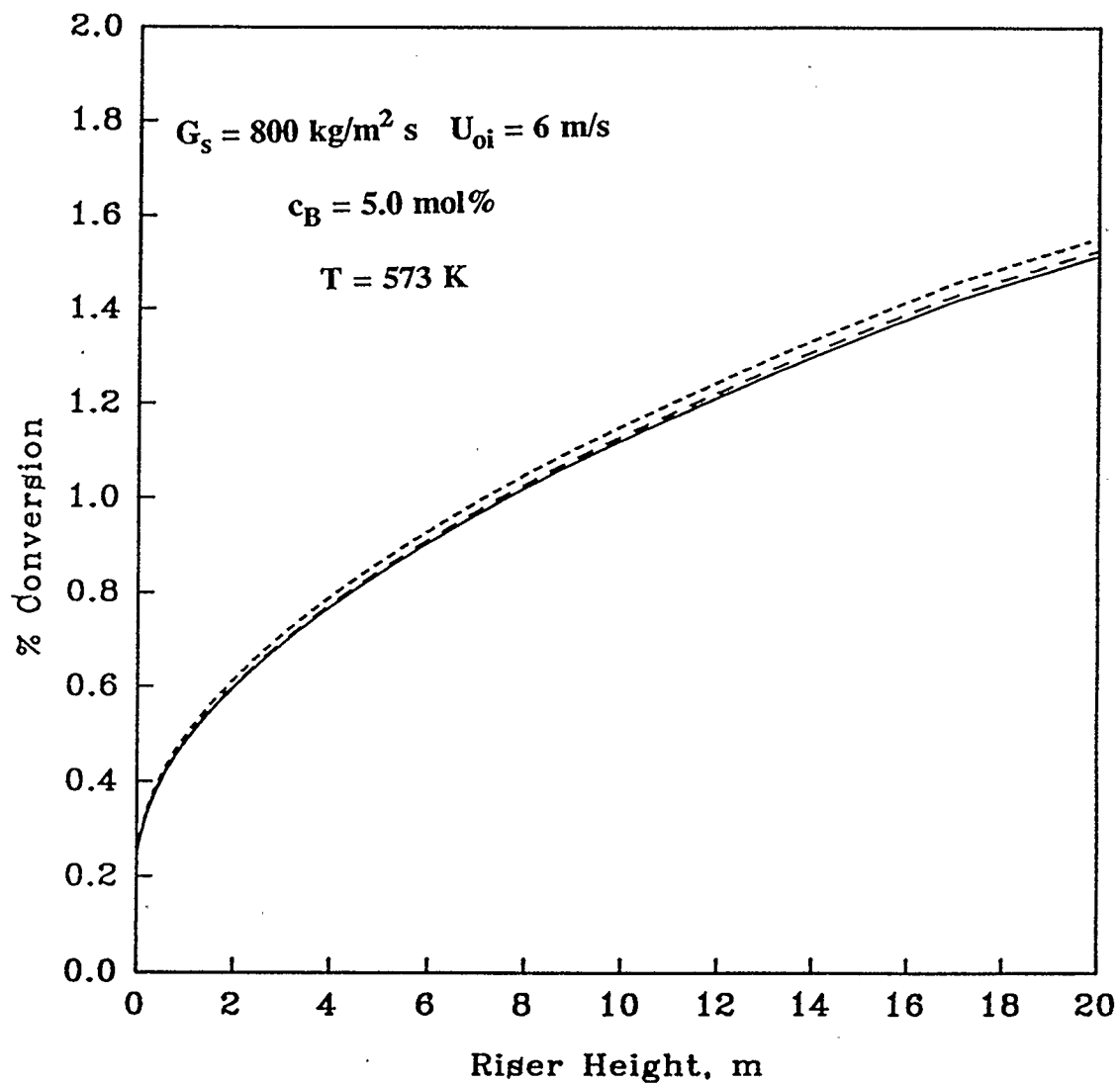


Figure 5.25 - Single Pass Butane Conversion for the Three Models of the Annular Voidage

## 5.6 Comparison of the CFB Reactor Model with CSTR and PFR Reactor Models

Gianetto et al. (1990) calculated selectivity and yield for complex reactions occurring in a Circulating Fluidized Bed Reactor and compared their results to the theoretical cases of a perfectly mixed reactor (CSTR) and a plug flow reactor (PFR). These authors stated that the gas phase in a CFB exhibits plug flow characteristics with minor axial dispersion. Contractor and Chaouki (1990) also suggested essentially plug flow of gases in CFB reactors. The CFB catalytic reactor model developed in this work was compared with the CSTR and PFR reactor models. The actual solids holdup predicted by the hydrodynamic model was used in the design equations of the two theoretical reactor models. The results, presented in Figure 5.26, indicate that the CFB reactor modelled in this work more closely approaches the performance of the CSTR. Conversion achieved in the PFR is much greater than that predicted by the model for the CFB reactor. The CFB reactor model appears to over-predict the amount of gas crossflow from the core to the annular region. As a result, the CFB reactor exhibits a great deal of axial dispersion and significant deviation from plug flow behavior. As discussed in section 2.6 concerning radial gas mixing, limited research has been undertaken into the gas flow in the risers of CFBs. It is possible that axial gas dispersion is greater than suspected. Also, the model used in this work for radial gas mixing is extremely simplified and, based on Figure 5.26, appears to predict very large axial dispersion of gas. At this point, only qualitative conclusions can be safely arrived at regarding the comparison of the CFB reactor model to the theoretical reactor cases: the CFB reactor performance is an improvement over a

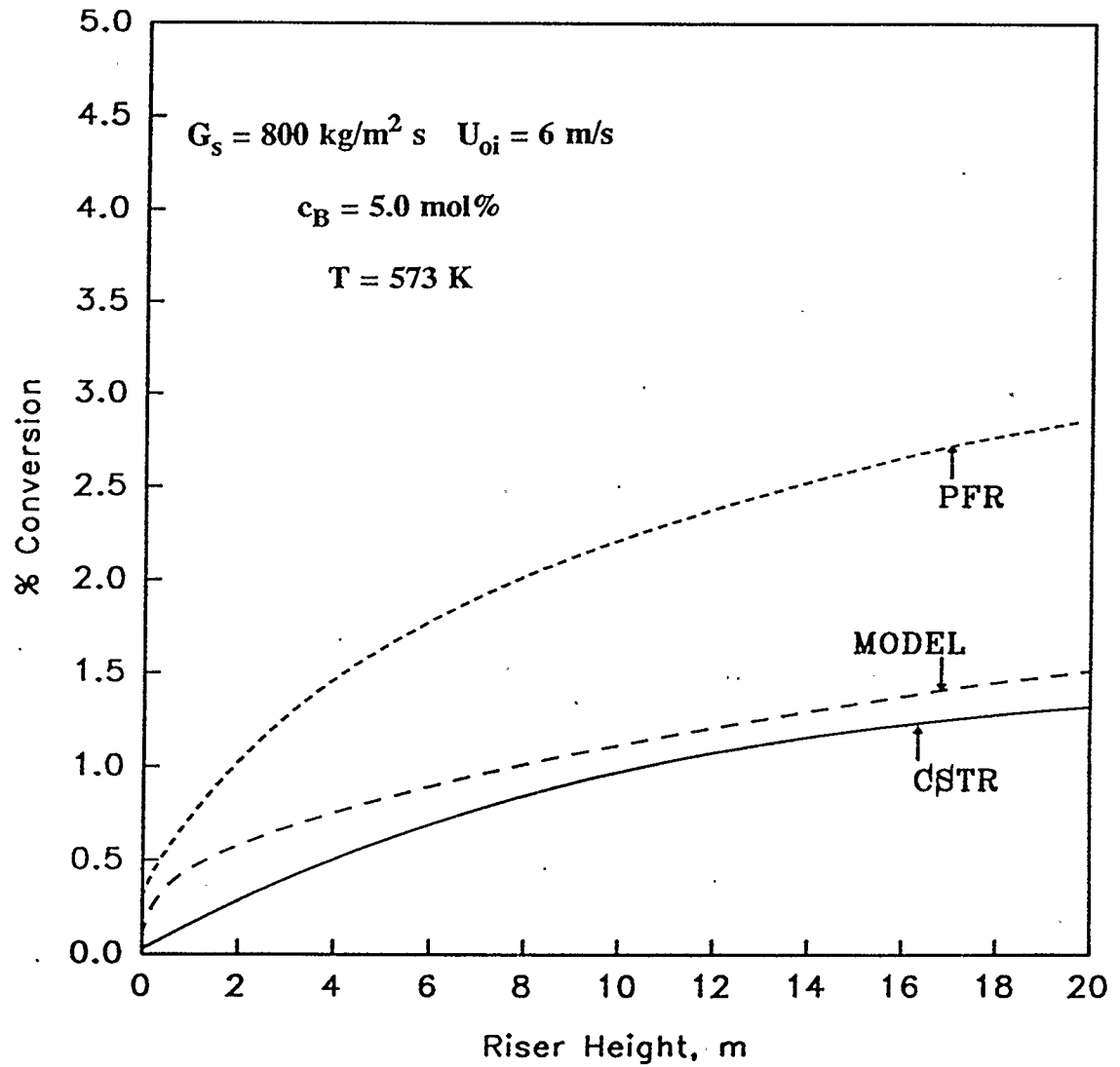


Figure 5.26 - Comparison of the CFB Reactor Model With CSTR and PFR Reactor Models

CSTR reactor, but deviates from the plug flow reactor performance. The magnitude of this deviation depends on the radial gas mixing which requires further investigation at this time. Although the conversions achieved in a CFB reactor may not be as great as those achieved in a PFR reactor, the backmixing of solids and gas will maintain a uniform temperature in the bed and avoid yield and selectivity losses associated with hot spots. Gianetto et al. (1990) found that formation of hot spots significantly reduced yield and selectivity of the desired intermediates of a complex reaction system in a PFR, although conversion was still high. They concluded that the very fine particles and the backmixing of solids in a CFB reactor can eliminate hot spots adverse to the desired reaction paths and catalyst life.

## CHAPTER 6

### CONCLUSIONS AND RECOMMENDATIONS

#### 6.1 Conclusions

The hydrodynamics of a Circulating Fluidized Bed (CFB) and a reaction kinetic model have been combined to form a computer simulation of the partial oxidation of *n*-butane to maleic anhydride.

A predictive model for the riser hydrodynamics based on a core/annular type of flow has been utilized which estimates the average axial voidage profile and the internal gas and solids flow structures. The model assumes that the riser may be divided into three sections: an acceleration zone at the base, a fully developed flow zone immediately above the acceleration zone, and a deceleration zone for risers with abrupt exit geometry. The model solves each section to predict the average voidage profile, the core voidage and radius, the core gas and solids velocities, and the solids interchange coefficients from core to annulus and annulus to core, all as a function of axial location.

Reaction kinetics developed for fixed bed technology have been utilized. The reaction network is a combination of series and parallel reaction steps involving formation of both the desired maleic anhydride product and total oxidation products (CO<sub>2</sub> and water), and subsequent decomposition of the desired product. The oxidation reaction is assumed to

occur in both the core and annular regions, the proportion of which is dependent on the local solids concentration as predicted by the hydrodynamic model. A simple first order catalyst deactivation model has been used and incorporated into the simulation.

The ability of the simulation to predict the trends of CFB reactor performance under various operating conditions was tested by performing numerous runs. The effects of solids circulation rate, superficial gas velocity, *n*-butane feed concentration, and reaction temperature were investigated. Also, the importance of increasing catalyst deactivation was examined. Increased conversion was observed for increased solids circulation rates due to the improved gas/solids contacting associated with larger solids holdup. Increased yields resulted from increased conversion. Conversely, increased superficial gas velocity decreased the conversion attainable. An increase in *n*-butane feed concentration resulted in a decrease in conversion. However, at very low concentrations, low selectivity to maleic anhydride resulted in poor yields of desired product. An increase in reaction temperature led to an increase in reaction rate, and hence improved conversion. For the higher temperatures, though, the total oxidation of *n*-butane to CO<sub>2</sub> and water was favored as the activation energy barrier for that reaction was overcome. As expected, increased catalyst deactivation lessened the conversion, although this effect was limited because of the short average residence time of solids in the riser.

The results of the computer simulation combined with the unique features of the CFB reactor clearly indicate that the CFB process for this reaction is superior to any other.

Since the oxygen required for the reaction is supplied by the layers of oxygen on the surface of the solid catalyst, and the catalyst is completely regenerated in the standpipe, the reactor may be operated in the absence of or with very low concentrations of gas phase oxygen in the riser. Therefore, the feed to the riser will have a high *n*-butane concentration and, as the model predicts, the yield and selectivity of maleic anhydride will be high. Although conversions at the higher *n*-butane concentrations will be low, the large throughputs associated with high gas velocities in CFBs will increase production. These high gas velocities combined with gas generation due to reaction allow for higher solids circulation rates and enhanced reaction rates while eliminating the onset of choking. Large solids-to-wall heat transfer coefficients combined with low single pass conversions will maintain isothermal operating conditions, and eliminate the formation of hot spots and the associated yield and selectivity losses. High gas velocities result in short average residence times of the solid catalyst particles, so even though the VPO catalyst becomes rapidly deactivated, the reaction will not be appreciably affected.

## 6.2 Recommendations

A current limit of the simulation is the use of reaction kinetics based on fixed bed reactor technology. Kinetics arising from CFB operation are expected to be significantly different because of the ability to operate in the absence or with very low concentrations of gas phase oxygen in the riser, the higher possible activity of the catalyst, and the different preparation of the attrition resistant catalyst used in a CFB. This would possibly lead to

large improvements in conversions and yields. Also, the kinetics of catalyst deactivation are more complicated than described by the simple first order kinetics model employed in this study. A more rigorous formulation is needed. In addition, there is a need for high temperature gas and solids RTD studies at high solids circulation rates, in order to further understand the internal flow of the gas and solids in the core and annular regions. This would help to quantify the gas interchange between the two zones and to trace the flow of solids which could potentially include deactivated catalyst recirculating in an industrial unit. Finally, the effect of the continuous cycling operation of the catalyst between the reduction and oxidation zones, which will possibly enhance the reaction rates and selectivities, must be studied further for the specific reaction of *n*-butane to maleic anhydride. The method of Lang et al. (1989) would be suitable for this with the study extended to the development of a kinetic model for the cyclical operation.

In order to validate and improve the proposed model there is a need for experimental data on the formation of maleic anhydride from *n*-butane in a CFB reactor. It is possible to perform such experiments in a laboratory scale unit and compare results with the model predictions, but in order to use the model in industry, there will eventually be a need for data from industrial scale CFBs. Such data are difficult to obtain in view of the extreme economic importance of the process and the protection placed on the technology and its performance by the major industrial installations.

## CHAPTER 7

## REFERENCES

## 7.1 References

Adams, C. K. *Gas Mixing in Fast Fluidized Beds*. Circulating Fluidized Bed Technology II (P. Basu and J. F. Large, Eds.), Pergamon Press, Toronto, Ontario, pp. 299 - 306, (1988).

Arena, U., Cammarota, A., Pistone, L. *High Velocity Fluidization Behavior of Solids in a Laboratory Scale Circulating Bed*. Circulating Fluidized Bed Technology (P. Basu, Ed.), Pergamon Press, Toronto, Ontario, pp. 119 - 125, (1986).

Bader, R., Findlay, J. and Knowlton, T.M. *Gas/Solids Flow Patterns in a 30.5 cm Diameter Circulating Fluidized Bed*. Circulating Fluidized Bed Technology II (P. Basu and J.F. Large, Eds.), Pergamon Press, Toronto, Ontario, pp. 123 - 127, (1988).

Bej, S. K., and Rao, M. S. *Selective Oxidation of n-Butane to Maleic Anhydride. 2. Identification of Rate Expression for the Reaction*. Ind. Eng. Chem. Res., **30**, 1824 - 1828, (1991).

Berruti, F. and Kalogerakis, N., *Modelling the Internal Flow Structure of Circulating*

*Fluidized Beds. Can. J. Chem. Eng., 67, 1010 - 1014, (1989).*

Bolton, L. W. and Davidson, J. F. *Recirculation of Particles in Fast Fluidized Risers. Circulating Fluidized Bed Technology II (P. Basu and J. F. Large, Eds.), Pergamon Press, Toronto, Ontario, pp. 139 - 146, (1988).*

Brereton, C.M.H., Grace, J. R., and Yu, J., *Axial Gas Mixing in a Circulating Fluidized Bed. Circulating Fluidized Technology II (P. Basu and J. F. Large, Eds.), Pergamon Press, Toronto, Ontario, pp. 307 - 314, (1988).*

Buchanan, J. S. and Sundaresan, S. Appl. Cat., 26, 211, (1986).

Centi, G., Fornasari, G., Trifiro, F. *N-Butane Oxidation to Maleic Anhydride on Vanadium - Phosphorus Oxides: Kinetic Analysis with a Tubular Flow Stacked - Pellet Reactor. Ind. Eng. Chem. Prod. Res. Dev., 24, 32 -37, (1985).*

Centi, G., Trifiro, F., Ebner, J. R., and Franchetti, V. M. *Mechanistic Aspects of Maleic Anhydride Synthesis from C<sub>4</sub> Hydrocarbons over Vanadium Phosphorus Oxides. Chem. Rev., 88, 55 - 80, (1988).*

Centi, G. Personal Correspondence, Sept. 6, (1991).

Choi, J. H., Yi, C. K., and Son, J. E. *Axial Voidage Profile in a Cold Mode Circulating Fluidized Bed*. Circulating Fluidized Bed Technology III (P. Basu, M. Horio, and M. Hasatani, Eds.), Pergamon Press, Toronto, Ontario, pp. 131 - 136, (1990).

Chong, Y. O. and Leung, L. S. *Comparison of Choking Velocity Correlations in Vertical Pneumatic Conveying*. Powder Technology, **47**, 43 - 50, (1986).

Chowdrury, J. (Ed.) *Inexpensive Butyrolactone by Direct Hydrogenation*. Chem. Eng., **98**, No. 9, p. 17, (1991).

Contractor, R. M. and Sleight, A. W. *Maleic Anhydride from C<sub>4</sub> Feedstocks Using Fluidized Bed Reactors*. Catalysis Today, **1**, 587 - 607, (1987).

Contractor, R. M., Bergna, H. E., Horowitz, H. S., Blackstone, C. M., Chowdhry, U., and Sleight, A. W. *Butane Oxidation to Maleic Anhydride in a Recirculating Solids Reactor*. Catalysis 1987 (J.W. Ward, Ed.), Elsevier Science Publishers, Amsterdam, (1988).

Contractor, R. M. *Butane Oxidation to Maleic Anhydride in a Recirculating Solids Riser Reactor*. Circulating Fluidized Technology II (P. Basu and J. F. Large, Eds.), Pergamon Press, Toronto, Ontario, pp. 467 - 474, (1988).

Contractor, R. M. and Chaouki, J. *Circulating Fluidized as a Catalytic Reactor*.

Circulating Fluidized Bed Technology III (P. Basu, M. Horio, and M. Hasatani, Eds.), Pergamon Press, Toronto, Ontario, pp. 39 - 48, (1990).

Dry, R. J. and La Nauze, R. D. *Combustion in Fluidized Beds*. Chem. Eng. Prog., **86**(7), 31 - 47, July, (1990).

Enick, R., Falkenberg, K. L., and Klinzing, G. E., *Acceleration Length Model for Pneumatic Transport*. Particulate and Multiphase Processes (T. Ariman and T. N. Vezirglu, Eds.), Hemisphere Publishing Corporation, New York, 307 - 317, (1987).

Escardino, A., Sola, C. and Ruiz, F. *Oxidacion Catalitica de Butano a Anhidrido Maleico*. An. Quim., **69**, 1157 - 1168, (1973).

Gianetto, A., Pagliolico, S., Rovero, G., and Ruggeri, B. *Theoretical and Practical Aspects of Circulating Fluidized Bed Reactors (CFBRs) for Complex Chemical Systems*. Chem. Eng. Sci., **45**, No. 8, 2219 - 2225, (1990).

Grace, J. R. *High Velocity Fluidized Bed Reactors*. Chem. Eng. Sci., **45**, No. 8, 1953 - 1966, (1990).

Higbie, R. Trans. AIChE, **31**, 365, (1935).

Irving - Monshaw, S. and Kislin, A. *Lively Markets Brighten Maleic Anhydride Horizons*. Chem. Eng., Aug. 17, 29 - 33, (1987).

Kunii, D. and Levenspiel, O. *Flow Modelling of Fast Fluidized Beds*. Circulating Fluidized Bed Technology III (P. Basu, M. Horio, and M. Hasatani, Eds.), Pergamon Press, Toronto, Ontario, pp. 91 - 98, (1990).

Kunii, D. and Levenspiel, O. Fluidization Engineering (3rd Edition), Butterworth - Heinemann, Boston, Massachusetts, (1991).

Lang, X., Hudgins, R. R., Silveston, P. L. *Application of Periodic Operation to Maleic Anhydride Production*. Can. J. Chem. Eng., **67**, 635 - 645, (1989).

Li, Y. Chemical Metallurgy, **4**, 20, (1980).

Martin, F. G., and Emig, G. *Kinetik der n-Butane Oxidation in der Wirbelschicht*. Chem.-Ing.-Tech., **61**, No. 10, 819 - 822, (1989).

Matros, Y. S., Unsteady Processes in Catalytic Reactors. Elsevier Science Publishers B. V., Amsterdam, Ch. 9, pp. 322 - 323, (1985).

Mori, S., Yan. Y., Kato, K., Matsubara, K., and Liu, D. *Hydrodynamics of a CFB*.

Circulating Fluidized Bed Technology III (P. Basu, M. Horio, and M. Hasatani, Eds.), Pergamon Press, Toronto, Ontario, pp. 113 - 118, (1990).

Patience, G. S. *Circulating Fluidized Beds: Hydrodynamics and Reactor Modelling*. Ph.D. Dissertation, École Polytechnique de Montréal, Montréal, PQ, (1990).

Patience, G. S., Chaouki, J., and Kennedy, G. *Solids Residence Time Distribution in CFB Reactors*. Circulating Fluidized Bed Technology III (P. Basu, M. Horio, and M. Hasatani, Eds.), Pergamon Press, Toronto, Ontario, pp. 599 - 604, (1990).

Patience, G. S., Chaouki, J., Berruti, F., Wong, R. *Scaling Considerations for Circulating Fluidized Bed Catalytic Risers*. Powder Technology, submitted for publication, (1991).

Perry, R.H. and Green, D. (Eds.) Perry's Chemical Engineering Handbook (6th Edition), McGraw Hill Book Company, New York, N. Y., (1984).

Schneider, P. *Katalysatorentwicklung und Kinetische Untersuchung am Beispiel der Maleinsaureanhydrid-Herstellung aus n-Butan*. Ph.D. Thesis, Uni. Erlangen-Nurnberg, W. Germany (1985).

Senior, R. C. and Brereton, C. *Modelling of Circulating Fluidized Bed Flow Structure and Heat Transfer*. Department of Chemical Engineering, University of British Columbia,

Sept. (1990).

Sharma, R. K., Cresswell, D. L., and Newson, E. J. *Kinetics and Fixed Bed Reactor Modelling of Butane Oxidation to Maleic Anhydride*. AICHE J., 37, No. 1, 39 - 47, (1991).

Smith, J. R. Chemical Engineering Kinetics. (3rd Edition), McGraw Hill Book Company, New York, N. Y., pp. 381 - 383, (1981).

Takeuchi, H. and Hiramata, T. *Flow Visualization in the Riser of a Circulating Fluidized Bed*. Circulating Fluidized Bed Technology III (P. Basu, M. Horio, and M. Hasatani, Eds.), Pergamon Press, Toronto, Ontario, pp. 177 - 182, (1990).

Weinstein, H., Shao, M. and Schnitzlein, M. *Radial Variation in Solid Density in High Velocity Fluidization*. Circulating Fluidized Bed Technology (P. Basu, Ed.), Pergamon Press, Toronto, Ontario, pp. 201 - 206, (1986).

Wohlfahrt, K. and Hoffmann, H. Chem. Ing. Tech., 52, 811, (1980).

Wong, R. *Modelling the Hydrodynamics of Circulating Fluidized Bed Risers*. M.Sc. Thesis, The University of Calgary, Calgary, AB, (1990).

Zhang, H., Xie, Y., Chen, Y., Hasatani, M. *Mathematical Modelling for Longitudinal Voidage Distribution of Fast Fluidized Beds. Circulating Fluidized Bed Technology III* (P. Basu, M. Horio, and M. Hasatani, Eds.), Pergamon Press, Toronto, Ontario, pp. 151 - 156, (1990).